CHEMISTRY

A EUROPEAN JOURNAL

19/26

2013

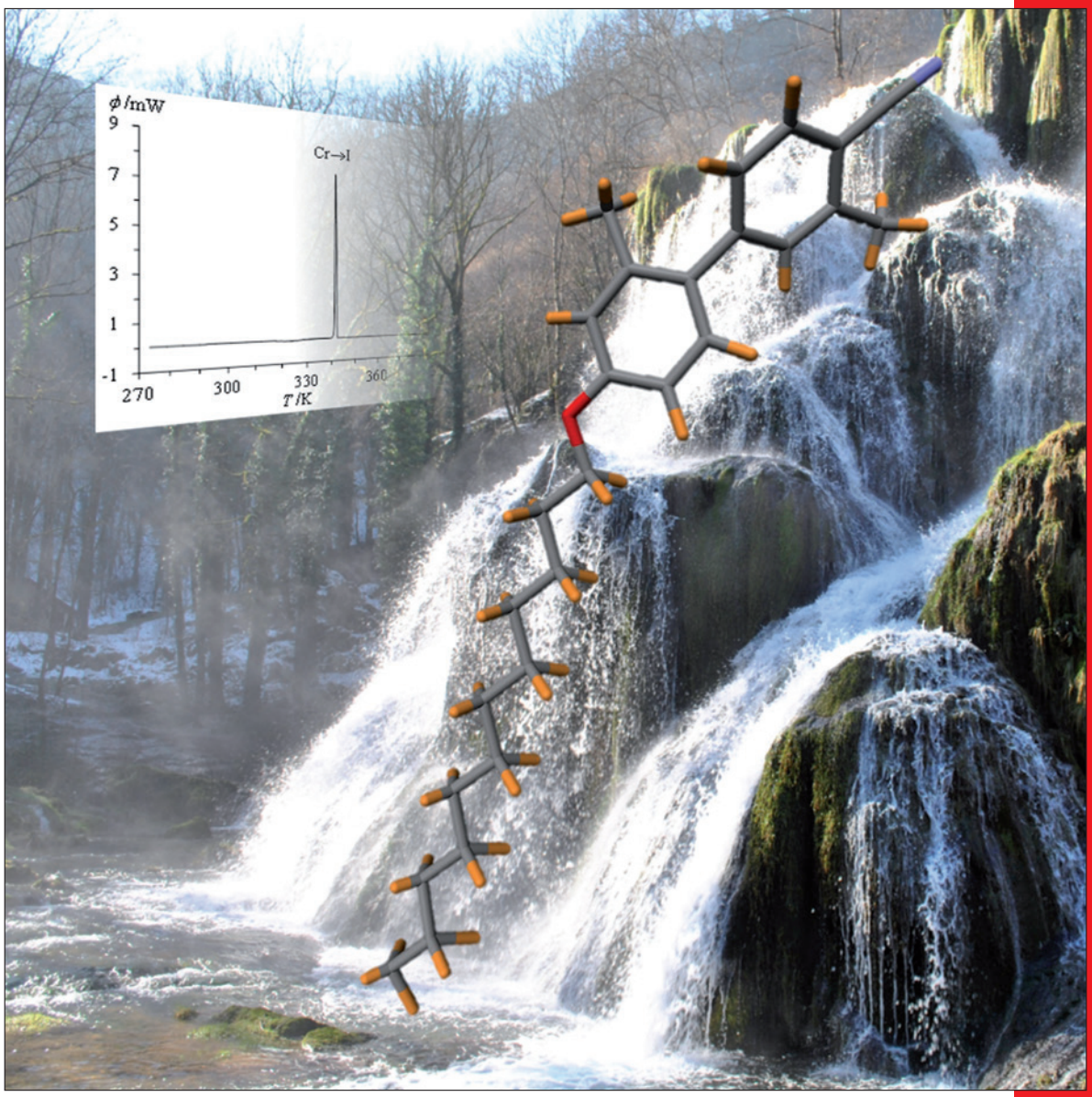

Concept

Transporting and Shielding Photosensitisers by Using Water-Soluble Organometallic Cages: A New Strategy in Drug Delivery and Photodynamic Therapy

B. Therrien

A Journal of

ChemPubSoc Europe

Supported by ACES

WILEY-VCH

CEUJED 19 (26) 8357–8688 (2013) · ISSN 0947-6539 · Vol. 19 · No. 26 · 2013

www.chemeurj.org

CHEMISTRY
A EUROPEAN JOURNAL

FULL PAPER

DOI: 10.1002/chem.201300587

Enthalpy–Entropy Compensation Combined with Cohesive Free-Energy Densities for Tuning the Melting Temperatures of Cyanobiphenyl Derivatives

Thibault Dutronc,[a] Emmanuel Terazzi,*[a] Laure Guénée,[b] Kerry-Lee Buchwalder,[a] Aurore Spoerri,[a] Daniel Emery,[c] Jiri Mareda,[c] Sébastien Floquet,[d] and Claude Piguet*[a]

Abstract: This work illustrates how minor structural perturbations produced by methylation of 4′-(dodecyloxy)-4-cyanobiphenyl leads to enthalpy–entropy compensation for their melting processes, a trend which can be analyzed within the frame of a simple intermolecular cohesive model. The transformation of the melting thermodynamic parameters collected at variable temperatures into cohesive free-energy densities expressed at a common reference temperature results in a novel linear correlation, from which melting temperatures can be simply predicted from molecular volumes.

Keywords: cohesive energy density · cyanobiphenyl · enthalpy–entropy compensation · intermolecular interactions · melting point

Introduction and Theoretical Background

Beyond the theoretically justified Gibbs free energy relationship $\Delta G = \Delta H - T\Delta S$, which links enthalpy ($\Delta H$) and entropy ($\Delta S$) with free energy ($\Delta G$) changes,[1] the extra-thermodynamic linear enthalpy–entropy correlation [Eq. (1)] may appear almost as familiar, because of its observation in an extremely wide range of areas covering chemical, physical, and biological processes.[2,3]

$$\Delta H_i = \alpha \Delta S_i + \gamma \quad (1)$$

The slope α has units of Kelvin and is often referred to as the compensation temperature, because all chemical processes i in a homogeneous series obeying Equation (1) display the same free-energy change γ (i.e. the compensation free energy) when conducted at this temperature.[4] Theoretical approaches of enthalpy–entropy correlation based on statistical thermodynamics include both attempts to refute its relevance,[5] as well as to establish its signature as the result of 1) minor perturbations of equilibrium constants,[3] 2) partition functions governed by a Gaussian density of states[6] or 3) underlying hidden thermodynamic processes.[7] Recent considerations further propose some physical rational for the operation of alternative nonlinear (rectangular hyperbolic) enthalpy–entropy compensation effects.[8] For broad scope (bio)chemists interested in controlling and tuning intermolecular interactions and phase-transition processes, but with no intention to specialize in statistical thermodynamics, Equation (1) is particularly attractive because of its intuitive interpretation, which suggests that an increasing enthalpic benefit of bonding is logically offset by an increasing adverse entropy of restricted motion.[9] Focussing on this idea, Williams[10] set a general parabolic form for H/S correlations, for which the entropic cost of any association between two molecular partners is some fraction of 50–60 kJ mol^{-1},[9] and is a sensitive function of the exothermicity of the interaction. In most cases, the experimentally accessible range of enthalpic contributions induced by molecular perturbations is too limited for detecting significant curvature, and linear H/S compensations are acceptable approximations.[11] Building on this concept, Ford derived with the help of Bjerrum's formalism, the two non-quantum Equations (2) and (3), which model the association between two molecular partner A and B bound by a single non-directional interaction obeying a simple harmonic potential ($u_{\min}^{A,B}$ is the well depth, $\kappa^{A,B}$ is the force constant, k_b is Boltzmann constant and $\beta = (k_b T)^{-1}$).[12]

[a] T. Dutronc, Dr. E. Terazzi, K.-L. Buchwalder, A. Spoerri, Prof. C. Piguet
Department of Inorganic and Analytical Chemistry
University of Geneva
30 quai E. Ansermet, 1211 Geneva 4 (Switzerland)
E-mail: Emmanuel.Terazzi@unige.ch
Claude.Piguet@unige.ch

[b] Dr. L. Guénée
Laboratory of X-ray Crystallography
University of Geneva
24 quai E. Ansermet, 1211 Geneva 4 (Switzerland)

[c] Dr. D. Emery, Dr. J. Mareda
Department of Organic Chemistry
University of Geneva
30 quai E. Ansermet, 1211 Geneva 4 (Switzerland)

[d] Dr. S. Floquet
Institut Lavoisier de Versailles, UMR 8180
University of Versailles Saint-Quentin
45 av. des Etats-Unis, 78035 Versailles (France)

Supporting information for this article is available on the WWW under http://dx.doi.org/10.1002/chem.201300587.

$$\Delta H_{asso}^{A,B} = u_{min}^{A,B} + \frac{3}{2}k_b T \quad (2)$$

$$\Delta S_{asso}^{A,B} = k_b \ln\left[c^{\theta}\left(\frac{2\pi e}{\beta\kappa^{A,B}}\right)^{3/2}\right] \quad (3)$$

The development of Ford's harmonic potential at the minimum of a standard Lennard–Jones (12,6) attractive well satisfyingly catches the two parameters used for characterizing the intermolecular interaction operating between the two molecular partners: 1) the absolute minimum of the attractive well depth $\varepsilon = -u_{min}^{A,B}$ and 2) the critical intermolecular A···B distance r_0 at which the potential of interaction is zero (Figure 1).[13] The consideration of the total energy of the

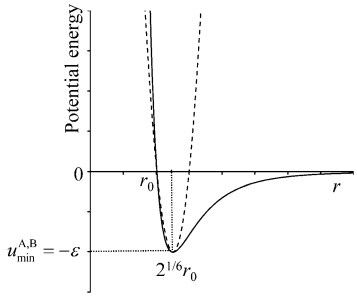

Figure 1. Representation of a Lennard–Jones (12,6) potential (full trace) with the interpretation of ε and r_0 parameters, and its harmonic approximation modelling the intermolecular interactions responsible for the formation of a AB complex. Adapted from reference [13].

harmonic oscillator for the special motion amplitude $r_0(2^{1/6}-1)$ eventually gives Equation (4) for the force constant $\kappa^{A,B}$, estimating the capacity of the bound system to gain residual degrees of freedom.

$$\frac{\kappa^{A,B}\left[r_0\left(1-2^{1/6}\right)\right]^2}{2} = \varepsilon \Rightarrow$$
$$\kappa^{A,B} = \frac{2}{(1-2^{1/6})^2}\frac{\varepsilon}{(r_0)^2} = -\frac{2}{(1-2^{1/6})^2}\frac{u_{min}^{A,B}}{(r_0)^2} \quad (4)$$

According to this simple model, the structural parameter r_0 represents the required hidden physicochemical process at the origin of H/S correlation.[7,14] When r_0 is constant along a perturbation applied to the molecular AB pair (i.e. the minimum contact distance at which the interaction potential is zero is retained along the perturbation), Equation (4) predicts that the force constant $\kappa^{A,B}$, controlling the association entropy, $\Delta S_{asso}^{A,B}$ [Eq. (3)] linearly depends on the well depth $u_{min}^{A,B}$, controlling the association enthalpy $\Delta H_{asso}^{A,B}$ [Eq. (2)].[12,15] Moreover, any change of $u_{min}^{A,B}$ induces a shift of $\kappa^{A,B}$ in the opposite direction resulting in the "natural" emergence of H/S compensation [$\alpha > 0$ in Eq. (1)]; hence $\Delta H_{asso}^{A,B}$ and $\Delta S_{asso}^{A,B}$ both decrease or both increase. Exact linear compensation as shown in Equation (1) further requires the expansion of the logarithmic function in Equation (3) as a first-order Taylor series around a central $\kappa_0^{A,B}$ estimate for the force constant of the process.[16] A plethora of H/S compensations obeying Equation (1) have been reported for the melting of solids subjected to minor structural variations (ΔG_m, ΔH_m, ΔS_m),[10,17] or during reverse condensation processes, in which isotropic liquids or liquid-crystalline phases transform into organized solids (ΔG_{asso}, ΔH_{asso}, ΔS_{asso}).[18] These processes can be idealized as reversible nth-order chemical reactions, in which n identical monomers associate into fully assembled entities with $\Delta G_m = -\Delta G_{asso}$, $\Delta H_m = -\Delta H_{asso}$ and $\Delta S_m = -\Delta S_{asso}$ [Eq. (5)].

$$nA \underset{\Delta G_m}{\overset{\Delta G_{asso}}{\rightleftharpoons}} A_n \quad (5)$$

A famous example concerns the melting of linear saturated hydrocarbons C_nH_{2n+2} of increasing length ($n > 1$), in which two terminal methyl tripods are separated by an increasing number ($n-2$) of methylene rotors.[19] The plot of ΔH_m (C_nH_{2n+2}) versus ΔS_m (C_nH_{2n+2}) indeed displays H/S compensation (Figure 2a). At the melting temperature T_m, the phase equilibrium condition requires $\Delta G_m = 0$ and we can write Equation (6).

$$\Delta G_m = \Delta H_m - T_m \Delta S_m = 0 \Rightarrow T_m = \frac{\Delta H_m}{\Delta S_m} = \frac{\Delta H_{asso}}{\Delta S_{asso}} \quad (6)$$

Introducing Equation (1) into Equation (6) yields Equation (7), in which the melting temperature can be simply deduced from the melting entropy (Figure 2b), a parameter

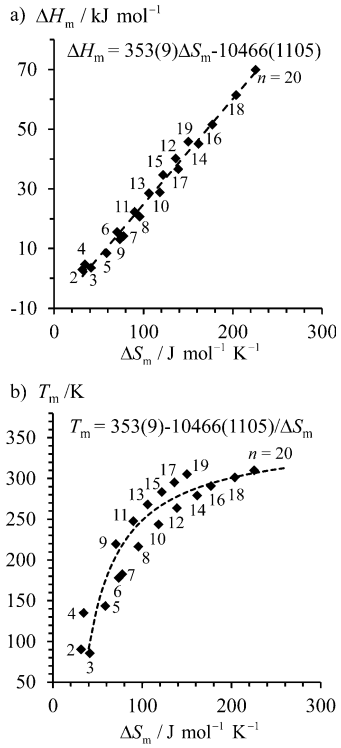

Figure 2. a) ΔH_m (C_nH_{2n+2}) versus ΔS_m (C_nH_{2n+2}) [Eq. (1)] and b) T_m versus ΔS_m (C_nH_{2n+2}) [Eq. (7)] correlation plots for the melting of saturated linear hydrocarbons CnH_{2n+2}.[19]

for which semi-empirical structure-based estimation schemes are available.[20]

$$T_m = \alpha + \frac{\gamma}{\Delta S_{asso}} = \alpha - \frac{\gamma}{\Delta S_m} \quad (7)$$

We note here that the sign of the compensation free energy is crucial and $\gamma = 10.5(1.1)\ kJ\,mol^{-1}$ found for the melting of linear alkanes induces larger melting temperatures when the melting entropies (hence the chain length) increase (Figure 2b). This trend is not general because decorrelation ($\gamma = 0$) was found, for instance, for the melting of silver *n*-alkanethiolate,[21] whilst opposite decreases of T_m with increasing melting entropies ($\gamma < 0$) were reported for polycatenar complexes.[22] Any predictive and rational correlation of the latter parameter with minor structural perturbations would bring an innovative tool for controlling melting temperatures within the frame of enthalpy–entropy compensation. However, melting enthalpies and entropies are collected at different temperatures for each compound (i.e., at T_m), and a common reference for comparing intermolecular cohesions within molecular solids is lacking. The closely related challenge of predicting boiling points was addressed by Hildebrand, who, taking Trouton's rule[23] into account for the vaporization of liquids, introduced the concept of cohesive energy density $ced = (\Delta H_v - RT)/V_m$ for estimating the average cohesive force in a liquid (ΔH_v is the vaporization enthalpy and V_m is the molar volume).[24] We suspect that this approach could be extended for melting processes, but the absence of Trouton's rule for solids requires the use of melting Gibbs free energy for estimating a cohesive free-energy density $CFED = -\Delta G^{\circ}_m/V_m$ along a homogeneous series of solid compounds at a common reference temperature. Considering the rodlike 4′-(dodecyloxy)-4-cyanobiphenyl compound **C12L$^{0',0}$** as a basic building block[25] for which thermochemical data[26] and intermolecular interactions[27] have been carefully investigated, we explore here the structural and thermodynamic consequences of its systematic substitution with methyl groups in 4′-(dodecyloxy)-*i*′-methyl-*j*-methyl-4-cyanobiphenyl (**C12L$^{i',j}$**; Scheme 1). Particular efforts are made for obtaining coherent sets of melting enthalpies and entropies at a common reference temperature, a prerequisite for the exploitation of cohesive free-energy densities within the frame of enthalpy–entropy compensation.

Results and Discussion

Synthesis and structural characterization of methyl-substituted 4′-dodecyloxy-4-cyanobiphenyls C12L$^{i',j}$: The target compounds **C12L$^{i',j}$** are obtained following Suzuki–Miyaura strategies for the formation of the inter-aromatic C–C bond in **5$^{i',j}$**,[15,28,29] followed by Williamson etherifications (Scheme 1).[30] The deleterious effect produced by a methyl group occupying the *ortho* position of the boronic esters **4^2** leads to low yield for **5$^{2',2}$** and **5$^{3',2}$**, and only traces for **5$^{0',2}$**. This drawback forced us to synthesize the alternative 4-alkoxyphenyl boronic acid **7** for the preparation of acceptable quantities of **C12L$^{0',2}$** (Scheme 1, right). All compounds were purified by thorough column chromatography and gave satisfying elemental analyses, ^{1}H and ^{13}C NMR spectra and adequate molecular peaks by using ESI-MS (see Experimental Section). Crystallization from hot methanol provided limited crops of X-ray quality prisms for all **C12L$^{i',j}$** compounds except for **C12L$^{0',3}$** and **C12L$^{2',2}$** (Table S1 and Figure S1, S2, Supporting Information).[31] In line with the crystal structure reported for the non-methylated reference compound **C12L$^{0',0}$**,[25] the molecular structures of the monomethyl **C12L$^{3',0}$**, **C12L$^{2',0}$**, and **C12L$^{0',2}$** (Figure 3a) and dimethyl

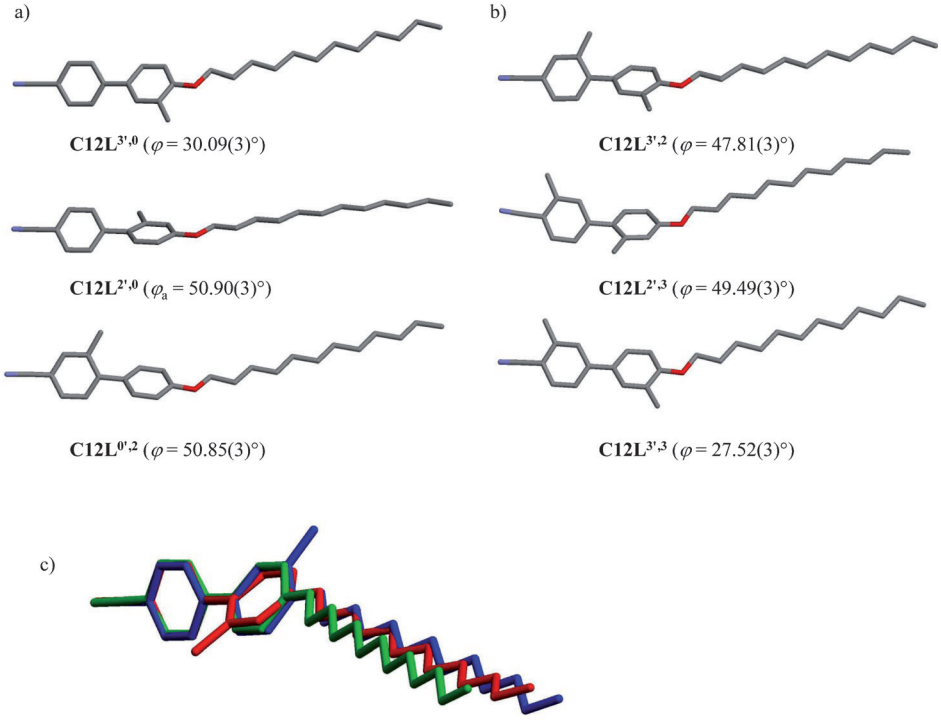

Figure 3. Molecular structures for a) monomethyl **C12L$^{3',0}$**, **C12L$^{2',0}$**, and **C12L$^{0',2}$**,[33] and b) dimethyl **C12L$^{3',2}$**, **C12L$^{2',3}$**, and **C12L$^{3',3}$** cyanobiphenyls. c) Superimposition of non-substituted **C12L$^{0',0}$** (green)[25] and monomethyl substituted at the 3-position **C12L$^{3',0}$** (blue) and at the 2-position **C12L$^{2',0}$** (red) showing the increase of φ interplanar angles between the connected aromatic rings. Hydrogen atoms are omitted for clarity.

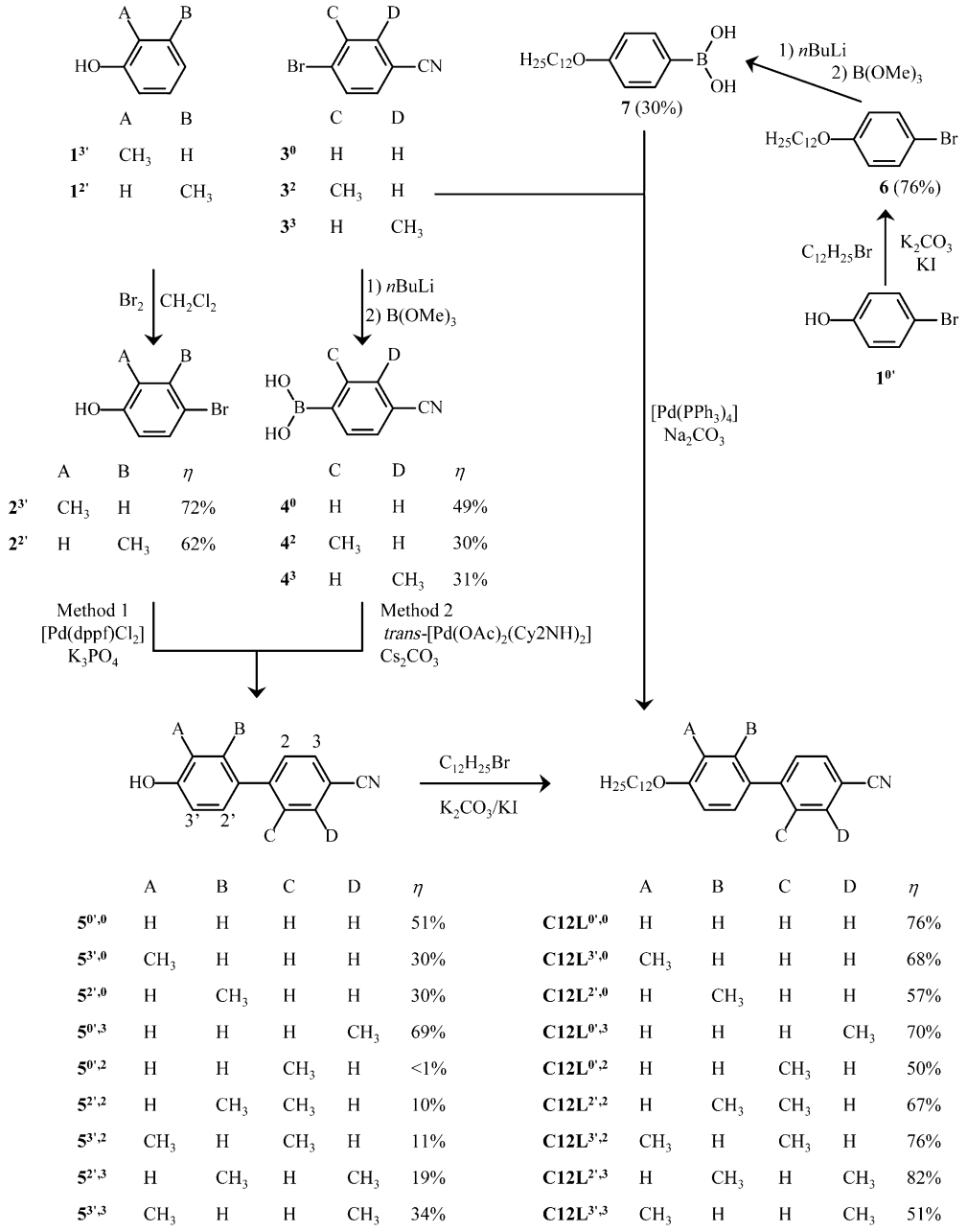

Scheme 1. Syntheses and chemical structures of the 4′-(dodecyloxy)-*i*′-methyl-*j*-methyl-4-cyanobiphenyl **C12L$^{i',j}$**. dppf = 1,10-Bis(diphenylphosphino)ferrocene and Cy_2NH = dicyclohexylamine.

C12L$^{3',2}$, **C12L$^{2',3}$**, and **C12L$^{3',3}$** (Figure 3b) cyanobiphenyls display variably twisted biaryl aromatic cores, to which planar all-*trans*-dodecyloxy chains are attached. The interaromatic twist angle φ is sensitive to the methyl groups bound to the 2- or 2′-positions, and it increases from $\varphi = 29.5(1.3)°$ in **C12L$^{0',0}$**, **C12L$^{3',0}$**, and **C12L$^{3',3}$** (no methyl group in the 2- or 2′-positions) to 51.1(3.1)° in **C12L$^{2',0}$**, **C12L$^{0',2}$**, **C12L$^{3',2}$**, and **C12L$^{2',3}$** (one methyl group in the 2- or 2′-positions, Figure 3c and Table S2).

All C–C, C–O, and C–N bond lengths are standard,[32] leading to elongated rodlike molecules 2.56(2) nm long and 0.515(7) nm wide (Appendix 1, Table A1-1 in the Supporting Information). In the crystal structures, each molecule is involved in several weak intermolecular C–H···N bonds,[34] together with stronger sheared antiparallel CN···CN motifs (Table 1 and Appendix 2 in the Supporting Information).[27] One immediately notices that methylation severely limits the latter processes, since four intermolecular CN···CN interactions are observed per **C12L$^{0',0}$** molecule, whilst only one related interaction per molecule could be identified for **C12L$^{0',2}$** and **C12L$^{2',3}$**, and none in the remaining compounds (Table 1). All crystallized **C12L$^{i',j}$** compounds display layered arrangements of the aromatic cyanobiphenyl units in the solid state and variable tilt angles with respect to the interfa-

Table 1. Number of intermolecular interactions[a] and distances identified in the crystal structures of **C12L$^{0',0}$**, **C12L$^{3',0}$**, **C12L$^{2',0}$**, **C12L$^{0',2}$**, **C12L$^{3',2}$**, **C12L$^{2',3}$** and **C12L$^{3',3}$**.

	CN···CN d(C···N) [Å]	C_{arom}H···N d(C···N) [Å]	C_{aliph}H···N d(C···N) [Å]
C12L$^{0',0}$	4/3.5(1)	4/3.46(1)	0
C12L$^{3',0}$	0	2/3.560(2)	2/3.814(2)
C12L$^{2',0}$	0	6/3.48(3)	4/3.6(2)
	0	4/3.53(2)	2/3.575(2)
C12L$^{0',2}$	1/3.563(2)	6/3.58(4)	2/3.926(2)
C12L$^{3',2}$	0	4/3.7(2)	5/3.7(2)
C12L$^{2',3}$	1/3.441(2)	6/3.7(1)	4/3.8(1)
C12L$^{3',3}$	0	2/3.598(2)	2/3.700(2)

[a] C–H···N hydrogen bonds are considered for bond lengths d(H···N) < 3.0 Å and bond angles θ(C-H···N) > 120°.[34] Antiparallel CN···CN interactions are considered for: d(C···N) ≤ 3.6 Å (see Appendix 2 in the Supporting Information).[27] The number of interactions is given first followed by the bond length.

ces produced by the head-to-tail CN groups (Appendix 3 in the Supporting Information). We note that **C12L$^{0',0}$** is the only compound of the series for which the cyanobiphenyl cores lie perpendicular to the interface in the crystal, as found in its SmA mesophase at higher temperature.

Thermodynamic and structural characterization of the melting processes for methyl-substituted 4′-dodecyloxy-4-cyanobiphenyls C12L$^{i',j}$: In order to minimize deviations from thermodynamic equilibria, differential scanning calorimetric (DSC) traces were recorded at 0.5 K min^{-1} for compounds **C12L$^{i',j}$** and they showed single first-order melting processes transforming the room temperature solids into isotropic liquids (confirmed by polarized optical microscopy, Figure 4a and S3a–S9a, and Table 2), except for the reference compound **C12L$^{0',0}$**, which was known to display an intermediate smectic A mesophase prior to isotropization (Figure S10).[26] The 8–15% decrease of the ratio between the molecular cross sections of the aliphatic chains and of the aromatic cores upon methylation $\delta = A_{mol}^{tail}/A_{mol}^{core}$ may partly explain the removal of any mesomorphism in the substituted cyanobiphenyls (Table A1,2 in Appendix 1 in the Supporting Infor-

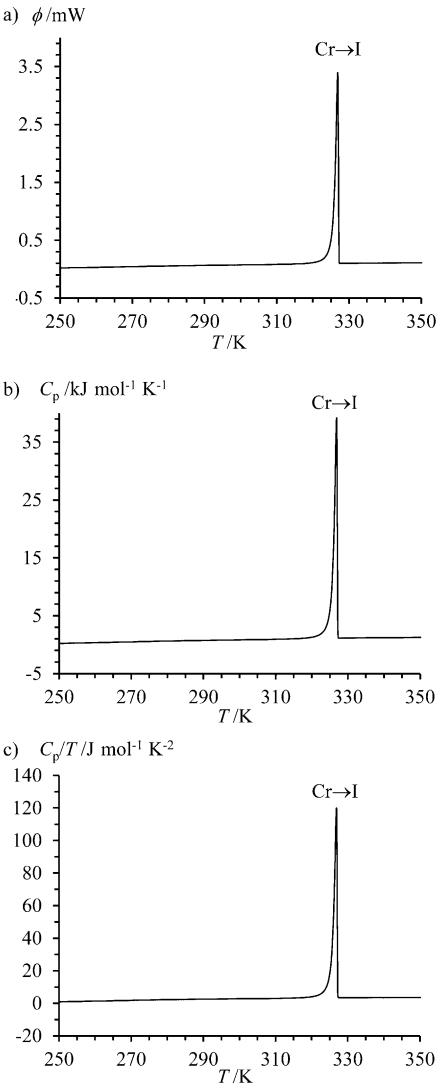

Figure 4. a) DSC trace recorded for the second heating of **C12L$^{2',3}$** and its transformation into b) molar heat capacity [Eq. (8)] and c) molar heat capacity per temperature unit.

Table 2. Thermodynamic parameters for the melting processes in **C12L$^{i',j}$**.[a]

	Transitions[b]	ΔH_m [J mol^{-1}]	ΔS_m [J mol^{-1} K^{-1}]	ΔG_m [kJ mol^{-1}]	T_m[c] [K]	ΔH_m^0 [kJ mol^{-1}]	ΔS_m^0 [J mol^{-1} K^{-1}]	ΔG_m^0 [kJ mol^{-1}]	T_{dec} [K]
C12L$^{0',0}$	Cr→SmA	41.7(2)	122.2(6)	0.0(4)	341.6	38.8(1.7)	118.6(5.3)	3.4(3.2)	327.2(20.5)
	SmA→I	4.6(2)	12.6(6)	0.0(6)	362.2	6.2(7)	13.4(7)	2.2(9)	462.7(57.6)
	′Cr→I′[d]	46.3(4)	134.8(1.1)	0.0(8)	–	45.0(2)	132.0(6)	5.7(3.7)	340.9(21.7)
C12L$^{3',0}$	Cr→I	57.0(5)	167.1(1.5)	0.0(1.0)	341.2	45.8(8)	132.0(2.4)	6.5(1.5)	347.0(8.8)
C12L$^{2',0}$	Cr→I	32.5(2)	103.5(6)	0.0(4)	314.0	31.3(8)	99.6(2.5)	1.6(1.5)	314.3(11.3)
C12L$^{0',3}$	Cr→I	50.7(7)	155.4(2.2)	0.0(1.4)	326.6	43.9(7)	133.2(2.2)	4.2(1.3)	329.6(7.6)
C12L$^{0',2}$	Cr→I	55.4(1.0)	171.1(3.1)	0.0(2.0)	323.8	46.7(2)	143.0(7)	4.1(4)	326.6(2.1)
C12L$^{2',2}$	Cr→I	34.4(5.5)	111.9(17.9)	0.0(11.0)	307.8	39.7(1)	128.7(1)	1.4(2)	308.5(8)
C12L$^{3',2}$	Cr→I	54.0(7)	155.5(2.0)	0.0(1.4)	347.5	46.2(5)	130.9(1.5)	7.2(9)	352.9(5.6)
C12L$^{2',3}$	Cr→I	46.3(2)	142.0(6)	0.0(4)	325.7	43.2(3)	132.0(9)	3.9(6)	327.3(3.2)
C12L$^{3',3}$	Cr→I	44.1(7)	137.8(2.2)	0.0(1.5)	329.3	41.3(9)	128.4(3.0)	3.1(1.8)	321.7(10.3)

[a] The parameters marked with a 0 index correspond to standard values at 298 K, whereas all other data are given at the melting temperature T_m. [b] Cr = crystal, SmA = smectic A, I = isotropic liquid. [c] Melting temperature taken at the onset of the DSC trace. [d] Sum of the two successive phase transitions.

mation), while the resort to empirical Hildebrand solubility parameters attributes this phenomenon to the decrease in polarity produced by methylation of the cyanobiphenyl cores (Appendix 4 in the Supporting Information).[35]

The energy flux $\phi = \Delta W/\Delta t$ measured by DSC at a constant scanning rate $v = \Delta T/\Delta t$ can be easily transformed 1) into molar constant pressure heat capacity C_p [Eq. (8) in which n is the number of moles, see also Figure 4b, Figures S3b–S10b in the Supporting Information] required for the determination of the melting enthalpies ΔH_m [Eq. (9), Figure 5, and Table 2 column 3] and 2) into temperature-normalized molar heat capacity C_p/T (Figure 4c and Figures S3c–S10c in the Supporting Information) required for the calculations of melting entropies ΔS_m [Eq. (10), Table 2 column 4). Evidently, the free energy of melting $\Delta G_m = \Delta H_m - T_m \Delta S_m$ is zero for all compounds at their melting temperatures (Table 2 column 5).

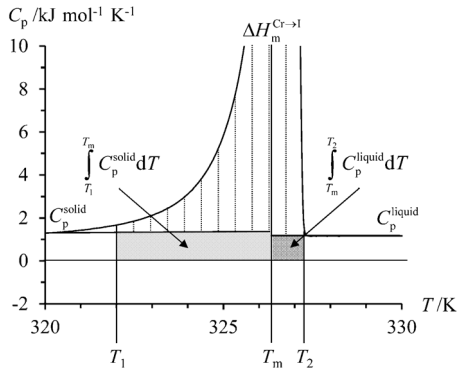

Figure 5. Molar heat capacity (C_p) trace recorded for **C12L$^{2',3}$** around its melting temperature with a graphical illustration of the method used for computing the thermodynamic melting enthalpy with Equation (9). T_1, T_m, and T_2 are respectively the starting, melting, and end temperatures of the Cr→I phase transition.[36]

$$\phi = \frac{\Delta W}{\Delta t} = \frac{nC_p \Delta T}{\Delta t} = nC_p v \Rightarrow C_p = \frac{\phi}{nv} \tag{8}$$

$$\Delta H_m = \int_{T_1}^{T_2} C_p dT - \int_{T_1}^{T_m} C_p^{solid} dT - \int_{T_m}^{T_2} C_p^{liquid} dT \tag{9}$$

$$\Delta S_m = \int_{T_1}^{T_2} \frac{C_p}{T} dT - \int_{T_1}^{T_m} \frac{C_p^{solid}}{T} dT - \int_{T_m}^{T_2} \frac{C_p^{liquid}}{T} dT \tag{10}$$

The minor change of the solid heat capacity below the melting temperature is reminiscent from the Dulong and Petit's law,[37] and linear approximations of C_p versus T curves for both solid and liquid states are valuable approximations in this temperature range.[38] Assuming that the linear correlation experimentally found for C_p^{liquid} versus T (Figure 5) also holds for the virtual liquid phase below its melting temperature, the associated Born–Haber cycle depicted in Figure 6 allows the estimation of "standard" melting enthalpies ΔH_m^0 [Eq. (11), Table 2 column 7] and entropies ΔS_m^0 [Eq. (12), Table 2 column 8] at a reference temperature T^0 (Appendix 5 in the Supporting Information).

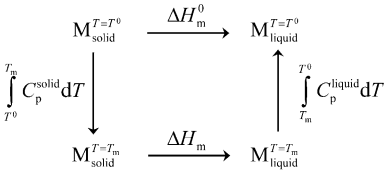

Figure 6. Born–Haber cycle used for estimating the standard enthalpy of melting in Equation (11).

$$\begin{aligned}\Delta H_m^0 &= \Delta H_m + \int_{T^0}^{T_m} C_p^{solid} dT - \int_{T^0}^{T_m} C_p^{liquid} dT \\ &= \int_{T^0}^{T_2} C_p dT - \int_{T^0}^{T_2} C_p^{liquid} dT\end{aligned} \tag{11}$$

$$\begin{aligned}\Delta S_m &= \Delta S_m + \int_{T^0}^{T_m} \frac{C_p^{solid}}{T} dT - \int_{T^0}^{T_m} \frac{C_p^{liquid}}{T} dT \\ &= \int_{T^0}^{T_2} \frac{C_p}{T} dT - \int_{T^0}^{T_2} \frac{C_p^{liquid}}{T} dT\end{aligned} \tag{12}$$

The resulting non-zero free energies of decohesion $\Delta G_m^0 = \Delta H_m^0 - T^0 \Delta S_m^0$ (Table 2, column 9) allow us to compare the trend for melting of the different compounds, whereas the associated temperatures of decohesion $T_{dec} = \Delta H_m^0/\Delta S_m^0$ (Table 2 column 10) fix the points at which melting is expected if ΔH_m^0 and ΔS_m^0 are temperature independent. A rapid inspection of Table 2 shows that the "standard" thermodynamic melting parameters obtained for **C12L$^{i',j}$** do not drastically differ from those collected at variable melting temperatures (Figure S11 in the Supporting Information) and the concept of free energy of decohesion at a common reference temperature can be reasonably extended to $\Delta G_m^0 = \Delta H_m - T^0 \Delta S_m$ (Figure S12 in the Supporting Information). Interestingly, the existence of an intermediate mesophase, as found for **C12L$^{0',0}$**, is no more a drastic limiting factor for comparison purposes, since the corrected enthalpy and entropy changes accompanying the successive melting and isotropization processes are now referred to a common temperature and can be added to provide a global thermodynamic parameter estimating a single virtual solid→liquid process (Table 2). The broadening of the melting process at a low scan rate for **C12L$^{3',3}$** (Figure S9 in the Supporting Information) and even its splitting for **C12L$^{2',0}$** (Figure S4 in the Supporting Information) suggest the existence of polymorphism in the solid state as previously established for **C12L$^{0',0}$**.[39] In our hands, the IR spectrum of solid **C12L$^{0',0}$** recorded in the 2200–2300 cm^{-1} range indeed showed the two separate bands of the C–N stretching vibrations as-

signed to the expected mixture between a minor thermodynamic form with $\nu(CN)=2222\ cm^{-1}$, and a major kinetic form with $\nu(CN)=2231\ cm^{-1}$ (Figure S13a in the Supporting Information).[40] Upon melting, these two bands coalesce to give a single peak at $\nu(CN)=2225\ cm^{-1}$ in line with the removal any strong CN···CN interactions (Figure S13b in the Supporting Information).[39,40] Reminiscent variable-temperature IR data can be collected for the melting of **C12L$^{3',3}$**, except that the thermodynamic form ($\nu(CN)=2217\ cm^{-1}$) represents the major polymorph for this compound in the solid state (Figure S14 in the Supporting Information).

Enthalpy–entropy compensation for the melting processes of methyl-substituted 4′-dodecyloxy-4-cyanobiphenyls C12L$^{i',j}$: The plot of ΔH^0_m versus ΔS^0_m for the solid to liquid melting processes is linear along the **C12L$^{i',j}$** series with a compensation temperature $\alpha=380(56)$ K and a compensation free energy $\gamma=-6(7)\ kJ\,mol^{-1}$ (Figure 7a). The same

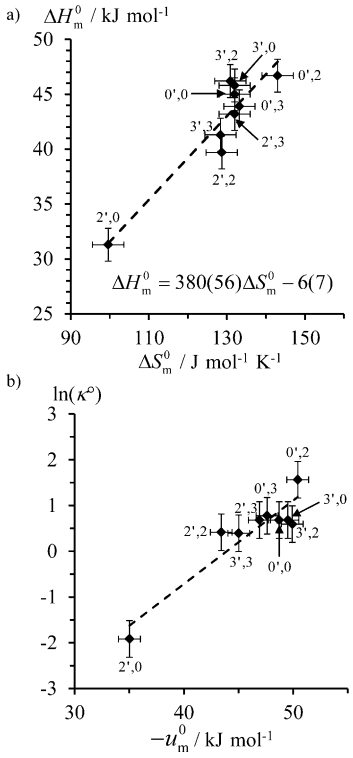

Figure 7. a) ΔH^0_m versus ΔS^0_m [Eq. (1)] and b) the logarithm of the force constants $\ln(\kappa^0)$ versus the potential well depth u^0_{min} for the melting of **C12L$^{i',j}$**.

enthalpy/entropy compensation (within experimental error) can be computed by using the thermodynamic parameters obtained at variable temperatures ($\Delta H_m=371(25)$ and $\Delta S_m-6(4)$, Figure S15 in the Supporting Information) and we conclude that the perturbations produced by methylation in **C12L$^{i',j}$** do not significantly affect the average minimum contact distance r_0 between the interacting entities in the solid state.

Interestingly, ΔH_m and ΔS_m values previously reported for **CnL$^{0',0}$** ($n=5$–11, Table S3)[26] fit the trend found for **C12L$^{i',j}$** and the linear H/S compensation also holds for change in chain length (Figure S15a in the Supporting Information). The logarithmic plot of the force constants κ^0 [computed with Eq. (3)] versus the attractive well depths u^0_{min} [computed with Eq. (2)] is evidently linear (Figure 7b and Figure S15b in the Supporting Information), but its interpretation within the frame of a single harmonic potential describing the intermolecular interactions in the solid state further requires the approximate Taylor series $\ln(\kappa^0)\approx\ln(\kappa^0_a)+[(\kappa^0-\kappa^0_a)/\kappa^0_a]$ developed around an optimum central value κ^0_a (Table S4).[12,13] The large dispersion of the force constants κ^0 estimated at various melting temperature is not appropriate for this purpose (Figure S16a in the Supporting Information), and the more confined set of κ^0 computed at a common reference temperature (298 K) is better suited for being approximated by a straight line generated around $\kappa^0_a=1.70\ kN\,m^{-1}$ (Figure S16b in the Supporting Information). Application of Equation (4) eventually gives $2^{1/6}r_0=1.3(2)$ Å for the average optimum contact distance between the surface of the cyanobiphenyl entities (Figure S16c in the Supporting Information).

Within the regime of H/S compensation produced by methylation of the aromatic core or by chain extension in **CnL$^{i',j}$**, the combination of Equations (1) and (6) leads to Equations (13)–(15), in which the standard thermodynamic parameters depend on the compensation temperature (α), the compensation free energy (γ), and the decohesion temperatures (T_{dec}).

$$\Delta H^0_m = \gamma\left(\frac{T_{dec}}{T_{dec}-\alpha}\right) \quad (13)$$

$$\Delta S^0_m = \gamma\left(\frac{1}{T_{dec}-\alpha}\right) \quad (14)$$

$$\Delta G^0_m = \gamma\left(\frac{T_{dec}-T^0}{T_{dec}-\alpha}\right) \quad (15)$$

Since the compensation free energy γ is close to zero within experimental error along the **C12L$^{i',j}$** series (Figure 7a), the decohesion or melting (Figures S17 and S18, respectively, in the Supporting Information) temperatures are only slightly influenced by the various thermodynamic parameters. Taking into account the molar volume $V_m=N_{av}\cdot V_{mol}$ estimated from the molecular volume (V_{mol}) computed for each **CnL$^{i',j}$** compound (N_{av} is Avogadro's number),[41] we deduce the target standard cohesive free-energy densities $CFED=\Delta G^0_m/V_m$ along the series (Table 3 and Table S5 in the Supporting Information). One immediately notices that CFED linearly increases with the decohesion temperature T_{dec} according to the empirical Equation (16) with $\lambda=-0.43(2)\ J\,K^{-1}\,cm^{-3}\,K^{-1}$ and $\mu=127(7)\ J\,cm^{-3}$, an observation in line with the redundancy of these two parameters for estimating the trend of the molecules to interact in solid **C12L$^{i',j}$** (Figure 8a and Figure S19a in the Supporting Information).

Table 3. Molecular (V_{mol}) and molar volumes (V_m), standard free energy of decohesion (ΔG^0_m) and cohesive free-energy densities (CFED) in **C12L$^{i',j}$**.

	Transitions[a]	V_{mol}[b] [Å]^3	V_m[c] [cm^3 mol^{-1}]	ΔG^0_m[d] [kJ mol^{-1}]	CFED[e] [J cm^{-3}]
C12L$^{0',0}$	'Cr→I'[f]	502.1	302.4	5.7(3.7)	−18.7(12.1)
C12L$^{3',0}$	Cr→I	530.7	319.7	6.5(1.5)	−20.2(4.6)
C12L$^{2',0}$	Cr→I	528.7	318.4	1.6(1.5)	−5.1(4.8)
C12L$^{0',3}$	Cr→I	528.4	318.3	4.2(1.3)	−13.2(4.2)
C12L$^{0',2}$	Cr→I	526.5	317.1	4.1(4)	−12.9(1.3)
C12L$^{2',2}$	Cr→I	548.1	330.1	1.4(2)	−4.1(4)
C12L$^{3',2}$	Cr→I	549.7	331.1	7.2(9)	−21.7(2.7)
C12L$^{2',3}$	Cr→I	548.5	330.4	3.9(6)	−11.7(1.7)
C12L$^{3',3}$	Cr→I	548.9	330.6	3.1(1.8)	−9.2(5.3)

[a] Cr = crystal, I = isotropic liquid. [b] Taken as the Connolly volume.[41] [c] $V_m = N_{av} \times V_{mol}$ in which N_{av} is the Avogadro number. [d] $\Delta G^0_m = \Delta H^0_m - T^0 \Delta S^0_m$ is taken from Table 2 column 9. [e] CFED $= -\Delta G^0_m / V_m$. [f] Sum of the two successive phase transitions leading to the isotropic liquid.

$$\mathrm{CFED} = \frac{\Delta G^0_m}{V_m} = \lambda T_{dec} + \mu \qquad (16)$$

The introduction of H/S compensation [Eq. (1)] together with $\Delta G^0_m = \Delta H^0_m - T^0 \Delta S^0_m$ and $T_{dec} = \Delta H^0_m / \Delta S^0_m$ into Equation (16) eventually gives Equation (17), in which the melting entropy, measuring the degrees of freedom relaxed upon melting, (Figure 2b),[44] can be deduced from the molar volume along the **CnL$^{i',j}$** series (Figure 8b and Figure S19b in the Supporting Information, domain of definition: $\Delta S^0_m \neq -\gamma/(\alpha + \mu/\lambda)$).[13]

$$V_m = \frac{(\Delta S^0_m)^2 (T^0 - \alpha) - \gamma \Delta S^0_m}{\Delta S^0_m (\lambda\alpha + \mu) + \lambda\gamma} \qquad (17)$$

Because of the very limited change in molar volumes induced by methylation in **C12L$^{i',j}$**, a satisfying fit with Equation (17) is difficult (Figure 8b), but the larger range of molar volumes explored with increasing chain length in **CnL$^{i',j}$** (n = 5–12) improves the quality of the correlation (Figure S19b in the Supporting Information).

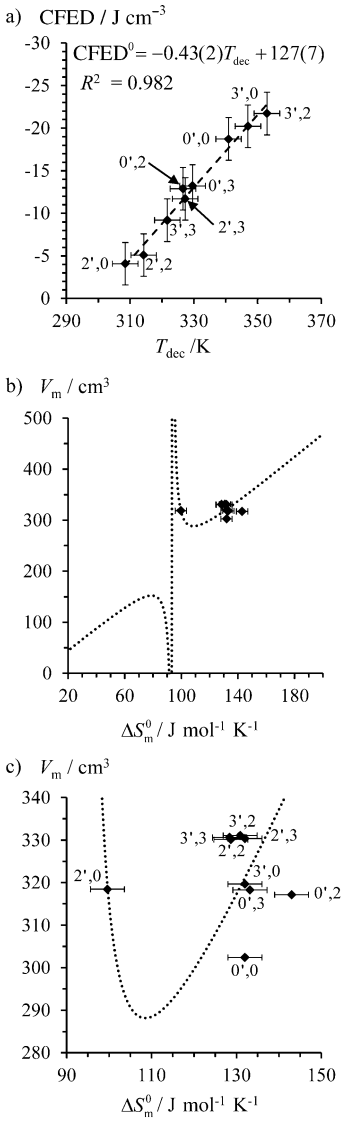

Figure 8. Plots of a) the standard cohesion free energy densities (CFED) versus the decohesion temperature (T_{dec}) and b) the molar volumes (V_m) versus ΔS^0_m for **CnL$^{i',j}$**. The dotted trace shows the theoretical curve computed with Equation (17) and c) shows the assignment for each compound.

Conclusion

The minor perturbations of the intermolecular interactions induced by successive methylation in **C12L$^{i',j}$** can be caught by a single harmonic potential with an average intermolecular contact distance of 1.3(2) Å. According to Ford's approach,[11–13] this situation leads to linear H/S compensation for the melting processes. Since the absolute melting temperatures of standard organic materials are globally close to that of the reference standard state (298 K), correcting enthalpies and entropies for temperature changes is not crucial and the usual assumption $\Delta H^0_m \approx \Delta H_m$ and $\Delta S^0_m \approx \Delta S_m$ is acceptable for extracting 1) average intermolecular contact distance r_0 in the solid state, 2) free energies of decohesion $\Delta G^0_m = \Delta H_m - T^0 \Delta S_m$ at T° = 298 K, and 3) standard cohesion free-energy densities CFED $= -\Delta G^0_m / V_m$. We have applied this approach for the melting of alkane C_nH_{2n+2} of increasing length (n = 2–20), for which H/S compensation is well established (Figure 2a). Firstly, the associated linear correlation established between the force constants and the potential well depth [Eqs. (2) and (3), and Figure S20a,b in the Supporting Information] yields an optimal contact distance of $2^{1/6} r_0 = 0.31(4)$ Å for the average optimum separation between the surface of the alkane entities [Eq. (4) and Figure S20c in the Supporting Information]. Secondly, the standard cohesion free energy densities (CFED) computed at 298 K are again linearly correlated with the melting temperatures (Figure 9a), and the relationship between the molar volumes and the melting entropies shown in Equation (17) allows simple predictions (Figure 9b). For instance, the molecular volume of V_{mol} = 738 Å^3 computed for tetraco-

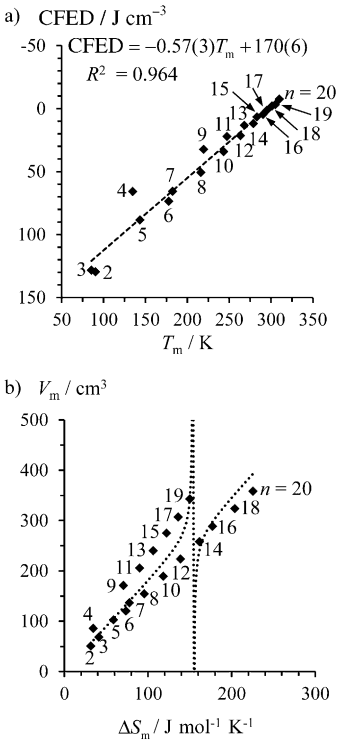

Figure 9. Plots of a) the cohesion free energy densities (CFED) versus the melting temperature (T_m) and b) the molar volumes (V_m) versus ΔS_m for saturated linear hydrocarbons C_nH_{2n+2}. The dotted trace shows the theoretical curve computed with Equation (17).

sane ($C_{24}H_{50}$)[41] is translated into a molar volume of V_m = 444.5 cm^3 mol^{-1}, from which a molar entropy of ΔS_m = 254 J mol^{-1} K can be estimated with Equation (17). Equation (14) then provides the melting temperature T_m = 312 K, whereas Equation (13) gives the melting enthalpy ΔH_m = 79.2 kJ mol^{-1} in good agreement with experimental calorimetric results of ΔH_m = 81.75 kJ mol^{-1}, ΔS_m = 253.9 J mol^{-1} K, and T_m = 322 K.[42] We are aware that multiparameter predictions along the alkane series have numerous precedences,[43] but the exploitation of the standard cohesion free energy densities (CFED) proposed in Equation (16) provides an unexpectedly simple and rational correlation between melting entropies and molecular volumes in Equation (17), which we believe to be useful for synthetic chemists in order to predict and tune melting temperatures beyond the limited predictions usually obtained with the exclusive resort of *H*/*S* compensation.[13] Efforts are currently focussed on the extension of the CFED concept for the rationalization and prediction of the successive melting processes characterizing the transformation of solids into liquid crystals and of liquid crystals into isotropic liquids.

Experimental Section

Solvents and starting materials: These were purchased from Strem, Acros, Fluka AG and Aldrich and used without further purification unless otherwise stated. Compounds **4^{0}**,[44] **42**,[45] **5$^{2',0}$**,[15] and **5$^{2',2}$**[15] were prepared according to litterature procedures. The synthesis of **22′**, **2$^{3'}$**, **4^{3}**, **5$^{0',0}$**, **5$^{3',0}$**, **5$^{3',2}$**, **5$^{0',3}$**, **5$^{2',3}$**, **5$^{3',3}$**, **6**, **7**, **C12L$^{0',0}$**, **C12L$^{3',0}$**, **C12L$^{2',0}$**, **C12L$^{0',3}$**, **C12L$^{2',2}$**, **C12L$^{3',2}$**, **C12L$^{2',3}$**, **C12L$^{3',3}$** and **C12L$^{0',2}$** are given in Appendix 6 (Supporting information). Acetonitrile and dichloromethane were distilled over calcium hydride. Silicagel plates Merck 60 F254 were used for thin layer chromatography (TLC) and Fluka silica gel 60 (0.04–0.063 mm) or Acros neutral activated alumina (0.050–0.200 mm) was used for preparative column chromatography.

Spectroscopic and analytical measurements: ^{1}H and ^{13}C NMR spectra were recorded at 25 °C on a Bruker Avance 400 MHz spectrometer. Chemical shifts are given in ppm with respect to TMS. Pneumatically-assisted electrospray (ESI-MS) mass spectra were recorded from 10^{-4} M solutions on an Applied Biosystems API 150EX LC/MS System equipped with a Turbo Ionspray source. Elemental analyses were performed by K. L. Buchwalder from the Microchemical Laboratory of the University of Geneva. TGA were performed with a thermogravimetric balance Mettler Toledo Star Systems (under N_2). DSC traces were obtained with a Mettler Toledo DSC1 Star Systems differential scanning calorimeters from 3–5 mg samples (5 and 0.5 °C min^{-1}, under N_2). The characterization of the mesophases and of the isotropic liquids were performed with a polarizing microscope Leitz Orthoplan-Pol with a Leitz LL 20x/0.40 polarizing lens, and equipped with a Linkam THMS 600 variable-temperature stage. The variable-temperature FT-IR spectra were recorded on an IRTF Nicolet iS10 spectrometrer in diffuse reflectance mode by using a high-temperature diffuse reflectance environmental chamber. The samples were diluted into a KBr matrix and the resulting mixtures containing about 10 % of compound were ground before being heated at 200 °C during few minutes. After cooling to room temperature the FT-IR spectra were recorded in the 20–200 °C and in the 200–20 °C temperature ranges using a heating or cooling rate of 2 °C min^{-1}. The spectra were recorded with a resolution of 0.4 cm^{-1}. The mathematical analyses were performed by using Igor Pro (WaveMetrics Inc.) and Excel (Microsoft) softwares.

X-ray crystallography: A summary of crystal data, intensity measurements and structure refinements for **C12L$^{3',0}$**, **C12L$^{2',0}$**, **C12L$^{0',2}$**, **C12L$^{3',2}$**, **C12L$^{2',3}$** and **C12L$^{3',3}$** is given in Table S1 (Supporting Information). All crystals were mounted on quartz fibers with protection oil. Cell dimensions and intensities were measured at 180–200 K on a Agilent Supernova diffractometer with mirror-monochromated $Cu_{K\alpha}$ radiation (λ = 1.54187 Å) and CCD camera. Data were corrected for Lorentz and polarization effects and for absorption. The structures were solved by direct methods (SIR97),[46] all other calculation were performed with SHELXL[47] systems and ORTEP[48] programs. CCDC-917848 (**C12L$^{3',0}$**), CCDC-917849 (**C12L$^{2',0}$**), CCDC-917850 (**C12L$^{0',2}$**), CCDC-917851 (**C12L$^{3',2}$**), CCDC-917852 (**C12L$^{2',3}$**), and CCDC-917853 (**C12L$^{3',3}$**) the supplementary crystallographic data for this paper. These data can be obtained free of charge from The Cambridge Crystallographic Data Centre via www.ccdc.cam.ac.uk/data_request/cif.

Acknowledgements

Financial support from the Swiss National Science Foundation is gratefully acknowledged.

[1] T. Engel, P. Reid, *Physical Chemistry*, Pearson Benjamin Cummings, San Francisco, **2006**, pp. 113–122.
[2] L. Liu, Q.-X. Guo, *Chem. Rev.* **2001**, *101*, 673.
[3] K. F. Freed, *J. Phys. Chem. B* **2011**, *115*, 1689.
[4] J. E. Leffler, *J. Org. Chem.* **1955**, *20*, 1202.
[5] A. Cornish-Bowden, *J. Biosci.* **2002**, *27*, 121.
[6] K. Sharp, *Protein Sci.* **2001**, *10*, 661.
[7] E. B. Starikov, B. Norden, *J. Phys. Chem. B* **2007**, *111*, 14431.
[8] E. B. Starikov, B. Norden, *J. Phys. Chem. B* **2009**, *113*, 4698.

[9] a) M. I. Page, W. P. Jencks, *Proc. Natl. Acad. Sci. USA* **1971**, *68*, 1678; b) W. P. Jencks, *Adv. Enzymol.* **1975**, *43*, 219; c) W. P. Jencks, *Proc. Natl. Acad. Sci. USA* **1981**, *78*, 4046.
[10] a) M. S. Searle, D. H. Williams, *J. Am. Chem. Soc.* **1992**, *114*, 10690; b) M. S. Searle, M. S. Westwell, D. H. Williams, *J. Chem. Soc. Perkin Trans. 2* **1995**, 141; c) D. H. Williams, D. P. O'Brien, B. Bardsley, *J. Am. Chem. Soc.* **2001**, *123*, 737.
[11] D. M. Ford, *Adsorption* **2005**, *11*, Suppl. 271.
[12] D. M. Ford, *J. Am. Chem. Soc.* **2005**, *127*, 16167.
[13] C. Piguet, *Dalton Trans.* **2011**, *40*, 8059.
[14] J. M. Ward, N. M. Gorenstein, J. Tian, S. F. Martin, C. B. Post, *J. Am. Chem. Soc.* **2010**, *132*, 11058.
[15] T. B. Jensen, E. Terazzi, K. Buchwalder, L. Guénée, H. Nozary, K. Schenk, B. Heinrich, B. Donnio, D. Guillon, C. Piguet, *Inorg. Chem.* **2010**, *49*, 8601.
[16] $\alpha=\kappa_0^{A,B}/3k_bf$ and $\gamma=9k_bTf-4\kappa_0^{A,B}\left\{\ln\left[c^\theta\left(\frac{2k_bT\pi e}{\kappa_0^{A,B}}\right)^{3/2}\right]+\frac{3}{2}\right\}/6f$, respectively, result for the compensation temperature α and for the compensation free energy γ; $f=[2^{1/2}/(1-2^{1/6})r_0]^2$.[13]
[17] a) E. Fisicaro, C. Compari, A. Braibanti, *Phys. Chem. Chem. Phys.* **2004**, *6*, 4156; b) D. H. Williams, E. Stephens, D. P. O'Brien, M. Zhou, *Angew. Chem.* **2004**, *116*, 6760; *Angew. Chem. Int. Ed.* **2004**, *43*, 6596; c) A. Escande, L. Guénée, E. Terazzi, T. B. Jensen, H. Nozary, C. Piguet, *Eur. J. Inorg. Chem.* **2010**, 2746, and references therein.
[18] a) J. D. Dunitz, *Chem. Biol.* **1995**, *2*, 709; b) J. D. Dunitz, *Chem. Commun.* **2003**, 545; c) D. Braga, *Chem. Commun.* **2003**, 2751; d) J. D. Dunitz, A. Gavezzotti, *Chem. Soc. Rev.* **2009**, *38*, 2622.
[19] D. R. Lide, H. V. Kehiaian, *Handbook of Thermophysical and Thermochemical Data*, CRC, Boca Raton, **1994**, pp. 99–108.
[20] a) E. S. Domalski, E. D. Hearing, *J. Phys. Chem. Ref. Data* **1988**, *17*, 1637; b) J. S. Chickos, D. G. Hesse, J. F. Liebman, *J. Org. Chem.* **1990**, *55*, 3833; c) R. Abramowitz, S. H. Yalkowsky, *Pharm. Res.* **1990**, *7*, 942; d) J. S. Chickos, C. M. Braton, J. F. Liebman, *J. Org. Chem.* **1991**, *56*, 927; e) R.-M. Dannenfelser, N. Surendren, S. H. Yalkowsky, *SAR QSAR Environ. Res.* **1993**, *1*, 273; f) R.-M. Dannenfelser, S. H. Yalkowsky, *Ind. Eng. Chem. Res.* **1996**, *35*, 1483; g) R.-M. Dannenfelser, S. H. Yalkowsky, *J. Pharm. Sci.* **1999**, *88*, 722; h) J. L. H. Johnson, S. H. Yalkowsky, *Ind. Eng. Chem. Res.* **2005**, *44*, 7559; i) D. C. Evans, S. H. Yalkowsky, *Fluid Phase Equilib.* **2011**, *303*, 10.
[21] A. A. Levchenko, C. K. Yee, A. N. Parikh, A. Navrotsky, *Chem. Mater.* **2005**, *17*, 5428.
[22] a) H. Nozary, C. Piguet, P. Tissot, G. Bernardinelli, J.-C. G. Bünzli, R. Deschenaux, D. Guillon, *J. Am. Chem. Soc.* **1998**, *120*, 12274; b) E. Terazzi, J.-M. Bénech, J.-P. Rivera, G. Bernardinelli, B. Donnio, D. Guillon, C. Piguet, *Dalton Trans.* **2003**, 769; c) E. Terazzi, S. Torelli, G. Bernardinelli, J.-P. Rivera, J.-M. Bénech, C. Bourgogne, B. Donnio, D. Guillon, D. Imbert, J.-C. G. Bünzli, A. Pinto, D. Jeannerat, C. Piguet, *J. Am. Chem. Soc.* **2005**, *127*, 888.
[23] Trouton's rule states that the entropy of vaporization for any liquid is almost the same value, about 85–88 $J\,K^{-1}\,mol^{-1}$. Consequently, the vaporization temperature entirely depends on the vaporization enthalpy. F. T. Trouton, *Philos. Mag.* **1884**, *18*, 54.
[24] a) M. Dunkel, *Z. Phys. Chem. Abt. A* **1928**, *138*, 42; b) J. H. Hildebrand, R. L. Scott, *The Solubility of Nonelectrolytes*, 3rd ed., Reinhold, New York, **1950**; c) R. F. Fedors, *Polym. Eng. Sci.* **1974**, *14*, 147; d) A. F. M. Barton, *Handbook of Solubility Parameters and Other Cohesion Parameters*, 2nd ed., CRC, Boca Raton, **1991**, p. 127.
[25] R. Gupta, V. K. Dinesh, A. Kumar, B. Varghese, *Mol. Cryst. Liq. Cryst.* **2002**, *383*, 99.
[26] G. A. Oweimreen, M. A. Morsy, *Thermochim. Acta* **2000**, *346*, 37.
[27] P. A. Wood, S. J. Borwick, D. J. Watkin, W. D. Motherwell, F. H. Allen, *Acta Crystallogr. Sect. B* **2008**, *64*, 393.
[28] N. Miyaura, A. Suzuki, *Chem. Rev.* **1995**, *95*, 2457.
[29] a) S. P. Stanforth, *Tetrahedron* **1998**, *54*, 263; b) B. Tao, D. W. Boykin, *J. Org. Chem.* **2004**, *69*, 4330; c) M. Tobisu, N. Chatani, *Angew. Chem.* **2009**, *121*, 3617; *Angew. Chem. Int. Ed.* **2009**, *48*, 3565.
[30] A. Williamson, *Philos. Mag.* **1850**, *37*, 350.
[31] We would like to stress here that the DSC traces of **C12L$^{0',3}$** and **C12L$^{2',2}$** display exceptionally large supercooling processes compared to the other related compounds, which may explain their reluctance to crystallize.
[32] F. H. Allen, O. Kennard, D. G. Watson, L. Brammer, A. G. Orpen, R. Taylor, *J. Chem. Soc. Perkin Trans. 2* **1987**, S1.
[33] The asymmetric unit contains two lightly different molecules (see Figure S1 in the Supporting Information), of which only one is depicted in Figure 3.
[34] a) G. R. Desiraju, T. Steiner, *The Weak Hydrogen Bond in Chemistry and Biology*, Oxford University Press, Oxford, **1999**; b) L. J. Prins, D. N. Reinhoudt, P. Timmerman, *Angew. Chem.* **2001**, *113*, 2446; *Angew. Chem. Int. Ed.* **2001**, *40*, 2382; c) T. Steiner, *Angew. Chem.* **2002**, *114*, 50; *Angew. Chem. Int. Ed.* **2002**, *41*, 48; d) S. J. Grabowski, *Chem. Rev.* **2011**, *111*, 2597.
[35] C. Tschierske, *Top. Curr. Chem.* **2012**, *318*, 1.
[36] Because the melting processes are first-order transitions with no intimate mixing of solid and liquid phase, we arbitrarily selected the maximum of the peaks in the DSC trace for defining T_m.
[37] a) A.-T. Petit, P.-L. Dulong, *Ann. Chim. Phys.* **1819**, *10*, 395; b) A. Einstein, *Ann. Phys.* **1907**, *22*, 180; c) P. Debye, *Ann. Phys.* **1912**, *344*, 789.
[38] a) A. S. Teja, *J. Chem. Eng. Data* **1983**, *28*, 83; b) A. Bondi, *Ind. Eng. Chem. Fundam.* **1966**, *5*, 442.
[39] E. Galbiati, G. Zerbi, *J. Chem. Phys.* **1987**, *87*, 3653.
[40] K. Hori, H. Wu, *Liq. Cryst.* **1999**, *26*, 37.
[41] The molecular volumes are taken as the Connolly volumes, which are obtained from the building of the Connolly surface around the molecular structures of complexes observed in their crystal structure (when available) or their gas-phase structure (semi-empirical PM3 method: J. J. P. Stewart, *J. Comput. Chem.* **1989**, *10*, 209; J. J. P. Stewart, *J. Comput. Chem.* **1989**, *10*, 221) and by using a probe radius of 1.4 Å for modelling water solvent molecule (M. L. Connolly, *Science* **1983**, *221*, 709; M. L. Connolly, *J. Appl. Crystallogr.* **1983**, *16*, 548).
[42] Z. I. Syunyaev, B. P. Tumanyan, S. I. Kolsnikov, N. I. Zhokhova, *Zhur. Prikl. Khim.* **1984**, *57*, 666.
[43] a) A. R. Katritzky, U. Maran, M. Karelson, V. S. Lobanov, *J. Chem. Inf. Comput. Sci.* **1997**, *37*, 913, and references therein; b) Y. Tsuchiya, H. Hasegawa, T. Iwatsubo, *J. Chem. Phys.* **2001**, *114*, 2484.
[44] G. J. Pernía, J. D. Kilburn, J. W. Essex, R. J. Mortishire-Smith, M. Rowley, *J. Am. Chem. Soc.* **1996**, *118*, 10220.
[45] D. Stones, S. Manky, X. Lu, D. G. Hall, *Chem. Eur. J.* **2004**, *10*, 92.
[46] A. Altomare, M. C. Burla, M. Camalli, G. Cascarano, C. Giacovazzo, A. Guagliardi, G. Moliterni, G. Polidori, R. Spagna, *J. Appl. Crystallogr.* **1999**, *32*, 115.
[47] G. M. Sheldrick, SHELXL97 Program for the Solution and Refinement of Crystal Structures, University of Göttingen, Germany, **1997**.
[48] ORTEP3: L. J. Farrugia, *J. Appl. Crystallogr.* **1997**, *30*, 565.

Received: February 14, 2013
Published online: May 21, 2013

CHEMISTRY
A EUROPEAN JOURNAL

Supporting Information

Enthalpy–Entropy Compensation Combined with Cohesive Free-Energy Densities for Tuning the Melting Temperatures of Cyanobiphenyl Derivatives

Thibault Dutronc,[a] Emmanuel Terazzi,*[a] Laure Guénée,[b] Kerry-Lee Buchwalder,[a] Aurore Spoerri,[a] Daniel Emery,[c] Jiri Mareda,[c] Sébastien Floquet,[d] and Claude Piguet*[a]

chem_201300587_sm_miscellaneous_information.pdf

Appendix 1: Geometrical shape analysis of the molecular structures of methyl-substituted 4'-dodecyloxy-4-cyanobiphenyls (C12L$^{i',j}$).

Each **C12L$^{i',j}$** compound can be roughly considered as a cyclinder (Fig. A1-1), whose total length L_{cyl} is given by the *d*N1···C25 distance (Table A1-1, column 3) and its approximate diameter d_{cyl} (Table A1-1, column 4) can be deduced from the molecular volume V_{mol} (Table A1-1, column 1) by using eqn (S1).

$$d_{cyl} = 2r_{cyl} = 2\sqrt{\left(V_{mol}/\pi L\right)} \qquad \text{(S1)}$$

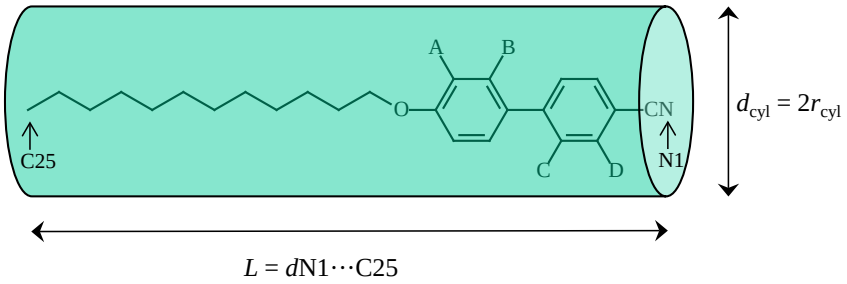

Figure A1-1 Representation of the circum cylinder for the cyanobiphenyls **C12L$^{i',j}$** .

Table A1-1 Molecular volumes (V_{mol}) and associated length (L_{cyl}), diameter (d_{cyl}), and anisometry (γ) for the rod-like **C12L$^{i',j}$** molecules considered as pseudo-cylinders.

Compound	V_m /Å^3 [a]	L_{cyl} /Å	d_{cyl} /Å	$\gamma = L_{cyl}/d_{cyl}$
No methyl				
C12L$^{0',0}$	506.71	25.41	5.04	5.04
Mono-methyl				
C12L$^{3',0}$	526.25	25.83	5.10	5.07
C12L$^{2',0}$	532.52	25.76	5.14	5.02
C12L$^{0',2}$	526.23	25.60	5.12	5.00
Average mono-methyl	528.3(3.6)	25.7(1)	5.12(1)	5.03(4)
Dimethyl				
C12L$^{3',2}$	550.56	25.84	5.20	4.96
C12L$^{2',3}$	546.40	25.34	5.24	4.84
C12L$^{3',3}$	546.53	25.59	5.22	4.91
Average di-methyl	547.8(2.4)	25.6(3)	5.22(1)	4.90(6)

[a] The molecular volumes are taken as the Connolly volumes, which are obtained from the building of the Connolly surface around the molecular structures of compounds observed in their crystal structure and by using a probe radius of 1.4 Å for modelling water solvent molecules (M. L. Connolly, *Science* **1983**, *221*, 709. M. L. Connolly, *J. Appl. Cryst.* **1983**, *16*, 548).

A more precise geometrical analysis decomposes the rodlike molecules into two co-axial cylinders of different diameters (Figure A1-2), from which specific parameters for the aliphatic tails (molecular volume V_{mol}^{tail}, length L_{cyl}^{tail} = *d*C14···C25, and molecular area $A_{cyl}^{tail} = V_m^{tail} / L_{cyl}^{tail}$) and for the aromatic biaryl cores (molecular volume V_{mol}^{core}, length L_{cyl}^{core} = *d*N1···O1, and molecular area $A_{cyl}^{core} = V_m^{core} / L_{cyl}^{core}$) are easily computed (Table A1-2).

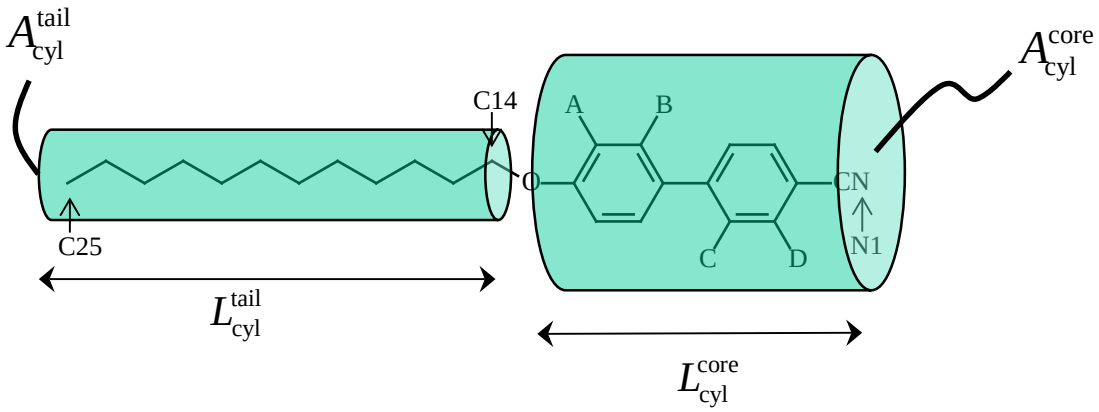

Figure A1-2 Representation of the combination of two circum cylinders confining the cyanobiphenyls **C12L$^{i',j}$** .

Table A1-2 Molecular volumes (V_{mol}) and associated length (L_{cyl}), molecular area (A_{cyl}), and ratios (δ) for the rod-like molecules **C12L$^{i',j}$** considered as made of two co-axial pseudo-cylinders.

Compound	V_{mol}^{tail} /Å^{3} [a]	L_{mol}^{tail} /Å	A_{mol}^{tail} /Å^{2}	V_{mol}^{core} /Å^{3} [a]	L_{mol}^{core} /Å	A_{mol}^{core} /Å^{2}	$\delta = A_{mol}^{tail} / A_{mol}^{core}$
No methyl							
C12L$^{0',0}$	354.33	13.91	25.47	303.98	11.00	27.64	0.92
Mono-methyl							
C12L$^{3',0}$	355.74	14.00	25.40	330.13	11.04	29.90	0.85
C12L$^{2',0}$	355.52	13.98	25.42	328.67	11.03	29.79	0.85
C12L$^{0',2}$	355.36	13.97	25.43	328.63	11.02	29.82	0.85
Average mono-methyl	355.5(2)	13.99(2)	25.42(2)	329.1(9)	11.03(1)	29.84(6)	0.85(0)
Dimethyl							
C12L$^{3',2}$	355.08	14.01	25.35	354.00	11.01	32.15	0.79
C12L$^{2',3}$	354.72	13.98	25.38	354.20	11.01	32.16	0.79
C12L$^{3',3}$	355.24	13.96	25.45	355.67	11.03	32.25	0.79
Average di-methyl	355.0(3)	13.98(3)	25.40(5)	354.6(9)	11.02(1)	32.19(6)	0.79(0)

[a] The molecular volumes are taken as the Connolly volumes, which are obtained from the building of the Connolly surface around the molecular structures of compounds observed in their crystal structures and by using a probe radius of 1.4 Å for modelling water solvent molecules (M. L. Connolly, *Science* **1983**, *221*, 709. M. L. Connolly, *J. Appl. Cryst.* **1983**, *16*, 548).

Appendix 2: Intermolecular interactions operating in the crystal structures C12L$^{0',0}$, C12L$^{3',0}$, C12L$^{2',0}$, C12L$^{0',2}$, C12L$^{3',2}$, C12L$^{2',3}$ and C12L$^{3',3}$.

Criteria for C-H···N hydrogen bonds:[34]

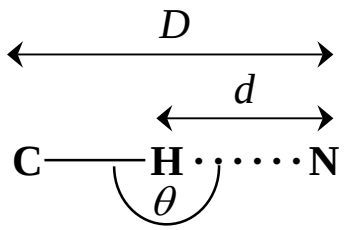

Bond distance d(H···N) < 3.0 Å and bond angle θ(C-H···N) > 120°.

Criteria for antiparallel C-N···C-N interactions:[27]

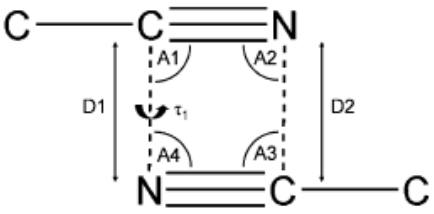

D1 d 3.6Å

C12L$^{0',0}$

C-H···N hydrogen bonds

Donor	**Acceptor**	***D* /Å**	***d* /Å**	***θ* /°**
C5-H3	N1^{i}	3.472	2.708	139.80
C5-H3^{ii}	N1	3.472	2.708	139.80
C3-H2	N1^{ii}	3.451	2.783	128.89
C3-H2^{i}	N1	3.451	2.783	128.89
Total :	4/mol	3.46(1)	2.75(4)	134(6)

^{i} for (–*x*, 1-*y*, 1-*z*) and ^{ii} (–*x*, -*y*, 1-*z*)

Antiparallel C-N···C-N interactions

Symmetry Op.	***D1* /Å**	***A1* /°**	***A2* /°**	***τ* /°**
(–*x*, -*y*, 1-*z*)	3.703	91.46	88.54	0
(–*x*, 1-*y*, 1-*z*)	3.504	93.71	86.29	0
(–*x*, *y*, 1.5-*z*)	3.433	107.98	72.01	0
(–*x*, *y*, 0.5-*z*)	3.497	102.13	77.86	0
Total : **4/mol**	3.5(1)	99(8)	81(8)	0(0)

C12L$^{3',0}$

C-H···N hydrogen bonds

Donor	**Acceptor**	***D* /Å**	***d* /Å**	***θ* /°**
C14-H14b	N1^{i}	3.814	2.822	171.9
C14-H14b^{i}	N1	3.814	2.822	171.9
C13-H13	N1^{ii}	3.560	2.647	158.0
C13-H13^{ii}	N1	3.560	2.647	158.0
Total :	4/mol	3.7(1)	2.7(1)	165(8)

^{i} for (2–*x*, -*y*, 1-*z*) and ^{ii} (2–*x*, -1-*y*, 1-*z*)

Antiparallel C-N···C-N interactions

Symmetry Op.	***D1* /Å**	***A1* /°**	***A2* /°**	***τ* /°**
(3–*x*, -*y*, 1-*z*)	5.386	120.56	59.44	0
Total : **0/mol**				

C12L$^{2',0}$

C-H···N hydrogen bonds (molecule a)

Donor	**Acceptor**	***D* /Å**	***d* /Å**	***θ* /°**
C26a-H26c^{ii}	N1a	3.434	2.606	142.4
C26a-H26c	N1a^{i}	3.434	2.606	142.4
C24a-H24b	N1b^{iii}	3.698	2.967	131.5
C24a-H24b^{iv}	N1b	3.698	2.967	131.5
C10a-H10^{i}	N1a	3.453	2.805	126.4
C10a-H10	N1a^{i}	3.453	2.805	126.4
C9a-H9a	N1a^{i}	3.521	2.925	121.9
C9a-H9a^{i}	N1a^{i}	3.521	2.925	121.9
C3a-H3a	N1b^{i}	3.467	2.818	126.4
C3a-H3a^{i}	N1b	3.467	2.818	126.4
Total :	10/mol	3.5(1)	2.8(1)	130(7)

^{i} for (–*x*, 2-*y*, -*z*) ; ^{ii} (-1 –*x*, 2-*y*, -*z*); ^{iii} (*x*, -1+*y*, 1+*z*), ^{iv} (x, 1+y, -1+z)

C-H···N hydrogen bonds (molecule b)

Donor	**Acceptor**	***D* /Å**	***d* /Å**	***θ* /°**
C7b-H7b[i]	N1a	3.511	2.670	147.7
C7b-H7b	N1a[i]	3.511	2.670	147.7
C9b-H9b[ii]	N1b	3.551	2.903	126.5
C10b-H10b[ii]	N1b	3.541	2.905	125.3
C26b-H26f[iii]	N1b	3.575	2.963	121.6
C26b-H26f	N1b[iii]	3.575	2.963	121.6
Total :	6/mol	3.54(2)	2.8(1)	132(13)

[i] for (–*x*, 2-*y*, -*z*) ; [ii] (–*x*, 1-*y*, -*z*); [iii] (1-*x*, 1-*y*, -*z*) ;

Antiparallel C-N···C-N interactions

Symmetry Op.	***D1* /Å**	***A1* /°**	***A2* /°**	***τ* /°**
N1b-C1a[i]	3.718	90.60	85.20	40.4
Total : **0/mol**				

[i](–*x*, 2-*y*, -*z*)

C12L$^{0',2}$

C-H···N hydrogen bonds

Donor	**Acceptor**	***D* /Å**	***d* /Å**	***θ* /°**
C7-H7	N1[i]	3.537	2.679	150.5
C7-H7[i]	N1	3.537	2.679	150.5
C9-H9	N1[ii]	3.612	2.676	168.93
C9-H9[ii]	N1	3.612	2.676	168.93
C44-H44	N1[ii]	3.926	2.997	158.58
C44-H44[ii]	N1	3.926	2.997	158.58
C13-H13	N1[iIi]	3.608	2.930	129.34
C13-H13[iIi]	N1	3.608	2.930	129.34
Total :	8/mol	3.7(2)	2.8(2)	152(16)

[i] for (3-*x*, 1-*y*, -*z*); [ii] (2–*x*, 1-*y*, -*z*); [iii] (2-*x*, 2-*y*, -*z*)

Antiparallel C-N···C-N interactions

Symmetry Op.	***D1* /Å**	***A1* /°**	***A2* /°**	***τ* /°**
(3–*x*, 1-*y*, -*z*)	3.563	83.94	96.06	0
Total : **1/mol**				

C12L$^{3',2}$

C-H···N hydrogen bonds

Donor	**Acceptor**	***D* /Å**	***d* /Å**	***θ* /°**
C7-H7ii	N1	3.509	2.602	159.9
C7-H7	N1^{ii}	3.509	2.602	159.9
C13-H13	N1^{i}	3.790	2.934	150.7
C13-H13^{i}	N1	3.790	2.934	150.7
C26-H26a	N1^{i}	3.715	2.803	155.08
C26-H26a^{i}	N1	3.715	2.803	155.08
C27-H27c^{ii}	N1	3.760	2.892	148.08
C27-H27c	N1^{ii}	3.760	2.892	148.08
C25-H25b^{iii}	N1	3.738	2.866	148.65
Total :	9/mol	3.7(1)	2.8(1)	153(5)

^{i} for (-2 –*x*, 1-*y*, -*z*) ; ^{ii} (-2–*x*, 2-*y*, -*z*) ; ^{iii} (-3+*x*, *y*, -1+*z*)

Antiparallel C-N···C-N interactions

Symmetry Op.	***D1* /Å**	***A1* /°**	***A2* /°**	***τ* /°**
(-2–*x*, 2-*y*, -*z*)	4.600	101.45	78.55	0
Total : **0/mol**				

C12L$^{2',3}$

C-H···N hydrogen bonds

Donor	**Acceptor**	***D* /Å**	***d* /Å**	***θ* /°**
C6-H6b	N1^{i}	3.704	2.983	133.7
C6-H6b^{vii}	N1	3.704	2.983	133.7
C27-H27c	N1^{i}	3.629	2.851	136.8
C27-H27c^{vii}	N1	3.629	2.851	136.8
C3-H3	N1^{ii}	3.511	2.851	127.2
C3-H3^{v}	N1	3.511	2.851	127.2
C12-H12	N1^{iii}	3.731	2.809	164.2
C12-H12^{vi}	N1	3.731	2.809	164.2
C26-H26a	N1^{iv}	3.801	2.969	143.3
C26-H26a^{iv}	N1	3.801	2.969	143.3
Total :	10/mol	3.7(1)	2.89(7)	141(13)

^{i} for (-1+*x*, *y*, *z*); ^{ii} (4–*x*, -*y*, 1-*z*); ^{iii} (-1+*x*, 1+*y*, *z*); ^{iv} (3–*x*, -*y*, 1-*z*); ^{v} (4–*x*, -*y*, 1-*z*); ^{vi} (1+*x*, -1+*y*, *z*); ^{vii} (1+*x*, *y*, *z*);

Antiparallel C-N···C-N interactions

Symmetry Op.	***D1* /Å**	***A1* /°**	***A2* /°**	***τ* /°**
(4–*x*, -*y*, 1-*z*)	3.441	87.11	92.89	0
Total : **1/mol**				

C12L$^{3',3}$

C-H···N hydrogen bonds

Donor	**Acceptor**	***D* /Å**	***d* /Å**	***θ* /°**
C6-H6	N1^{i}	3.598	2.851	136.3
C6-H6^{iii}	N1	3.598	2.851	136.3
C27-H27c	N1^{ii}	3.700	2.972	131.9
C27-H27c^{ii}	N1	3.700	2.972	131.9
Total :	4/mol	3.65(6)	2.91(7)	134(3)

^{i} for (1+*x*, *y*, *z*); ^{ii} (-1–*x*, 2-*y*, 2-*z*); ^{iii} (-1+*x*, *y*, *z*)

Antiparallel C-N···C-N interactions

Symmetry Op.	***D1* /Å**	***A1* /°**	***A2* /°**	***τ* /°**
(-1–*x*,2-*y*, 2-*z*)	4.526	66.34	113.66	0
Total : **0/mol**				

Appendix 3: Analysis of the layered organizations of methyl-substituted 4'-dodecyloxy-4-cyanobiphenyls (C12L$^{i',j}$).

Layered organizations were systematically found for the crystallized compounds **C12L$^{i',j}$** even though the interfaces between layers were disturbed by the presence of methyl groups. In order to monitor these perturbations, atomic planes composed of similar nitrogen atoms (*i.e.* oriented in the same direction) were considered to describe the interface (Figure A2-1). A positive value of the interface separation d_i reflected an absolute segregation of the different layers, whilst a negative value indicated an effective interpenetration of the layers. The tilt angles of the cyanobiphenyl (α_{NO}) and of alkoxy groups (α_{OC}) were computed between the interface planes' normal lines and the N1-O1 axis and the O1-C25 axis, respectively. (see Figure A3-1 for a global description, Figures A3-2 to A3-8 for each specific case and Table A3-1 for numerical data).

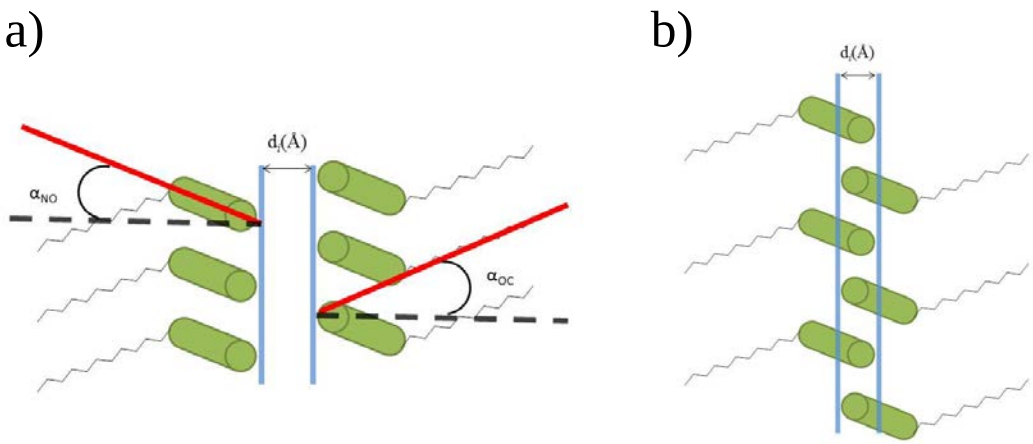

Figure A33-1 Schematic description of the interface planes in alkoxycyanobiphenyls showing interplanar distances (d_i) and tilt angles (α_{NO} and α_{CO}). a) A positive value ($d_i > 0$) indicates a segregation of the layers and b) a negative value ($d_i < 0$) holds for an interpenetration of the layers.

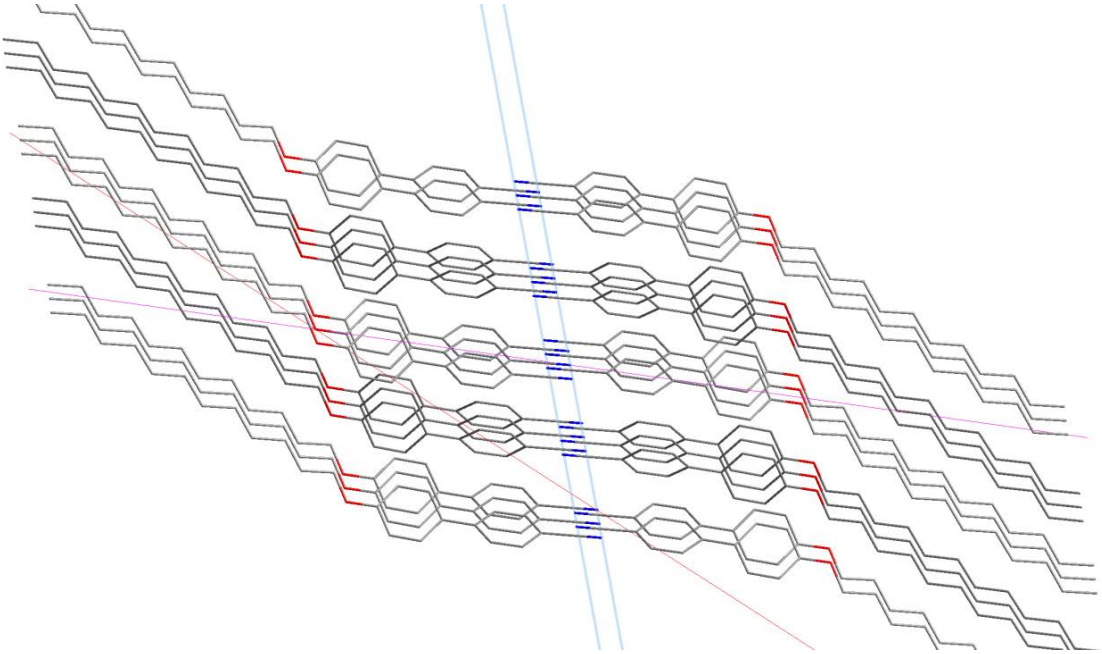

Figure A3-2 Layered organization in **C12L$^{0',0}$.** The planar interfaces are shown with blue lines and the N1-O1 and O1-C25 axis with red lines.

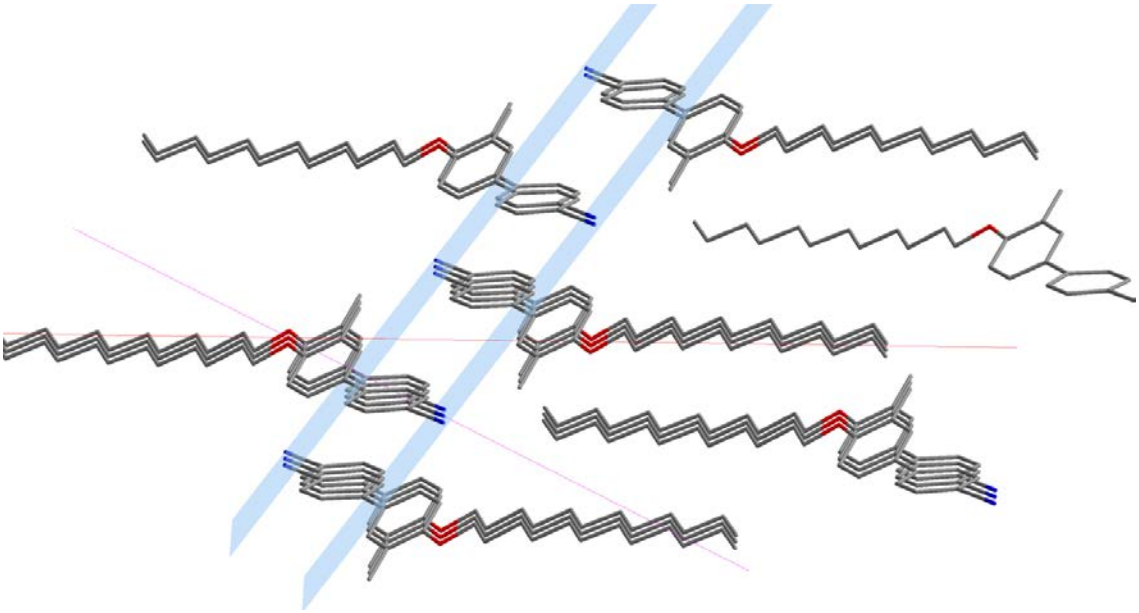

Figure A3-3 Layered organization in **C12L$^{3',0}$.** The planar interfaces are shown with blue lines and the N1-O1 and O1-C25 axis with red lines.

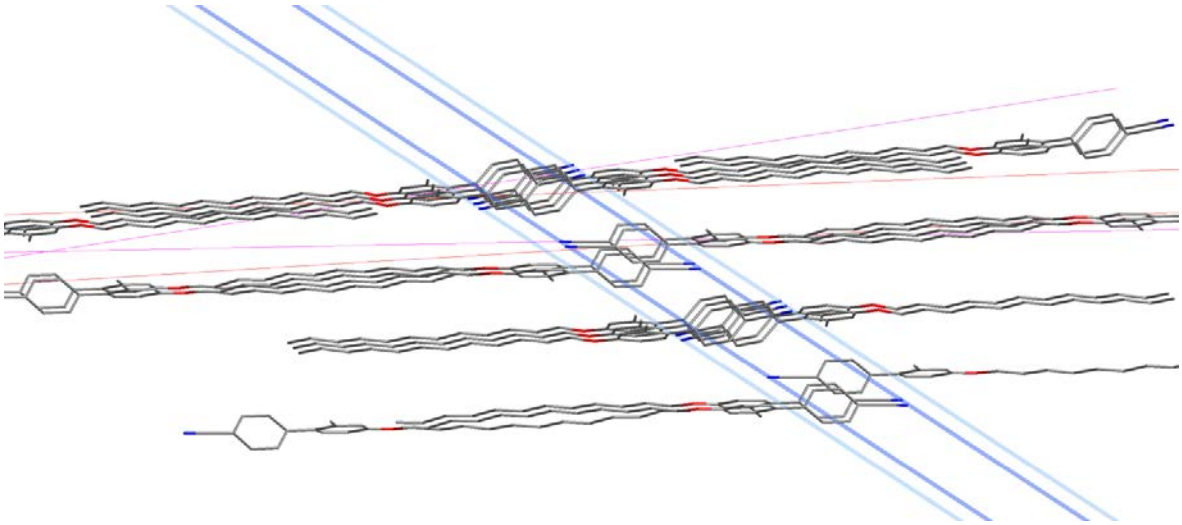

Figure A3-4 Layered organization in **C12L$^{2',0}$**. The planar interfaces are shown with blue lines and the N1-O1 and O1-C25 axis with red lines.

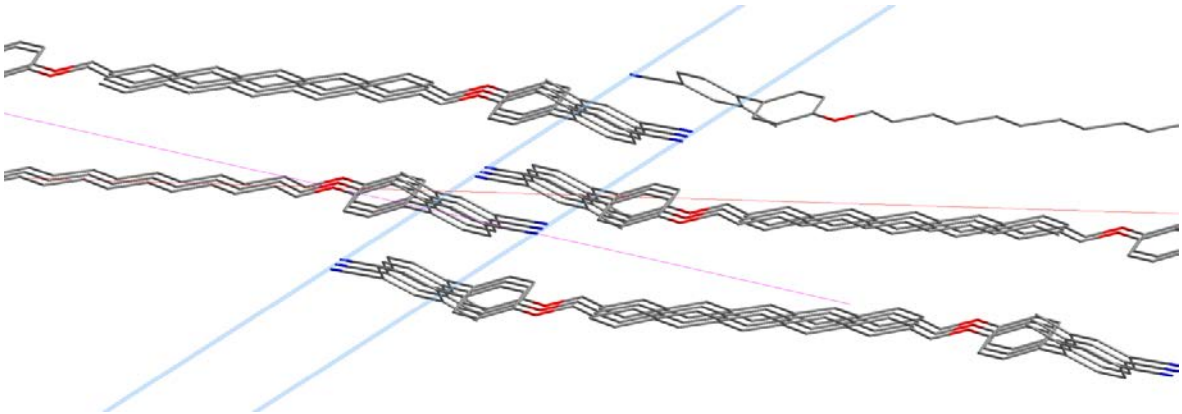

Figure A3-5 Layered organization in **C12L$^{0',2}$**. The planar interfaces are shown with blue lines and the N1-O1 and O1-C25 axis with red lines.

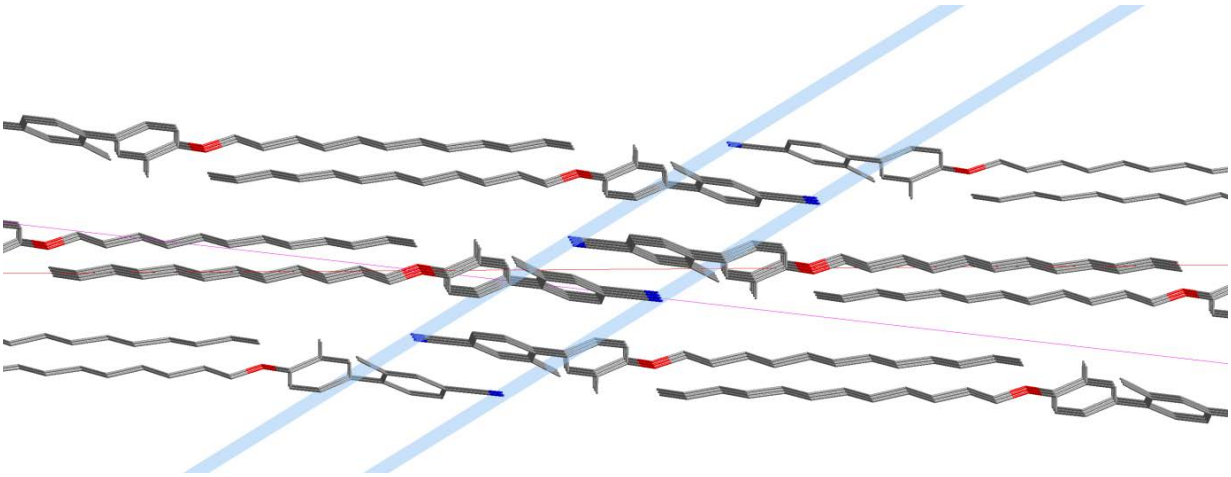

Figure A3-6 Layered organization of **C12L$^{3',2}$.** . The planar interfaces are shown with blue lines and the N1-O1 and O1-C25 axis with red lines.

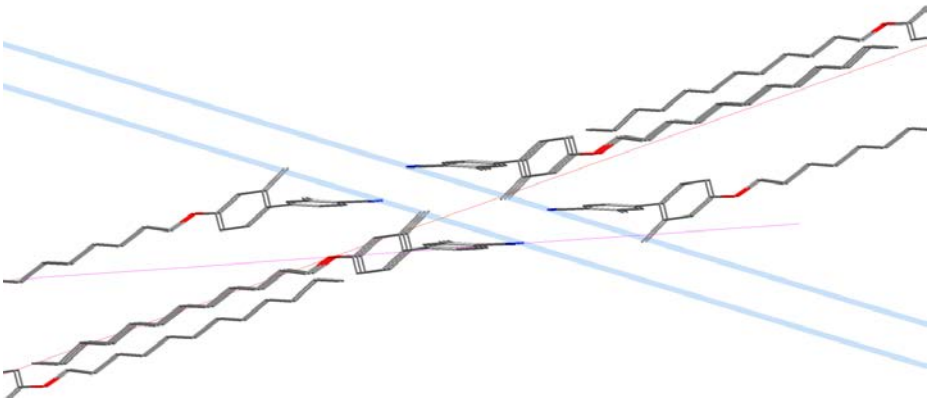

Figure A3-7 Layered organization in **C12L$^{2',3}$**. The planar interfaces are shown with blue lines and the N1-O1 and O1-C25 axis with red lines.

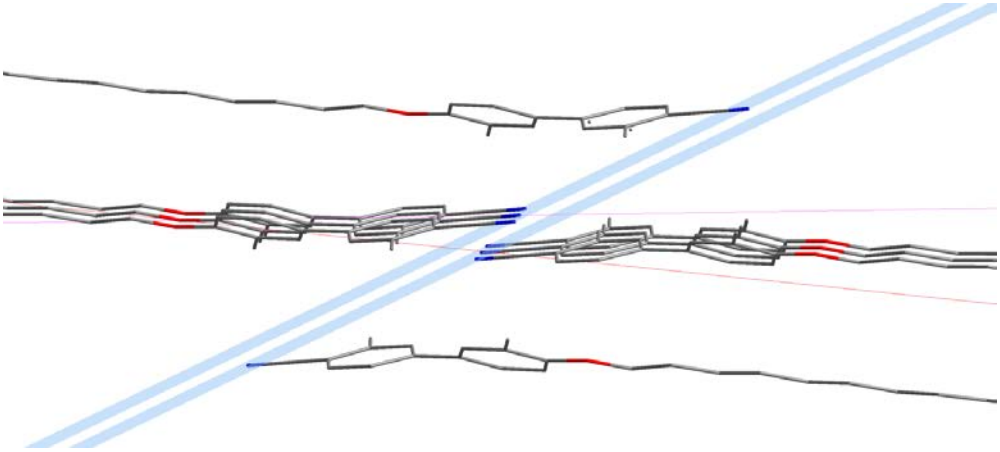

Figure A3-8 Layered organization in **C12L$^{3',3}$**. The planar interfaces are shown with blue lines and the N1-O1 and O1-C25 axis with red lines.

Table A3-1 Segregation of the cyanobiphenyls (d_i /Å) and tilt angles (α_{NO} and α_{OC}) in methyl-substituted 4'-dodecyloxy-4-cyanobiphenyls (**C12L$^{i',j}$**).

Compounds		d_i /Å[a]	α_{NO} /° [a]	α_{OC} /° [a]
C12L$^{0',0}$		-0.955	18.50	43.18
C12L$^{3',0}$		-3.100	59.20	58.77
C12L$^{2',0}$	(a)[b]	-2.689	57.53	52.30
C12L$^{2',0}$	(b)[b]	-4.302	53.48	54.90
C12L$^{0',2}$		-2.998	60.25	58.62
C12L$^{3',2}$		-3.756	57.59	59.76
C12L$^{2',3}$		1.882	73.26	54.44
C12L$^{3',3}$		0.543	68.89	58.80

[a] see Figure A3-1. [b] Two different molecules are present within the asymmetric unit.

Appendix 4: Analysis of microsegregation according to Hildebrand parameters in 4'-dodecyloxy-4-cyanobiphenyls (C12L$^{i',j}$).

Microsegregation can be thought as the demixion of the polar and apolar parts of an amphilphilic molecule at the molecular level. A criteria for estimating the trend of microsegregation can be thus approached byy considering the macroscopic mixing properties of binary mixtures of liquids.[A4-1] Following Trouton's rule,[23] the mixing free energy $\Delta G_{mix} = \Delta H_{mix} - T \cdot \Delta S_{mix}$ characterizing two different liquids mainly depends on the enthalpic contribution, which is correlated to the difference between the *Hildebrand*'s cohesive energy density $ced = \left(\Delta H_{\mathrm{v}} - RT\right)/V_{\mathrm{m}}$ (eqn S2),[35] the square root of it being often referred to as the *Hildebrand* solubility parameter δ_{T} tabulated in thermodynamic tables (eqn S3).[A4-1] A large difference $\Delta\delta_{\mathrm{T}}$ = $|\delta_{\mathrm{T}}$(rigid part)- δ_{T}(flexible part)| corresponds to a binary system with minor, if any, miscibility (Table A4-1).

$$\Delta H_{mix} \propto (ced_{\mathrm{A}} - ced_{\mathrm{B}}) \quad \text{(S2)}$$

$$\delta_{\mathrm{T}} = (ced)^{1/2} \quad \text{(S3)}$$

Table A4-1 Binary Mixture of Solvents with associated Hildebrand Parameter δ_{T} at 298 K.[A4-1]

Solvent A	δ_{T} /MPa$^{1/2}$	Solvent B	δ_{T} /MPa$^{1/2}$	$\Delta\delta_{\mathrm{T}}$ /MPa$^{1/2}$	Miscibility
Water	47.9	Cyclohexane	16.8	31.1	No
Methanol	29.6	Cyclohexane	16.8	12.8	No
Dimethylsulfoxyde	24.5	Cyclohexane	16.8	7.7	No
Acetonitrile	24.7	Cyclohexane	16.8	7.9	No
Acetone	20.2	Cyclohexane	16.8	3.4	Yes
Benzene	18.8	Cyclohexane	16.8	2	Yes

Focussing now on the amphiphilic molecules, the **C12L$^{i',j}$** compounds can be are considered are made of a rigid methyl-substituted cyanobiphenyl core attached to a dodecyloxy chain, each part being charaterized by a specific *Hildebrand* parameter obtained by the incremental method introduced by Dunkel[A4-2] (eqn S4) and popularized by Fedors ($^{z}\Delta U$ and ^{z}V are the internal energies of vaporization and molar volumes, respectively, for each incremental part in the molecule, Table A4-2).[A4-3]

$$\delta_T = \left(\frac{-\Delta U}{V_m}\right)^{1/2} = \left(\frac{\sum_Z \Delta^Z U}{\sum_Z {}^Z V}\right)^{1/2} \quad \text{(S4)}$$

Table A4-2 Hildebrand Parameters δ_T Computed with Eqn (S4) for the Substituted Cyanobiphenyl Rigid Cores in **C12L$^{i',j}$** at 298 K.[A4-3]

Z group	${}^Z\Delta H$ / kJ·mol^{-1}	${}^Z\Delta U$ / kJ·mol^{-1}	${}^Z V$/ cm^3·mol^{-1}	δ_T MPa$^{1/2}$
-CH_3	7.45	4.71	33.5	
Phenyl (disubstituted)	-	31.9	52.4	
Phenyl (trisubstituted)		31.9	33.4	
-O-	6.82	3.35	3.8	
-CN	-	25.5	24.0	
Non methylated **C12L^{0,0}**		92.65	132.6	26.43
Mono-methylated **C12L$^{2',0}$**, **C12L$^{3',0}$**, **C12L^{0,2}**,**C12L^{0,3}**		97.36	147.1	25.73
di-methylated **C12L$^{2',2}$**, **C12L$^{3',2}$**, **C12L$^{2',2}$**,**C12L$^{3',3}$**		102.07	161.6	25.13

Compared to the fixed value of δ_T(dodecane) = 16.1 Mpa$^{1/2}$ characterizing the flexible tails in **C12L$^{i',j}$**, we conclude that $\Delta\delta_T$ stepwise decreases upon successive methylation of the rigid core in agreement with a reduced trend to microsegregation and the loss of liquid crystalline properties for the methylated compounds.

References

[A4-1] (a) J. H. Hildebrand, R. L. Scott, *The Solubility of Nonelectrolytes*, 3rd Ed., Reinhold Pub Group, New York, 1950. (b) A. F. M. Barton, *Handook of Solubility Parameters and Other Cohesion Parameters 2nd edition* 1991, 76.

[A4-2] M. Dunkel, *Z. Phys. Chem.* **1928**, *A138*, 42.

[A4-3] R. F. Fedors, *Polym. Eng. Sci.* **1974**, *51*, 891.

Appendix 5: Derivation of eqns (11)-(12). The Born-Haber cycles adapted to enthalpy changes (Figure 6) gives the left part of eqn (11), whereas its straightforward extension to the entropy change provides the left part of eqn (12).

$$\Delta H_{\mathrm{m}}^{0} = \Delta H_{\mathrm{m}} + \int_{T^0}^{T_{\mathrm{m}}} C_{\mathrm{p}}^{\mathrm{solid}} dT - \int_{T^0}^{T_{\mathrm{m}}} C_{\mathrm{p}}^{\mathrm{liquid}} dT \qquad \text{(11-left)}$$

$$\Delta S_{\mathrm{m}}^{0} = \Delta S_{\mathrm{m}} + \int_{T^0}^{T_{\mathrm{m}}} \frac{C_{\mathrm{p}}^{\mathrm{solid}}}{T} dT - \int_{T^0}^{T_{\mathrm{m}}} \frac{C_{\mathrm{p}}^{\mathrm{liquid}}}{T} dT \qquad \text{(12-left)}$$

The global enthalpy change between the reference temperature T^0 and the end temperature T_2 can be partitioned according to eqn S5 (Figure 5). Straightforward algebraic transformations leads to eqn (S6).

$$\int_{T^0}^{T_2} C_{\mathrm{p}} dT = \Delta H_{\mathrm{m}} + \int_{T^0}^{T_{\mathrm{m}}} C_{\mathrm{p}}^{\mathrm{solid}} dT + \int_{T_{\mathrm{m}}}^{T_2} C_{\mathrm{p}}^{\mathrm{liquid}} dT \qquad \text{(S5)}$$

$$\int_{T^0}^{T_{\mathrm{m}}} C_{\mathrm{p}}^{\mathrm{solid}} dT = \int_{T^0}^{T_2} C_{\mathrm{p}} dT - \Delta H_{\mathrm{m}} - \int_{T_{\mathrm{m}}}^{T_2} C_{\mathrm{p}}^{\mathrm{liquid}} dT \qquad \text{(S6)}$$

Introduction of eqn (S6) into eqn (11) followed by reorganization leads to the right part of eqn (11), which is well adapted for experimentally calculating $\Delta H_{\mathrm{m}}^{0}$ (Scheme A5-1).

$$\Delta H_{\mathrm{m}}^{0} = \int_{T_0}^{T_2} C_{\mathrm{p}} dT - \int_{T_0}^{T_2} C_{\mathrm{p}}^{\mathrm{liquid}} dT \qquad \text{(11-right)}$$

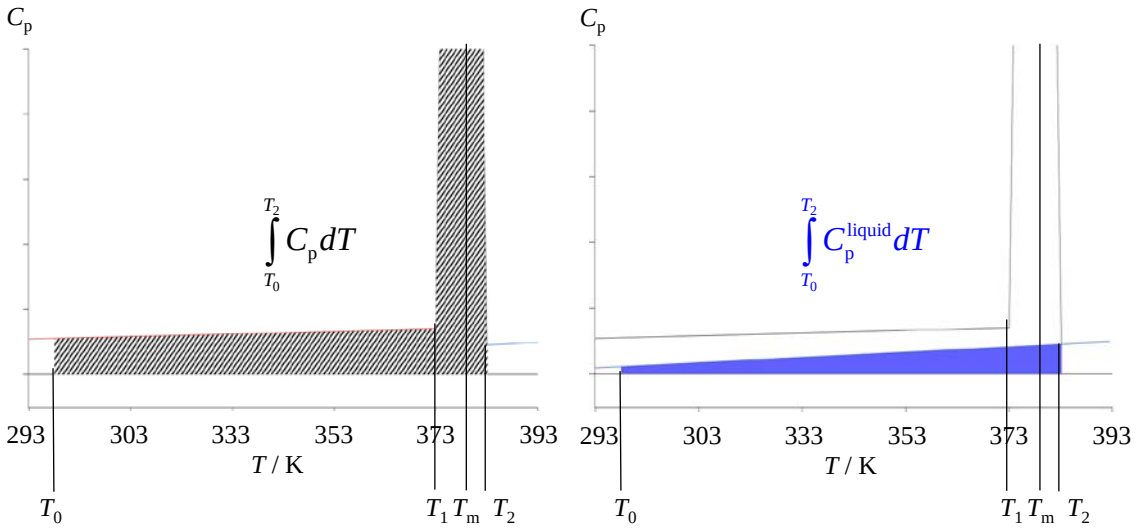

Scheme A5-1 Experimental determination of the standard melting enthalpy from the molar heat capacity (C_p) trace by using eqn (11).

The same method applied to entropies gives

$$\int_{T_0}^{T_2} \frac{C_\mathrm{p}}{T} dT = \Delta S_\mathrm{m} + \int_{T_0}^{T_\mathrm{m}} \frac{C_\mathrm{p}^\mathrm{solid}}{T} dT + \int_{T_\mathrm{m}}^{T_2} \frac{C_\mathrm{p}^\mathrm{liquid}}{T} dT \tag{S7}$$

$$\int_{T_0}^{T_\mathrm{m}} \frac{C_\mathrm{p}^\mathrm{solid}}{T} dT = \int_{T_0}^{T_2} \frac{C_\mathrm{p}}{T} dT - \Delta S_\mathrm{m} - \int_{T_\mathrm{m}}^{T_2} \frac{C_\mathrm{p}^\mathrm{liquid}}{T} dT \tag{S8}$$

Introduction of eqn (S8) into eqn (12) followed by reorganization leads to the right part of eqn (12),

$$\Delta S_\mathrm{m}^0 = \int_{T_0}^{T_2} \frac{C_\mathrm{p}}{T} dT - \int_{T_0}^{T_2} \frac{C_\mathrm{p}^\mathrm{liquid}}{T} dT \tag{12-right}$$

Appendix 6: Preparations of compounds $2^{2'}$, $2^{3'}$, 4^{3}, $5^{0',0}$, $5^{3',0}$, $5^{3',2}$, $5^{0',3}$, $5^{2',3}$, $5^{3',3}$, 6, 7, $C12L^{0',0}$, $C12L^{3',0}$, $C12L^{2',0}$, $C12L^{0',3}$, $C12L^{2',2}$, $C12L^{3',2}$, $C12L^{2',3}$, $C12L^{3',3}$ and $C_{12}L^{0',2}$.

Preparation of 4-bromo-3-methylphenol ($2^{2'}$). Bromine (16.11 g, 0.1008 mol) in CH_2Cl_2 (200 mL) was added dropwise to a solution of *m*-cresol (13.02g, 0.1204 mol) in CH_2Cl_2 (200 mL) at 0°C. The solution was allowed to warm up to room temperature overnight. The reaction mixture was evaporated to dryness. The crude product was dissolved in CH_2Cl_2 (40 mL), washed with brine (2 x 50 mL). The organic phase was dried over $MgSO_4$ and then evaporated to dryness. The solid residue was crystallized from benzene/hexane at -15°C to give 4-bromo-3-methylphenol ($2^{2'}$, 11.6g, 0.061 mol, 62% yield) as white crystals. ^{1}H NMR (400 MHz, $CDCl_3$): δ/ppm = 7.38 (d, ^3J = 8.6 Hz, 1H), 6.76 (s, 1H), 6.58 (d, ^3J = 8.6 Hz, 1H), 4.65 (s, 1H), 2.37 (s, 3H). ^{13}C NMR (101 MHz, $CDCl_3$): δ/ppm = 154.74, 139.15, 133.04, 117.85, 115.39, 114.55, 22.97. ESI-MS (CH_2Cl_2/MeOH 9:1): *m/z*: 184.9 $[M-H]^-$.

Preparation of 4-bromo-2-methylphenol ($2^{3'}$). Bromine (16.11 g, 0.1008 mol) in CH_2Cl_2 (200 mL) was added dropwise to a solution of o-cresol (13.02g, 0.1204 mol) in CH_2Cl_2 (200 mL) at 0°C. The solution was allowed to warm up to room temperature overnight. The reaction mixture was evaporated to dryness. The crude product was dissolved in CH_2Cl_2 (40 mL), washed with brine (2 x 50 mL). The organic phase was dried over $MgSO_4$ and then evaporated to dryness. The residual solid was crystallized from benzene/hexane at -15°C to give 4-bromo-2-methylphenol ($2^{3'}$,13.4 g, 0.072 mol, 72% yield) as white crystals. ^{1}H NMR (400 MHz, $CDCl_3$): δ/ppm = 7.27 (s, 1H), 7.20 (d, ^3J = 8.5 Hz, 1H), 6.67 (d, ^3J = 8.5 Hz, 1H), 4.87 (s, 1H), 2.25 (s, 3H). ^{13}C NMR (101 MHz, $CDCl_3$): δ/ppm = 152.88, 133.54, 129.75, 126.30, 116.57, 112.60, 15.64. ESI-MS (CH_2Cl_2/MeOH 9:1): *m/z*: 185.1 $[M-H]^-$.

Preparation of (4-cyano-2methyl-phenyl)boronic acid (4^{3}). 4-Bromo-2-methylbenzonitrile (2 g, 10 mmol) was dissolved in THF (30 mL) and cooled to -98°C. A solution of *n*-butyllithium 1.6 M in hexane (12 mL, 19.6 mmol, 2 eq) was added dropwise while the temperature was maintained

below -90°C. The solution was stirred for 30 min, trimethyl borate (12 mL, 124 mmol, 12 eq) was then slowly added. The reaction was allowed to warm up to room temperature overnight and evaporated to dryness. The solid residue was triturated with 2 M hydrochloric acid (50 mL) for 30 min and diethyl ether (50 mL) was added. The organic layer was separated and the aqueous phase extracted with diethyl ether (4×25mL). The combined organic layers were dryed over Na_2SO_4, filtered and evaporated to dryness. The crude product was purified by precipitation from a hot water solution to give (4-cyano-2methyl-phenyl)boronic acid (**4^3**, 0.5 g, 3.1 mmol, 31% yield). The product was quickly identified by mass spectrometry and used as is.

ESI-MS (CH_2Cl_2/MeOH 9:1): *m/z*: 159.9 $[M-H]^-$

Preparation of 4'-hydroxy-[1,1'-biphenyl]-4-carbonitrile (**5$^{0',0}$**). A solution of 4-bromophenol (1.06 g, 6.18 mmol), 4-cyanophenylboronic acid (**4^0**, 1 g, 6.8 mmol, 1.1 eq), K_3PO_4 (3.93 g, 18.5 mmol, 2.9 eq) in 2-propanol (40 mL) and H_2O (12 mL) was flushed with N_2 for 30 min. A catalytic amount $Pd(dppf)Cl_2$ (catalytic) was added, and the solution was stirred under dinitrogen for 15h at 70°C. The solution was filtered, CH_2Cl_2 (40 mL) was added, and the phases were separated. The aqueous phase was extracted with CH_2Cl_2 (40 mL), and the combined organic phases were dried over Na_2SO_4, filtered and evaporated to dryness. The crude product was purified by column chromatography (silica; CH_2Cl_2) to give 4'-hydroxy-[1,1'-biphenyl]-4-carbonitrile (**5$^{0',0}$**, 0.62 g, 3.15 mmol, 51% yield) as a white solid. ^{1}H NMR (400 MHz, $CDCl_3$): δ/ppm = 7.72 (d, ^3J = 8.6 Hz, 2H), 7.66 (d, ^3J = 8.6 Hz, 2H), 7.52 (d, ^3J = 8.7 Hz, 2H), 6.97 (d, ^3J = 8.7 Hz, 2H), 5.08 (s, 1H). ^{13}C NMR (101 MHz, $CDCl_3$): δ/ppm = 156.35, 145.26, 134.29, 132.92, 132.61, 131.75, 128.63, 127.96, 127.14, 116.33, 116.06, 110.10.

The same procedure was used for the preparation of:

4'-hydroxy-3'-methyl-[1,1'-biphenyl]-4-carbonitrile (**5$^{3',0}$**, 30% yield). ^{1}H NMR (400 MHz, $CDCl_3$): δ/ppm = 7.71 (d, ^3J = 8.4 Hz, 2H), 7.65 (d, ^3J = 8.4 Hz, 2H), 7.40 (s, 1H), 7.35 (d, ^3J = 8.4 Hz, 1H), 6.90 (d, ^3J = 8.3 Hz, 1H), 5.07 (s, 1H), 2.35 (s, 3H). ^{13}C NMR (101 MHz, $CDCl_3$):

δ/ppm = 154.74, 145.46, 132.91, 132.55, 131.59, 129.93, 127.96, 127.13, 125.99, 124.70, 115.56, 109.93, 15.94. ESI-MS (CH_2Cl_2/MeOH 9:1): *m/z*: 208.1 $[M-H]^-$.

4'-hydroxy-2,3'-dimethyl-[1,1'-biphenyl]-4-carbonitrile (**5$^{3',2}$**, 10% yield). ^{1}H NMR (400 MHz, $CDCl_3$): δ/ppm = ´ 7.56 (s, 1H), 7.52 (d, ^3J = 7.9 Hz, 1H), 7.31 (d, ^3J = 7.9 Hz, 1H), 7.08 (s, 1H), 7.03 (dd, ^3J = 8.1, ^4J = 2.0 Hz, 1H), 6.87 (d, ^3J = 8.1 Hz, 1H), 5.14 (s, 1H), 2.33 (s, 6H). ^{13}C NMR (101 MHz, $CDCl_3$): δ/ppm = 153.69, 146.63, 136.94, 133.78, 132.47, 131.45, 130.58, 129.43, 127.53, 123.94, 119.16, 114.82, 110.40, 20.43, 15.82. ESI-MS (CH_2Cl_2/MeOH 9:1): *m/z*: 222.5 $[M-H]^-$.

Preparation of 4'-hydroxy-3-methyl-[1,1'-biphenyl]-4-carbonitrile (**5$^{0',3}$**). 4-Bromophenol (448 mg, 2.6 mmol), 4-cyano-3-methylphenylboronic acid (**4^3**, 500 mg, 3.11 mmol, 1.2 eq) and Cs_2CO_3 (1.69 g, 5.2 mmol, 2 eq) were added to ethanol (8 mL). The mixture was flushed with N_2 for 30 min. A catalytic amount of trans-$(Cy2NH)_2Pd(OAc)_2$ was added and the mixture was stirred at room temperature for 15 h. The reaction was quenched with ethyl acetate (250 mL). The organic phase was washed with water (4×50mL) and evaporated to dryness. The crude product was purified by column chromatography (silica; CH_2Cl_2) to give 4'-hydroxy-3-methyl-[1,1'-biphenyl]-4-carbonitrile (**5$^{0',3}$**, 337 mg, 1.80 mmol, 69% yield) as a white solid. ^{1}H NMR (400 MHz, $CDCl_3$): δ/ppm = 7.65 (d, ^3J = 8.0 Hz, 1H), 7.50 (d, ^3J = 8.5 Hz, 2H), 7.50 (s, 1H), 7.46 (d, ^3J = 8.0 Hz, 1H), 6.96 (d, ^3J = 8.6 Hz, 2H), 5.20 (s, 1H), 2.62 (s, 3H). ^{13}C NMR (101 MHz, $CDCl_3$): δ/ppm = 156.31, 145.15, 142.33, 134.49, 132.93, 128.58, 128.28, 124.42, 118.39, 117.19, 115.98, 113.70, 110.48, 20.64. ESI-MS (CH_2Cl_2/MeOH 9:1): *m/z*: 208.1 $[M-H]^-$.

The same procedure was used for the preparation of:

4'-hydroxy-2',3-dimethyl-[1,1'-biphenyl]-4-carbonitrile (**5$^{2',3}$**, 19% yield). ^{1}H NMR (400 MHz, $CDCl_3$): δ/ppm = 7.64 (d, ^3J = 7.9 Hz, 1H), 7.27 (s, 1H), 7.23 (d, ^3J = 8.0 Hz, 1H), 7.08 (d, ^3J = 8.2 Hz, 1H), 6.82 (d, ^4J = 2.4 Hz, 1H), 6.79 (dd, ^3J = 8.2, ^4J = 2.5 Hz, 1H), 5.73 (s, 1H), 2.60 (s, 3H), 2.24 (s, 3H). ^{13}C NMR (101 MHz, $CDCl_3$): δ/ppm = 155.77, 146.68, 141.82, 136.78, 132.69,

132.27, 131.32, 130.78, 127.47, 118.41, 117.39, 113.14, 110.37, 20.54, 20.48. ESI-MS (CH_2Cl_2/MeOH 9:1): *m/z*: 222.5 $[M-H]^-$.

4'-hydroxy-3,3'-dimethyl-[1,1'-biphenyl]-4-carbonitrile (**5**$^{3',3}$, 34% yield). ^{1}H NMR (400 MHz, $CDCl_3$): δ/ppm7.64 (d, ^3J = 8.0 Hz, 1H), 7.50 (s, 1H), 7.45 (d, ^3J = 8.1 Hz, 1H), 7.39 (s, 1H), 7.34 (d, ^3J = 8.3 Hz, 1H), 6.91 (d, ^3J = 8.3 Hz, 1H), 5.35 (s, 1H), 2.61 (s, 3H), 2.35 (s, 3H). ^{13}C NMR (101 MHz, $CDCl_3$): δ/ppm = 154.70, 145.38, 142.27, 132.88, 131.73, 129.90, 128.26, 125.97, 124.66, 124.42, 118.49, 115.51, 110.29, 20.65, 15.96. ESI-MS (CH_2Cl_2/MeOH 9:1): *m/z*: 222.5 $[M-H]^-$.

Preparation of 1-bromo-4-(dodecyloxy)benzene (**6**). 4-bromophenol (2 g, 11.5 mmol), bromododecane (2.88 g, 11.5 mmol, 1 eq), K_2CO_3 (12 g, 86.8 mmol, 7.5 eq) and a catalytic amount of KI (catalytic) were dissolved in acetone (400 mL). The mixture was stirred under reflux for three days, then evaporated to dryness. The resulting solid was partitioned between CH_2Cl_2 (100 mL) and H_2O (100 mL), and the phases were separated. The organic phase was washed with H_2O (4×50mL), dried over Na_2SO_4, filtered and evaporated to dryness. The crude product was purified by column chromatography (silica; CH_2Cl_2) to give 1-bromo-4-docelyoxybenzene (**6**, 3.9 g, 8.74 mmol, 76% yield) as a waxy solid. ^{1}H NMR (400 MHz, $CDCl_3$): δ/ppm = 7.37 (d, ^3J = 8.5 Hz, 2H), 6.79 (d, ^3J = 8.7 Hz, 2H), 3.93 (t, ^3J = 6.6 Hz, 2H), 1.82 – 1.73 (m, 2H), 1.49 – 1.41 (m, 2H), 1.40 – 1.25 (m, 16H), 0.90 (t, ^3J = 6.7 Hz, 3H). ^{13}C NMR (101 MHz, $CDCl_3$): δ/ppm = 158.24, 132.15, 116.28, 112.53, 68.26, 29.67, 29.65, 29.60, 29.57, 29.38, 29.36, 29.18, 14.13. ESI-MS (CH_2Cl_2/MeOH 9:1): *m/z*: 358.6 $[M+NH_4]^+$.

Preparation of 4-dodecyloxyphenylboronic acid (**7**). 1-bromo-4-(dodecyloxy)benzene (**6**, 1 g, 2.93 mmol) was dissolved in THF (50 mL) and cooled to -98°C. A solution of n-butyllithium 1.6 M in hexane (10 mL, 16 mmol, 5 eq) was added dropwise while the temperature was maintained below -90°C. The solution was stirred for 30 min, trimethyl borate (5 mL, 45 mmol, 15 eq) was then added slowly. The reaction was allowed to warm up to room temperature overnight and was evaporated to

dryness. The solid residue was treated with 2M hydrochloric acid (50 mL) for 30 min, diethyl ether (50 mL) was added and the phases were separated. The aqueous phase was extracted with diethyl ether (4×25mL) and the combined organic phases were dryed over Na_2SO_4, filtered and evaporated to dryness. The crude product was purified by precipitation from a hot water solution to obtain a pale yellow powder(**7**, 300 mg, 0.88 mmol, 30%yield). The product was quickly identified by mass spectrometry and used as is. ESI-MS (CH_2Cl_2/MeOH 9:1): *m/z*: 305.3 $[M-H]^-$.

Preparation of 4'-(dodecyloxy)-[1,1'-biphenyl]-4-carbonitrile (**C12L$^{0',0}$**). A mixture of 4'-hydroxy-[1,1'-biphenyl]-4-carbonitrile (**5$^{0',0}$**, 500 mg, 2.6 mmol), bromododecane (722 mg, 2.9 mmol, 1.1 eq), K_2CO_3 (3.165 g, 22.9 mmol, 9 eq) and KI (catalytic amount) in acetone (80 mL) was stirred under reflux for three days. The mixture was evaporated to dryness. The resulting solid was partitioned between CH_2Cl_2 (25 mL) and H_2O (25 mL), and the phases were separated. The organic phase was washed with H_2O (4×15mL), dried over Na_2SO_4, filtered and evaporated to dryness. The crude product was purified by column chromatography (silica; CH_2Cl_2) to give 4'-(dodecyloxy)-[1,1'-biphenyl]-4-carbonitrile (**C$_{12}$L$^{0',0}$**, 710 mg, 1.98 mmol, 76% yield) as a white solid. ^{1}H NMR (400 MHz, $CDCl_3$): δ/ppm = 7.70 (d, ^3J = 8.3 Hz, 2H), 7.65 (d, ^3J = 8.4 Hz, 2H), 7.55 (d, ^3J = 8.7 Hz, 2H), 7.02 (d, ^3J = 8.7 Hz, 2H), 4.03 (t, ^3J = 6.5 Hz, 2H), 1.84 (q, ^3J = 6.7 Hz, 2H), 1.55 – 1.44 (m, 2H), 1.42 – 1.25 (m, 16H), 0.91 (t, ^3J = 6.7 Hz, 3H). ^{13}C NMR (101 MHz, $CDCl_3$): δ/ppm = 159.85, 145.29, 132.56, 131.21, 128.31, 127.06, 119.12, 115.10, 110.03, 68.19, 31.95, 29.69, 29.67, 29.63, 29.61, 29.42, 29.38, 29.25, 26.06, 22.72, 14.14. ESI-MS (CH_2Cl_2/MeOH 9:1): *m/z*: 364.4 $[M+H]^+$; 381.6 $[M+H_3O]^+$. Elemental analysis for $C_{25}H_{33}NO{\cdot}0.13H_2O$: calcd (found) C, 82.07 (82.08); H, 9.16 (9.55); N, 3.83 (3.75).

The same procedure was used for the preparation of:

4'-(dodecyloxy)-3'-methyl-[1,1'-biphenyl]-4-carbonitrile (**C12L$^{3',0}$**, 68% yield). ^{1}H NMR (400 MHz, $CDCl_3$) ´ = 7.70 (d, ^3J = 8.6 Hz, 2H), 7.66 (d, ^3J = 8.5 Hz, *2H*), 7.42 (s, 1H), 7.41 (d, *J* = 3.5 Hz, 1H), 6.94 – 6.89 (m, 1H), 4.04 (t, ^3J = 6.4 Hz, 2H), 2.32 (s, 3H), 1.90 – 1.81 (m, 2H), 1.56 –

1.48 (m, 2H), 1.44 – 1.26 (m, 16H), 0.91 (t, ^{3}J = 6.8 Hz, 3H). ^{13}C NMR (101 MHz, $CDCl_3$) ´ = 158.02, 145.57, 132.51, 130.76, 129.38, 127.65, 127.07, 125.63, 119.21, 111.21, 109.84, 68.16, 31.94, 29.68, 29.66, 29.61, 29.39, 29.37, 29.29, 26.14, 22.71, 16.43, 14.14. ESI-MS (CH_2Cl_2/MeOH 9:1): *m/z*: 378.5 $[M+H]^+$; 395.5 $[M+H_3O]^+$. Elemental analysis for $C_{26}H_{35}NO{\cdot}0.19H_2O$: calcd (found) C, 81.97 (81.97); H, 9.36 (9.53); N, 3.68 (3.67).

4'-(dodecyloxy)-2'-methyl-[1,1'-biphenyl]-4-carbonitrile (**C12L$^{2',0}$**, 57% yield). ^{1}H NMR (400 MHz, $CDCl_3$) ´ = 7.70 (d, ^{3}J = 8.5 Hz, 2H), 7.43 (d, ^{3}J = 8.5 Hz, 2H), 7.14 (d, ^{3}J = 8.3 Hz, 1H), 6.86 (d, ^{4}J = 2.5 Hz, 1H), 6.83 (dd, ^{3} *J* = 8.3, ^{4}J= 2.6 Hz, 1H), 4.01 (t, ^{3}J = 6.6 Hz, 2H), 2.27 (s, 3H), 1.87 – 1.77 (m, 2H), 1.53 – 1.45 (m, 2H), 1.43 – 1.26 (m, 16H), 0.91 (t, ^{3}J = 7.1 Hz, 1H). ^{13}C NMR (101 MHz, $CDCl_3$) ´ = 159.10, 146.65, 136.47, 132.37, 131.88, 130.61, 130.15, 119.06, 116.67, 112.02, 110.23, 68.05, 31.93, 29.68, 29.65, 29.62, 29.60, 29.40, 29.36, 29.29, 26.07, 22.70, 20.63, 14.13. ESI-MS (CH_2Cl_2/MeOH 9:1): *m/z*: 378.4 $[M+H]^+$; 395.5 $[M+H_3O]^+$. Elemental analysis for $C_{26}H_{35}NO{\cdot}0.05H_2O$: calcd (found) C, 82.50 (82.51); H, 9.35 (9.67); N, 3.70 (3.71).

4'-(dodecyloxy)-3-methyl-[1,1'-biphenyl]-4-carbonitrile (**C12L$^{0',3}$**, 70% yield). ^{1}H NMR (400 MHz, $CDCl_3$) ´ = 7.61 (d, ^{3}J = 8.0 Hz, 1H), 7.53 (d, ^{3}J = 8.7 Hz, 2H), 7.50 – 7.48 (m, 1H), 7.44 (dd, ^{3} *J* = 8.1, ^{4}J= 1.8 Hz, 1H), 7.00 (d, ^{3}J = 8.7 Hz, 2H), 4.01 (t, ^{3}J = 6.6 Hz, 2H), 2.60 (s, 3H), 1.87 – 1.79 (m, 2H), 1.55 – 1.46 (m, 2H), 1.43 – 1.27 (m, 16H), 0.92 (t, ^{3}J = 6.8 Hz, 3H). ^{13}C NMR (101 MHz, $CDCl_3$) ´ = 159.74, 145.11, 142.22, 132.86, 131.38, 128.27, 128.17, 124.34, 118.41, 115.02, 110.49, 68.17, 31.96, 29.71, 29.68, 29.65, 29.63, 29.44, 29.40, 29.28, 26.08, 22.73, 20.64, 14.16. ESI-MS (CH_2Cl_2/MeOH 9:1): *m/z*: 378.5 $[M+H]^+$; 395.5 $[M+H_2O]$. Elemental analysis for $C_{26}H_{35}NO$: calcd (found) C, 82.71 (82.69); H, 9.34 (9.57); N, 3.71 (3.72).

4'-(dodecyloxy)-2,2'-dimethyl-[1,1'-biphenyl]-4-carbonitrile (**C12L$^{2',2}$**, 67% yield). ^{1}H NMR (400 MHz, $CDCl_3$) ´ = 7.57 (s, 1H), 7.51 (d, ^{3}J = 7.9 Hz, 1H), 7.22 (d, ^{3}J = 7.8 Hz, 1H), 6.97 (d, ^{3}J = 8.3 Hz, 1H), 6.87 (d, ^{4}J = 2.2 Hz, 1H), 6.82 (dd, ^{3}J = 8.3, ^{4}J= 2.4 Hz, 1H), 4.02 (t, ^{3}J = 6.5 Hz, 2H), 2.13 (s, 3H), 2.04 (s, 3H), 1.89 – 1.76 (m, 2H), 1.58 – 1.46 (m, 2H), 1.46 – 1.26 (m, 16H), 0.92

(t, ^{3}J = 6.7 Hz, 3H). ^{13}C NMR (101 MHz, $CDCl_3$) ´ = 158.86, 146.59, 138.03, 136.53, 133.28, 131.93, 130.74, 129.59, 129.28, 119.04, 116.13, 111.71, 110.93, 67.94, 31.97, 29.73, 29.70, 29.67, 29.65, 29.47, 29.40, 29.39, 26.15, 22.74, 19.97, 19.73, 14.16. ESI-MS (CH_2Cl_2/MeOH 9:1): *m/z*: 392.4$[M+H]^+$; 409.5 $[M+H_3O]^+$. Elemental analysis for $C_{27}H_{37}NO{\cdot}0.2H_2O$: calcd (found) C, 82.04 (82.08); H, 9.62 (9.98); N, 3.49 (3.44).

4'-(dodecyloxy)-2,3'-dimethyl-[1,1'-biphenyl]-4-carbonitrile (**C12L$^{3',2}$**, 76% yield). ^{1}H NMR (400 MHz, $CDCl_3$) ´ = 7.53 (s, 1H), 7.50 (d, ^{3}J = 7.9 Hz, 1H), 7.30 (d, ^{3}J = 8.1 Hz, 1H), 7.09 – 7.04 (m, 2H), 6.87 (d, ^{3}J = 9.0 Hz, 1H), 4.01 (t, ^{3}J = 6.4 Hz, 2H), 2.31 (s, 3H), 2.27 (s, 3H), 1.88 – 1.77 (m, 2H), 1.55 – 1.46 (m, 2H), 1.43 – 1.24 (m, 16H), 0.89 (t, ^{3}J = 6.8 Hz, 3H). ^{13}C NMR (101 MHz, $CDCl_3$) ´ = 157.00, 146.74, 136.91, 133.75, 131.70, 131.02, 130.58, 129.39, 127.15, 126.83, 119.22, 110.51, 110.34, 68.07, 31.93, 29.68, 29.66, 29.65, 29.62, 29.41, 29.36, 29.35, 26.17, 22.70, 20.49, 16.32, 14.13. ESI-MS (CH_2Cl_2/MeOH 9:1): 392.4$[M+H]^+$; 409.5 $[M+H_3O]^+$. Elemental analysis for $C_{27}H_{37}NO{\cdot}0.4H_2O$: calcd (found) C, 81.32 (81.36); H, 9.62 (9.96); N, 3.46 (3.22).

4'-(dodecyloxy)-2',3-dimethyl-[1,1'-biphenyl]-4-carbonitrile (**C12L$^{2',3}$**, 82% yield). ^{1}H NMR (400 MHz, $CDCl_3$) ´ = 7.64 (d, ^{3}J = 7.9 Hz, 1H), 7.24 (d, ^{3}J = 7.9 Hz, 1H), 7.13 (d, ^{3}J = 8.3 Hz, 1H), 6.85 (s, 1H), 6.82 (d, ^{3}J = 8.3 Hz, 1H), 4.01 (t, ^{3}J = 6.5 Hz, 2), 2.61 (s, 3H), 2.27 (s, 3H), 1.88 – 1.75 (m, 2H), 1.55 – 1.44 (m, 2H), 1.44 – 1.25 (m, 16H), 0.91 (t, ^{3}J = 6.7 Hz, 3H). ^{13}C NMR (101 MHz, $CDCl_3$) ´ = 159.00, 146.51, 141.66, 136.45, 132.57, 132.17, 131.25, 130.54, 127.40, 118.37, 116.61, 111.93, 110.65, 68.03, 31.94, 29.69, 29.66, 29.63, 29.61, 29.42, 29.37, 29.30, 26.08, 22.71, 20.65, 20.56, 14.14. ESI-MS (CH_2Cl_2/MeOH 9:1): 392.4$[M+H]^+$; 409.5 $[M+H_2O]$. Elemental analysis for $C_{27}H_{37}NO{\cdot}0.1CH_3OH$: calcd (found) C, 81.46 (82.47); H, 9.55 (9.76); N, 3.40 (3.58).

4'-(dodecyloxy)-3,3'-dimethyl-[1,1'-biphenyl]-4-carbonitrile (**C12L$^{3',3}$**, 51% yield). ^{1}H NMR (400 MHz, $CDCl_3$) ´ = 7.64 (d, ^{3}J = 8.0 Hz, 1H), 7.50 (s, 1H), 7.46 (dd, ^{3}J = 8.1, ^{4}J= *1*.4 Hz, 1H), 7.42 – 7.37 (m, 2H), 6.91 (d, ^{3}J = 9.1 Hz, 1H), 4.03 (t, ^{3}J = 6.4 Hz, 2H), 2.62 (s, 3H), 2.31 (s, 3H), 1.89 – 1.80 (m, 2H), 1.55 – 1.47 (m, 2H), 1.44 – 1.25 (m, 16H), 0.91 (t, ^{3}J = 6.8 Hz, 3H). ^{13}C NMR

(101 MHz, $CDCl_3$) δ = 157.89 , 145.41 , 142.18 , 132.84 , 130.94 , 129.38 , 128.21 , 127.54 , 125.59 , 124.38 , 118.53 , 111.14 , 110.30 , 68.14 , 31.93 , 29.68 , 29.66 , 29.61 , 29.39 , 29.37 , 29.30 , 26.14 , 22.71 , 20.67 , 16.43 , 14.14 . ESI-MS (CH_2Cl_2/MeOH 9:1): *m/z*: 392.4$[M+H]^+$; 409.5 $[M+H_3O]^+$. Elemental analysis for $C_{27}H_{37}NO$: calcd (found) C, 82.81 (82.47); H, 9.52 (9.13); N, 3.58 (3.33).

Preparation of 4'-(dodecyloxy)-2-methyl-[1,1'-biphenyl]-4-carbonitrile ($C_{12}L^{0',2}$). 4-dodecyloxyphenylboronic acid (**7**, 100 mg, 0.33 mmol) and 4-bromo-3-methylbenzonitrile (**3**^{2}, 51 mg, 0.26 mmol, 0.8 eq) were dissolved in a mixture of benzene (1 mL), ethanol (2 mL) and 2M aqueous Na_2CO_3 (1 mL). The mixture was flushed with N_2 for 15 min. A catalytic amount of $Pd(PPh_3)_4$ was added and the reaction was heated at 75°C for 20 h under a dinitrogen atmosphere. The solvents were evaporated and water (5 mL) was added. The aqueous phase was extracted with diethyl ether (4×15mL) and the combined organic phases were dried over Na_2SO_4, filtered and evaporated. The crude product was purified by column chromatography (silica; CH_2Cl_2) to give 4'-(dodecyloxy)-2-methyl-[1,1'-biphenyl]-4-carbonitrile (**$C_{12}L^{0',2}$**, 50 mg, 0.13 mmol, 50% yield) as a white solid. ^{1}H NMR (400 MHz, $CDCl_3$) ´ = 7.56 (s, 1H), 7.53 (d, ^3J = 8.0 Hz, 1H), 7.32 (d, ^3J = 7.8 Hz, 1H), 7.23 (d, ^3J = 8.4 Hz, 2H), 6.98 (d, ^3J = 8.3 Hz, 2H), 4.02 (t, ^3J = 6.5 Hz, 2H), 2.33 (s, 3H), 1.84 (q, ^3J = 6.8 Hz, 2H), 1.54 – 1.45 (m, 2H), 1.42 – 1.25 (m, 16H), 0.91 (t, ^3J = 6.6 Hz, 3H). ^{13}C NMR (101 MHz, $CDCl_3$) ´ = 158.86, 146.46, 136.91, 133.81, 132.12, 130.56, 129.92, 129.46, 114.34, 110.52, 68.11, 31.93, 29.67, 29.65, 29.61, 29.59, 29.41, 29.36, 29.28, 26.08, 22.70, 20.45, 14.13. ESI-MS (CH_2Cl_2/MeOH 9:1): *m/z*: 378.5 $[M+H]^+$; 395.5 $[M+H_3O]^+$. $]^+$. Elemental analysis for $C_{26}H_{35}NO$: calcd (found) C, 82.71 (82.74); H, 9.34 (9.65); N, 3.71 (3.57).

Table S1 Summary of crystal data, intensity measurements and structure refinements for **C12L$^{3',0}$, C12L$^{2',0}$**, **C12L$^{0',2}$**, **C12L$^{3',2}$**, **C12L$^{2',3}$** and **C12L$^{3',3}$.**

	C12L$^{3',0}$	**C12L$^{2',0}$**	**C12L$^{0',2}$**
Empirical formula	$C_{26}H_{35}NO$	$C_{26}H_{35}NO$	$C_{26}H_{35}NO$
Formula weight	377.55	377.55	377.55
Temperature	180(2) K	180(2) K	180(2) K
Wavelength	1.54184 Å	1.54184 Å	1.54184 Å
Crystal System, Space group	Triclinic, *P*-1	Triclinic, *P*-1	Triclinic, *P*-1
Unit cell dimensions	a = 8.2164(8) Å	a = 9.8501(3) Å	a = 7.3851(3) Å
	b = 9.2342(9) Å	b = 13.0601(5) Å	b = 9.3425(4) Å
	c = 16.4517(15) Å	c = 18.5745(7) Å	c = 17.4961(10) Å
	α = 90.886(7)°	α = 85.249(3)°	α = 77.231(4)°
	β = 96.759(8)°	β = 88.996(3)°	β = 89.480(4)°
	γ = 115.412(9)°	γ = 72.465(3)°	γ = 75.528(4)°
Volume in Å^3	1116.6(2)	2270.56(15)	1138.57(9)
Z,	2	4	2
Calculated density	1.123 Mg/m^3	1.104 Mg/m^3	1.101 Mg/m^3
Absorption coefficient	0.508 mm^{-1}	0.500 mm^{-1}	0.498 mm^{-1}
F(000)	412	824	412
Theta range for data collection	2.71 to 73.38°	3.56 to 73.32°	2.59 to 73.27°
Limiting indices	-10<=*h*<=8,	-10<=*h*<=12,	-8<=*h*<=7,
	-11<=*k*<=10,	-16<=*k*<=13,	-11<=*k*<=11,
	-20<=*l*<=20	-22<=*l*<=22	-21<=*l*<=20
Reflections collected / unique	7446 / 4348	17402 / 8836	8559 / 4418
	[*R*(int) = 0.0170]	[*R*(int) = 0.0145]	[*R*(int) = 0.0142]
Completeness to theta	66.97°/ 99.9 %	66.97°/ 99.9 %	67.00°/ 100 %
Data / restraints / parameters	4348 / 0 / 255	8836 / 0 / 509	4418 / 0 / 255
Goodness-of-fit on F^2	1.038	1.019	1.034
Final *R* indices [I>2σ(I)]	R_1 = 0.0401,	R_1 = 0.0381,	R_1 = 0.0432,
	ωR_2 = 0.1143	ωR_2 = 0.1067	ωR_2 = 0.1251
R indices (all data)	R_1 = 0.0469,	R_1 = 0.0452,	R_1 = 0.0555,
	ωR_2 = 0.1239	ωR_2 = 0.1144	ωR_2 = 0.1364
Largest diff. peak and hole	0.199 and -0.170 e·Å^{-3}	0.194 and -0.164 e·Å^{-3}	0.439 and -0.161 e·Å^{-3}

Table S1 (continued)**.**

	C12L$^{3',2}$	**C12L$^{2',3}$**	**C12L$^{3',3}$**
Empirical formula	$C_{27}H_{37}NO$	$C_{27}H_{37}NO$	$C_{27}H_{37}NO$
Formula weight	391.58	391.58	391.58
Temperature	200(2) K	180(2) K	180(2) K
Wavelength	1.54184 Å	1.54184 Å	1.54184 Å
Crystal System, Space group	Triclinic, *P*-1	Triclinic, *P*-1	Triclinic, *P*-1
Unit cell dimensions	*a* = 7.7992(4) Å	*a* = 6.8986(5) Å	*a* = 7.3011(4) Å
	b = 9.7490(5) Å	*b* = 9.5377(7) Å	*b* = 9.6303(6) Å
	c = 17.1569(9) Å	*c* = 18.1034(12) Å	*c* = 16.9491(10) Å
	α = 93.584(5)°	α = 83.061(6)°	α = 81.894(5)°
	β = 101.634(5)°	β = 87.050(5)°	β = 89.584(5)°
	γ = 109.593(5)°	γ = 89.910(6)°	γ = 87.265(4)°
Volume in Å^3	1191.70(11)	1180.85(14)	1178.48(12)
Z	2	2	2
Calculated density	1.091 Mg/m^3	1.101 Mg/m^3	1.104 Mg/m^3
Absorption coefficient	0.491 mm^{-1}	0.496 mm^{-1}	0.497 mm^{-1}
F(000)	428	428	428
Theta range for data collection	2.66 to 73.39°	2.46 to 73.33°	2.63 to 73.34°
Limiting indices	-8<=*h*<=9,	-8<=*h*<=7,	-8<=*h*<=8,
	-12<=*k*<=10,	-11<=*k*<=11,	-11<=*k*<=11,
	-21<=*l*<=18	-22<=*l*<=20	-20<=*l*<=21
Reflections collected / unique	8968 / 4634	7557 / 4595	8844 / 4547
	[*R*(int) = 0.0369]	[*R*(int) = 0.0448]	[*R*(int) = 0.0209]
Completeness to theta	66.97°/ 99.9 %	66.97°/ 99.9 %	66.97°/ 99.7 %
Data / restraints / parameters	4634 / 0 / 265	4595 / 0 / 265	4547 / 0 / 265
Goodness-of-fit on F^2	1.075	1.023	1.041
Final *R* indices [$I>2\sigma(I)$]	R_1 = 0.0507,	R_1 = 0.0607,	R_1 = 0.0448,
	ωR_2 = 0.1465	ωR_2 = 0.1746	ωR_2 = 0.1200
R indices (all data)	R_1 = 0.0626,	R_1 = 0.0800,	R_1 = 0.0620,
	ωR_2 = 0.1568	ωR_2 = 0.1954	ωR_2 = 0.1370
Largest diff. peak and hole	0.252 and -0.277 e·Å^{-3}	0.280 and -0.226 e·Å^{-3}	0.239 and -0.157 e·Å^{-3}

Table S2 Selected least-squares planes data for **C12L$^{3',0}$, C12L$^{2',0}$, C12L$^{0',2}$, C12L$^{3',2}$, C12L$^{2',3}$** and **C12L$^{3',3}$.**

C12L$^{3',0}$

Least-squares planes description	Abbreviation	Max. deviation /Å	Atom
Phenyl 1 C2 C3 C4 C5 C6 C7	Ph1	0.0164	C5
Phenyl 2 C8 C9 C10 C11 C12 C13	Ph2	0.0071	C9
Dodecyloxy chain O1 C14 C15 C16 C17 C18 C19 C20 C21 C22 C23 C24 C25	Chain	0.1564	O1

Interplanar angles (°)

	Ph2	Chain
Ph1	30.09(3)	33.12(4)
Ph2		4.26(3)

C12L$^{2',0}$

Least-squares planes description	Abbreviation	Max. deviation /Å	Atom
Phenyl 1 C2A C3A C4A C5A C6A C7A	Ph1A	0.0104	C2A
Phenyl 2 C8A C9A C10A C11A C12A C13A	Ph2A	0.0096	C8A
Dodecyloxy Chain O1A C14A C15A C16A C17A C18A C19A C20A C21A C22A C23A C24A C25A	ChainA	0.2009	O1A
Phenyl 1 C2B C3B C4B C5B C6B C7B	Ph1B	0.0107	C5B
Phenyl 2 C8B C9B C10B C11B C12B C13B	Ph2B	0.0067	C10B
Dodecyloxy Chain O1B C14B C15B C16B C17B C18B C19B C20B C21B C22B C23B C24B C25B	ChainB	0.1022	C21B

Interplanar angles (°)

	Ph2A	ChainA	Ph1B	Ph2B	ChainB
Ph1A	50.90(3)	52.05(4)	29.78(3)	52.75(3)	55.43(4)
Ph2A		1.26(4)	53.35(3)	2.91(3)	5.35(4)
ChainA			54.58(4)	1.87(3)	4.11(5)
Ph1B				56.18(3)	58.69(4)
Ph2B					2.74(4)

C12L$^{0',2}$

Least-squares planes description	Abbreviation	Max. deviation /Å	Atom
Phenyl 1 C2 C3 C4 C5 C6 C7	Ph1	0.0074	C3
Phenyl 2 C8 C9 C10 C11 C12 C13	Ph2	0.0083	C8
Dodecyloxy chain O1 C14 C15 C16 C17 C18 C19 C20 C21 C22 C23 C24 C25	Chain	0.0901	O1

Interplanar angles (°)

	Ph2	Chain
Ph1	50.85(3)	44.79(4)
Ph2		6.79 (4)

C12L$^{3',2}$

Least-squares planes description	Abbreviation	Max. deviation /Å	Atom
Phenyl 1 C2 C3 C4 C5 C6 C7	Ph1	0.0038	C5
Phenyl 2 C8 C9 C10 C11 C12 C13	Ph2	0.0043	C8
Dodecyloxy chain O1 C14 C15 C16 C17 C18 C19 C20 C21 C22 C23 C24 C25	Chain	0.0884	C22

Interplanar angles (°)

	Ph2	Chain
Ph1	47.81(3)	38.17(4)

Ph2		9.73(4)

C12L$^{2',3}$

Least-squares planes description	Abbreviation	Max. deviation /Å	Atom
Phenyl 1 C2 C3 C4 C5 C6 C7	Ph1	0.0064	C7
Phenyl 2 C8 C9 C10 C11 C12 C13	Ph2	0.0141	C11
Dodecyloxy chain O1 C14 C15 C16 C17 C18 C19 C20 C21 C22 C23 C24 C25	Chain	0.2137	O1

Interplanar angles (°)

	Ph2	Chain
Ph1	49.49(3)	46.31(4)
Ph2		3.36(4)

C12L$^{3',3}$

Least-squares planes description	Abbreviation	Max. deviation /Å	Atom
Phenyl 1 C2 C3 C4 C5 C6 C7	Ph1	0.0148	C5
Phenyl 2 C8 C9 C10 C11 C12 C13	Ph2	0.0087	C8 // C11
Dodecyloxy chain O1 C14 C15 C16 C17 C18 C19 C20 C21 C22 C23 C24 C25	Chain	0.1080	C14

Interplanar angles (°)

	Ph2	Chain
Ph1	27.52(3)	21.30(4)
Ph2		6.91(4)

Table S3 Thermodynamic parameters for the melting processes in **C*n*L$^{0',0}$**.[26]

Compounds	Transitions[a]	ΔH_m kJ/mol	ΔS_m J/mol·K	ΔG_m kJ/mol	T_m K	ΔG_m^0 [b] kJ/mol
C5L$^{0',0}$	Cr→N	29.58	92.31	0.00	320.4	2.07
	N→I	0.42	1.23	0.00	341.5	0.05
	'Cr→I'[c]	30	93.55	-	-	2.12
C6L$^{0',0}$	Cr→N	34.18	103.56	0.00	330.1	3.32
	N→I	0.63	1.8	0.00	350.0	0.09
	'Cr→I'[c]	34.81	105.36	-	-	3.41
C7L$^{0',0}$	Cr→N	28.07	86.71	0.00	323.7	2.23
	N→I	0.54	1.55	0.00	348.4	0.08
	'Cr→I'[c]	28.61	88.26	-	-	2.31
C8L$^{0',0}$	Cr→SmA	29.79	91.38	0.00	326.0	2.56
	SmA→N	0.04	0.13	0.00	307.7	0.00
	N→I	0.88	2.5	0.00	352.0	0.14
	'Cr→I'[c]	30.71	94.01	-	-	2.70
C9L$^{0',0}$	Cr→SmA	35.48	105.72	0.00	335.6	3.98
	SmA→N	0.38	1.08	0.00	351.9	0.06
	N→I	0.92	2.61	-	352.5	0.14
	'Cr→I'[c]	36.78	109.41	0.00	-	4.18
C10L$^{0',0}$	Cr→SmA	36.07	109.07	0.00	330.7	3.57
	SmA→I	3.31	9.27	0.00	357.1	0.55
	'Cr→I'[c]	39.38	118.33	-	-	4.12

Table S3 (continued)

C11L$^{0',0}$	Cr→SmA	44.73	130.88	0.00	341.8	5.73
	SmA→I	4.1	11.4	0.0	359.6	0.70
	'Cr→I'[c]	48.83	142.27	-	-	6.43
C12L$^{0',0}$	Cr→SmA	41.7	122.2	0.0	341.6	5.28
	SmA→I	4.6	12.6	0.0	362.2	0.85
	'Cr→I'[c]	46.3	134.8	-	-	6.13

[a] Cr = crystal, SmA = smectic A, N = nematic, I = isotropic liquid. [b] $\Delta G_m^0 = \Delta H_m - T^0 \Delta S_m$ are calculated at T^0 = 298 K by using the melting enthalpies and entropies determined at the melting temperatures T_m. [c] Sum of the successive phase transitions.

Table S4 Attractive well depths u_{min}^{0} (kJ/mol, eqn 2) and force constants κ^{0} (kN/m, eqn 3) computed for **C*n*L**$^{i',j}$.[a]

Compounds	Transitions	T_m	$-u_{min}$	κ	$-u_{min}^{0}$	κ^{0}
C5L$^{0',0}$	'Cr→I'[b]	320.7	34.0	0.1	-	-
C6L$^{0',0}$	'Cr→I'[b]	330.4	38.9	0.3	-	-
C7L$^{0',0}$	'Cr→I'[b]	324.2	32.7	0.1	-	-
C8L$^{0',0}$	'Cr→I'[b]	326.7	34.8	0.1	-	-
C9L$^{0',0}$	'Cr→I'[b]	336.2	41.0	0.4	-	-
C10L$^{0',0}$	'Cr→I'[b]	332.8	43.5	0.7	-	-
C11L$^{0',0}$	'Cr→I'[b]	343.2	53.1	5.2	-	-
C12L$^{0',0}$	'Cr→I'[b]	343.5	50.6	1.0	48.7	0.7
C12L$^{3',0}$	Cr→I	341.1	61.3	0.0	49.5	0.0
C12L$^{2',0}$	Cr→I	314.0	36.4	2.9	35.0	2.0
C12L$^{0',3}$	Cr→I	326.3	54.8	37.7	47.6	2.0
C12L$^{0',2}$	Cr→I	323.8	59.4	0.2	50.4	0.1
C12L$^{2'2}$	Cr→I	307.4	38.2	14.1	43.4	2.2
C12L$^{3',2}$	Cr→I	347.3	58.3	49.3	49.9	4.8
C12L$^{2',3}$	Cr→I	326.1	50.4	0.4	46.9	1.5
C12L$^{3',3}$	Cr→I	320.0	48.1	15.2	45.0	1.8

[a] The parameters marked with a 0 index correspond to standard values at 298 K, whereas all other data are given at the melting temperature T_m. [b] Sum of the successive phase transitions.

Table S5 Molecular (V_{mol}) and molar volumes (V_m), free energy of decohesion (ΔG_m^0) and cohesive free energy densities (*cfed*) in **C*n*L$^{i',j}$**.

Compounds	Transitions [a]	V_{mol} [b]	V_m [c]	ΔG_m^0 [d]	*cfed* [e]
		Å^3	cm^3/mol	kJ/mol	J/cm^3
C5L$^{0',0}$	'Cr→I'[f]	351.2	211.5	2.1	-10.0
C6L$^{0',0}$	'Cr→I'[f]	372.6	224.4	3.4	-15.2
C7L$^{0',0}$	'Cr→I'[f]	397.3	239.3	2.3	-9.6
C8L$^{0',0}$	'Cr→I'[f]	419.1	252.4	2.7	-10.7
C9L$^{0',0}$	'Cr→I'[f]	436.4	262.8	4.2	-15.9
C10L$^{0',0}$	'Cr→I'[f]	460.2	277.2	4.1	-14.9
C11L$^{0',0}$	'Cr→I'[f]	481.3	289.9	6.4	-22.2
C12L$^{0',0}$	'Cr→I'[f]	502.1	302.4	6.1(5)	-20.3(1.8)
C12L$^{3',0}$	Cr→I	530.7	319.7	7.2(7)	-22.5(2.1)
C12L$^{2',0}$	Cr→I	528.7	318.4	1.7(3)	-5.2(9)
C12L$^{0',3}$	Cr→I	528.4	318.3	4.4(1.0)	-13.8(3.0)
C12L$^{0',2}$	Cr→I	526.5	317.1	4.4(1.4)	-13.9(4.3)
C12L$^{2'2}$	Cr→I	548.1	330.1	1.1(7.7)	-3.2(23.2)
C12L$^{3',2}$	Cr→I	549.7	331.1	7.7(9)	-23.1(2.8)
C12L$^{2',3}$	Cr→I	548.5	330.4	4.0(3)	-12.1(8)
C12L$^{3',3}$	Cr→I	548.9	330.6	3.0(1.0)	-9.2(2.9)

[a] Cr = crystal, I = isotropic liquid. [b] Taken as the Connolly volume.[41] [c] $V_m = N_{av} \cdot V_{mol}$ where N_{av} is Avogadro number and V_{mol} taken as the Connolly volumes (see Table A1-1). [d] $\Delta G_m^0 = \Delta H_m - T^0 \Delta S_m$ are calculated at T^0 = 298 K by using the melting enthalpies and entropies determined at the melting temperatures T_m. [e] $cfed = -\Delta G_m^\circ / V_m$. [f] Sum of the successive phase transitions leading to the isotropic fluid.

a)

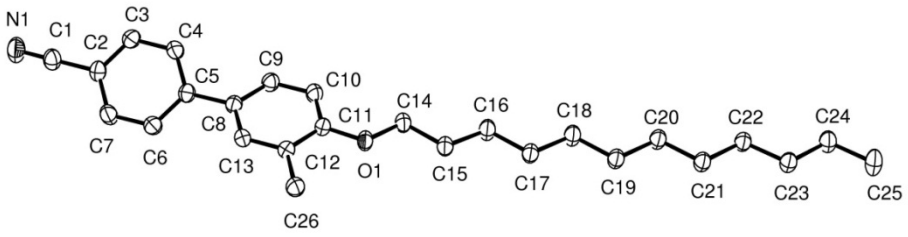

C12L$^{3',0}$ (φ = 30.09(3)°)

b)

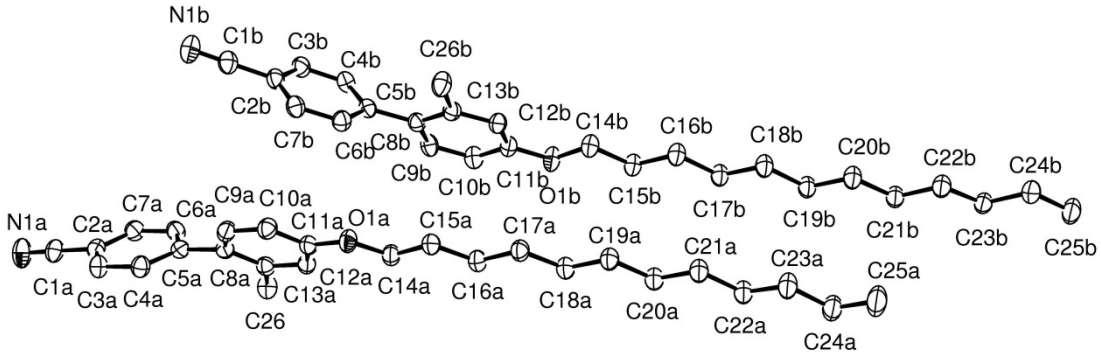

C12L$^{2',0}$ (φ_a = 50.90(3)°, φ_b = 56.18(3)°)

c)

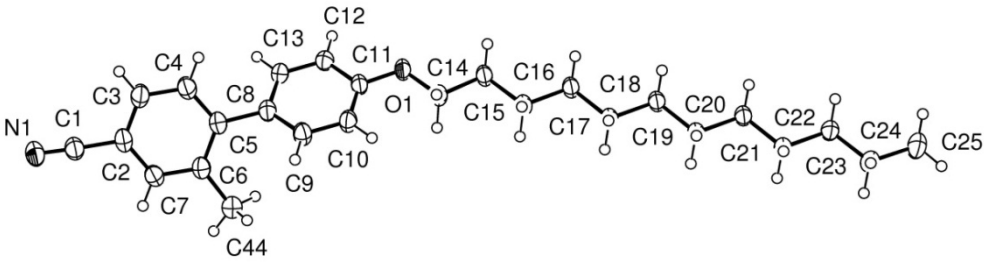

C12L$^{0',2}$ (φ = 50.85(3)°)

Figure S1 Molecular structures with numbering schemes of the asymmetric units for the mono-methyl cyanobiphenyl a) **C12L$^{3',0}$**, b) **C12L$^{2',0}$** and c) **C12L$^{0',2}$** (thermal ellipsoids are represented at the 50% probability level). Hydrogen atoms are omitted in (a) and (b) for clarity and φ is the interplanar angle between the connected aromatic rings.

a)

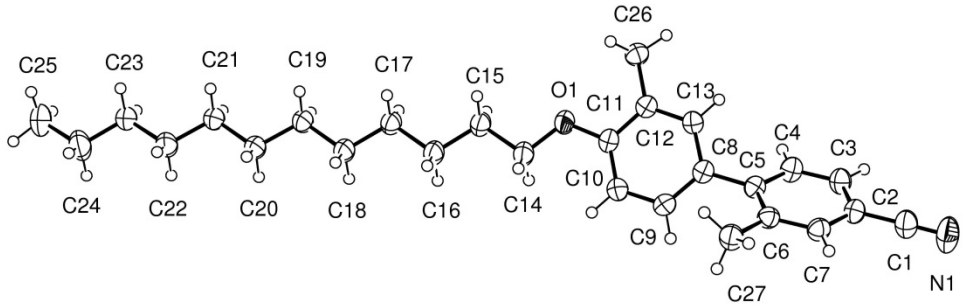

C12L$^{3',2}$ (φ = 47.81(3)°)

b)

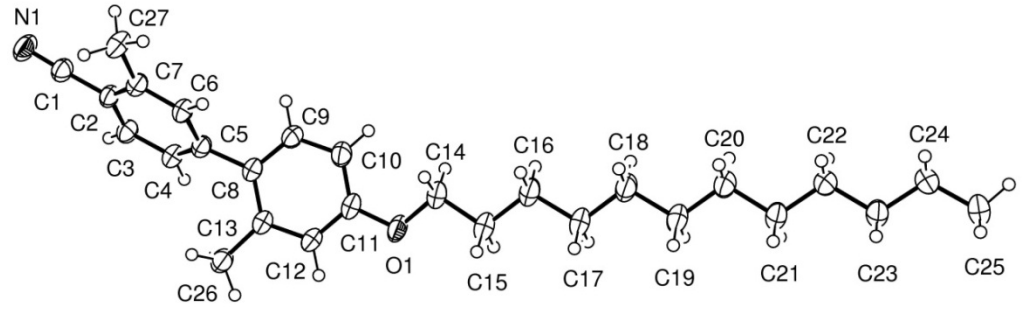

C12L$^{2',3}$ (φ = 49.49(3)°)

c)

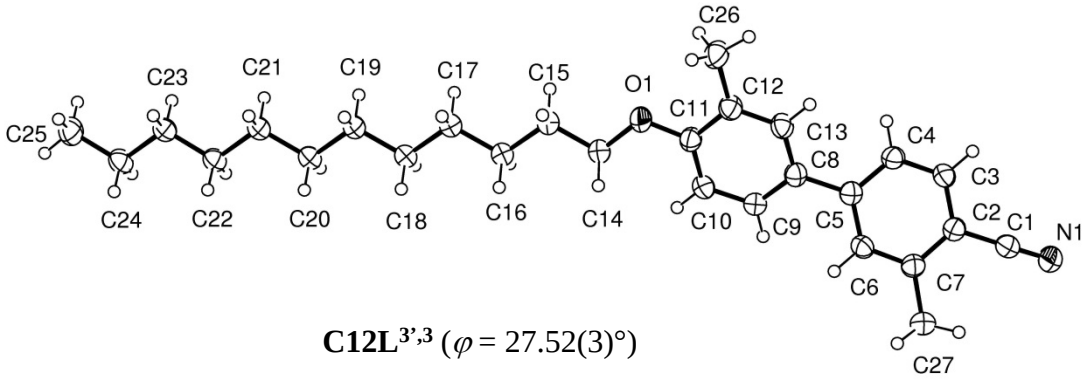

C12L$^{3',3}$ (φ = 27.52(3)°)

Figure S2 Molecular structures with numbering schemes of the asymmetric units for the dimethyl cyanobiphenyl a) **C12L$^{3',2}$**, b) **C12L$^{2',3}$** and c) **C12L$^{3',3}$** (thermal ellipsoids are represented at the 50% probability level). φ is the interplanar angle between the connected aromatic rings.

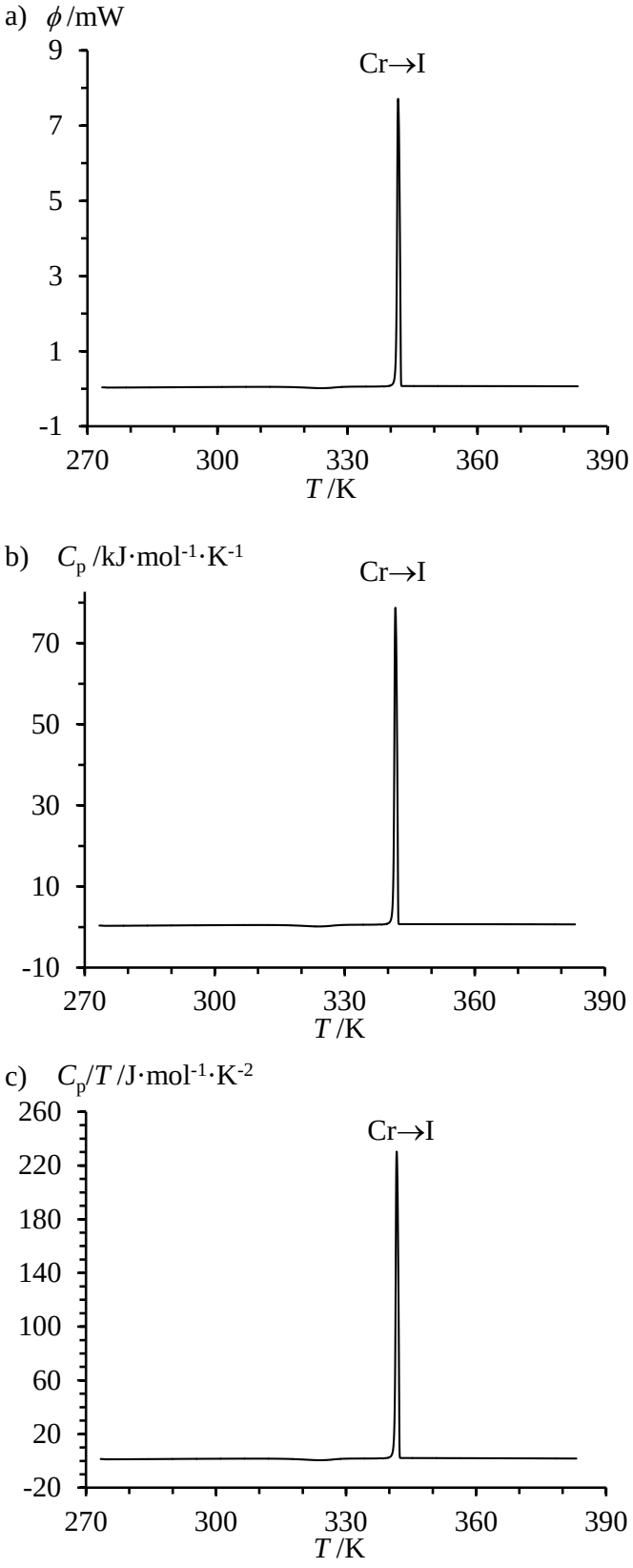

Figure S3 a) DSC trace recorded for the second heating of **C12L$^{3',0}$** and its transformation into b) molar heat capacity (eqn 8) and c) molar heat capacity per temperature unit.

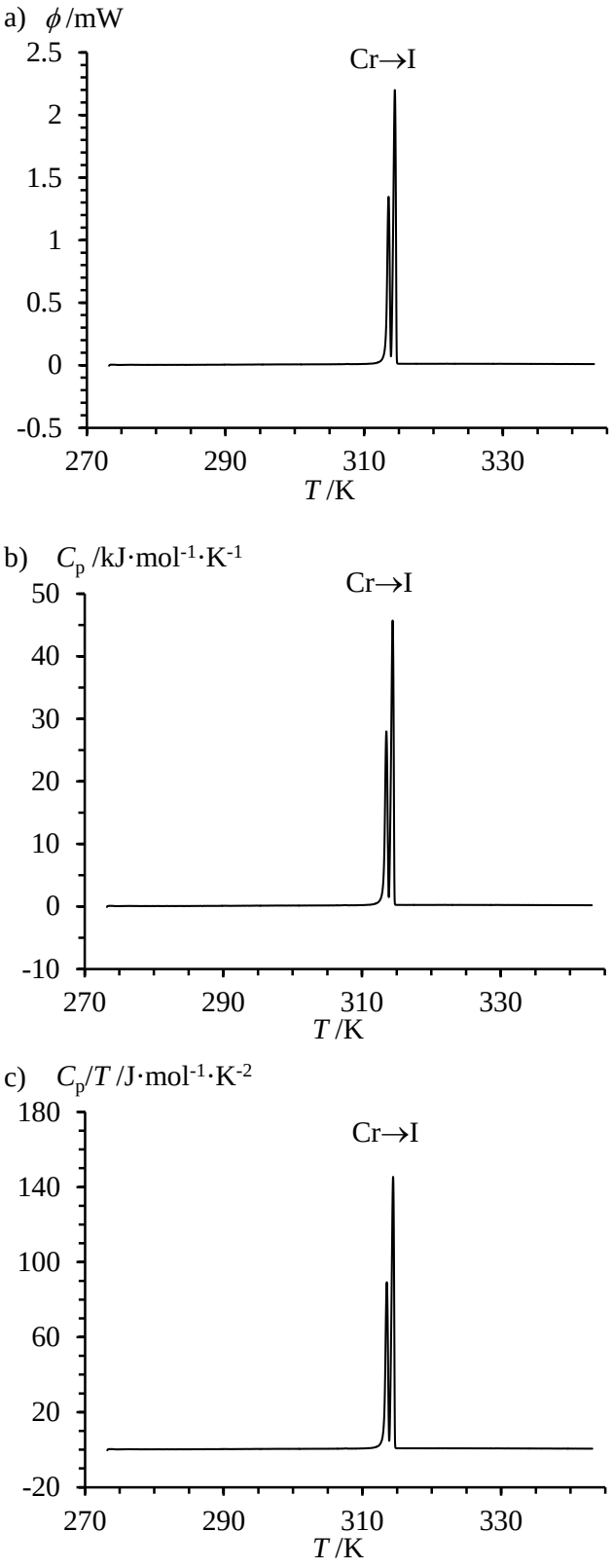

Figure S4 a) DSC trace recorded for the second heating of **C12L$^{2',0}$** and its transformation into b) molar heat capacity (eqn 8) and c) molar heat capacity per temperature unit.

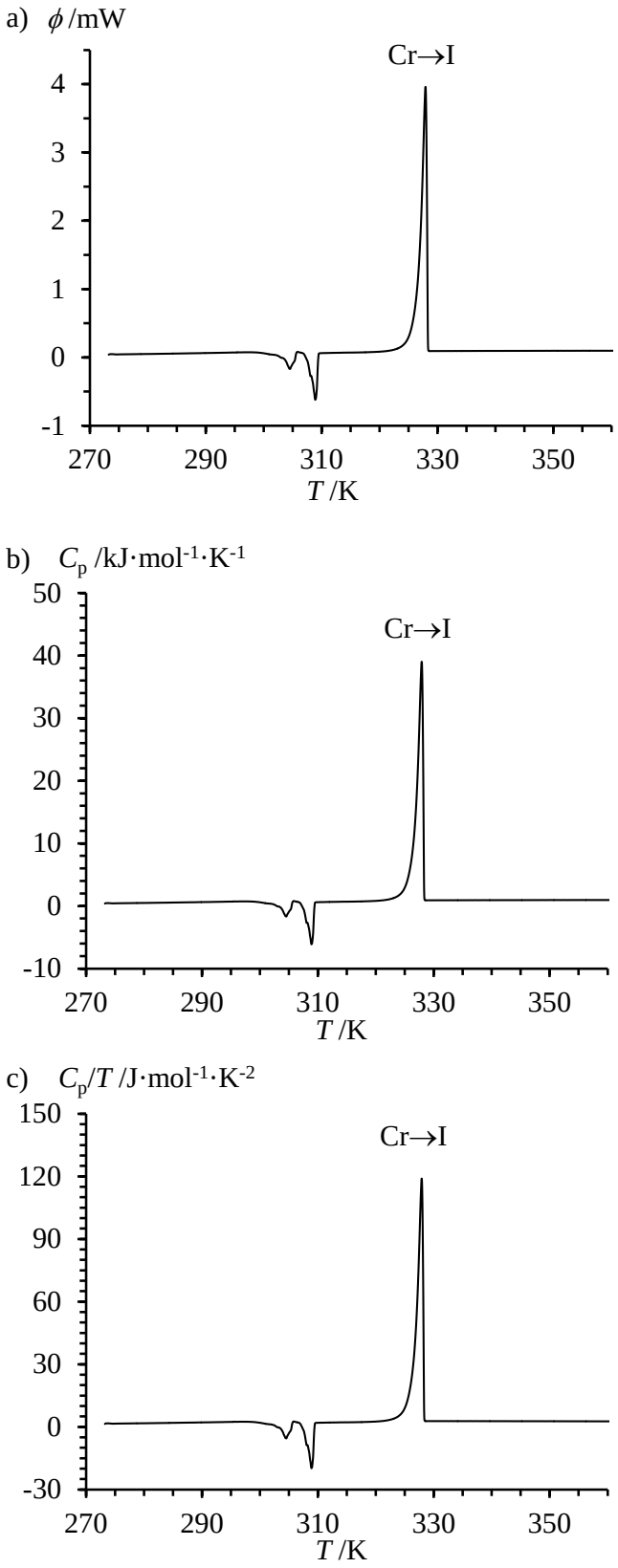

Figure S5 a) DSC trace recorded for the second heating of **C12L$^{0',3}$** and its transformation into b) molar heat capacity (eqn 8) and c) molar heat capacity per temperature unit.

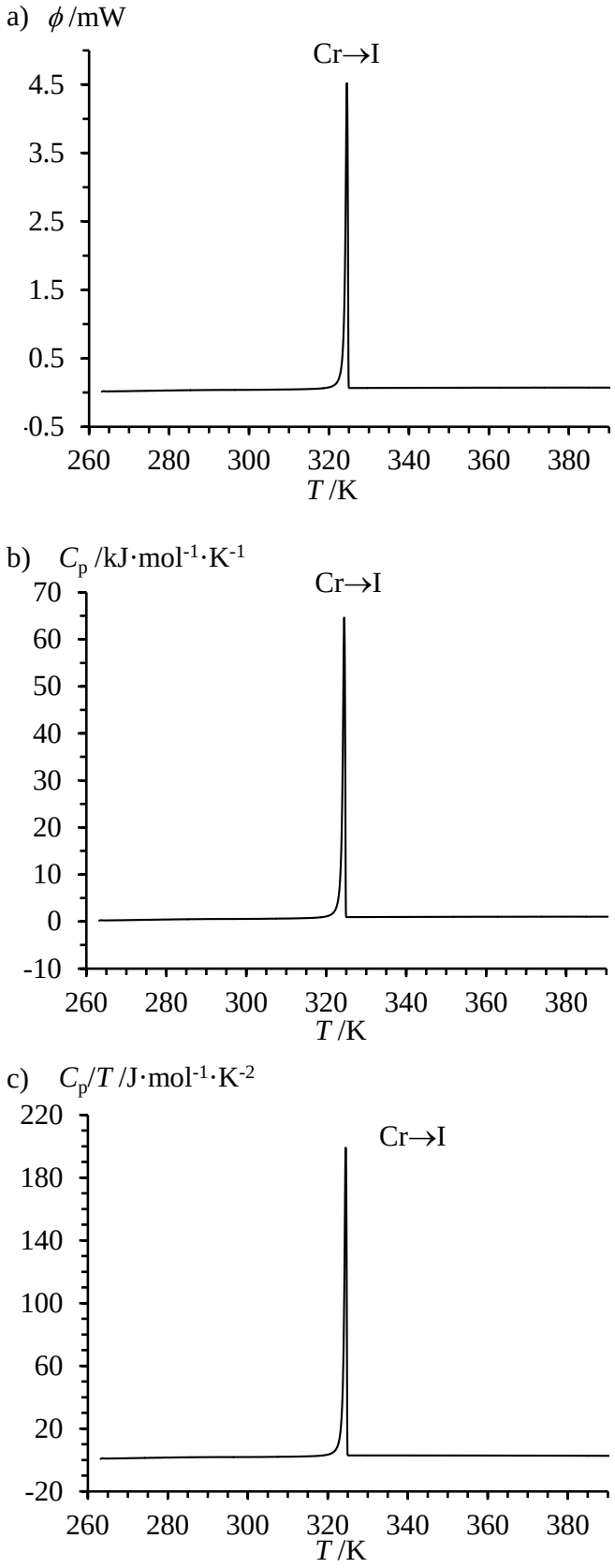

Figure S6 a) DSC trace recorded for the second heating of **C12L$^{0',2}$** and its transformation into b) molar heat capacity (eqn 8) and c) molar heat capacity per temperature unit.

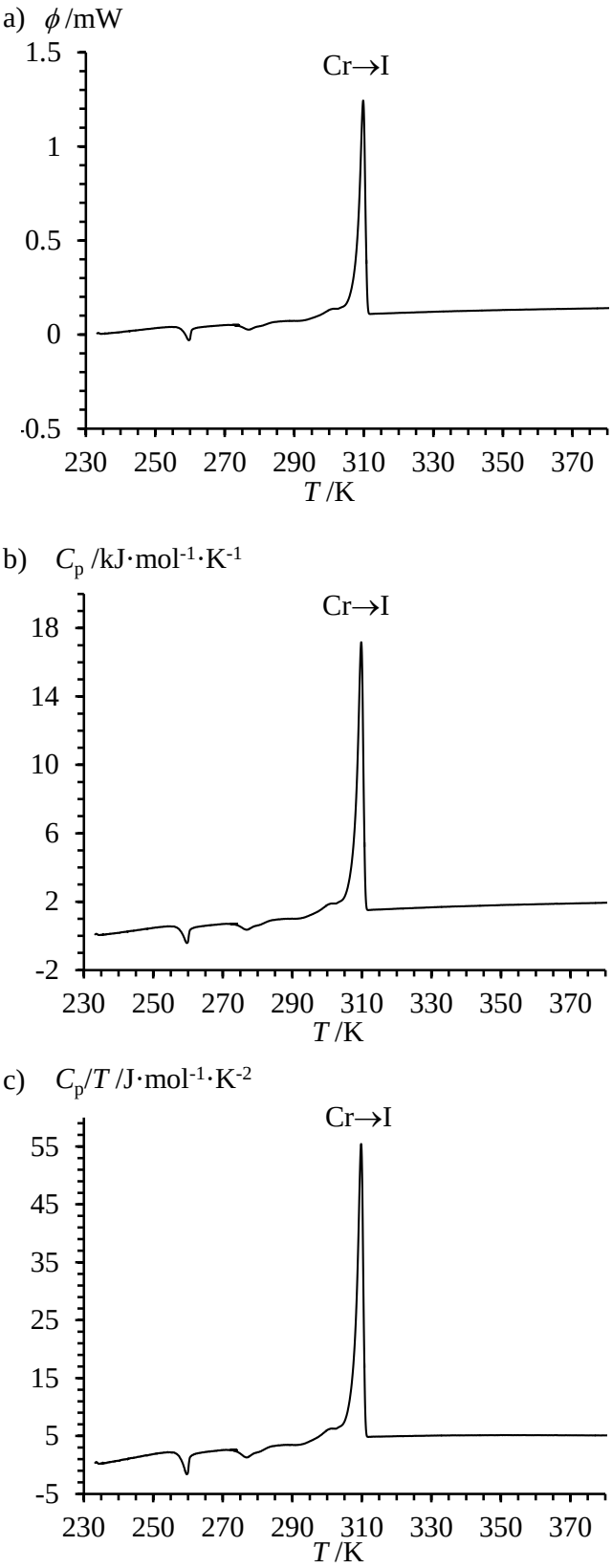

Figure S7 a) DSC trace recorded for the second heating of **C12L$^{2',2}$** and its transformation into b) molar heat capacity (eqn 8) and c) molar heat capacity per temperature unit.

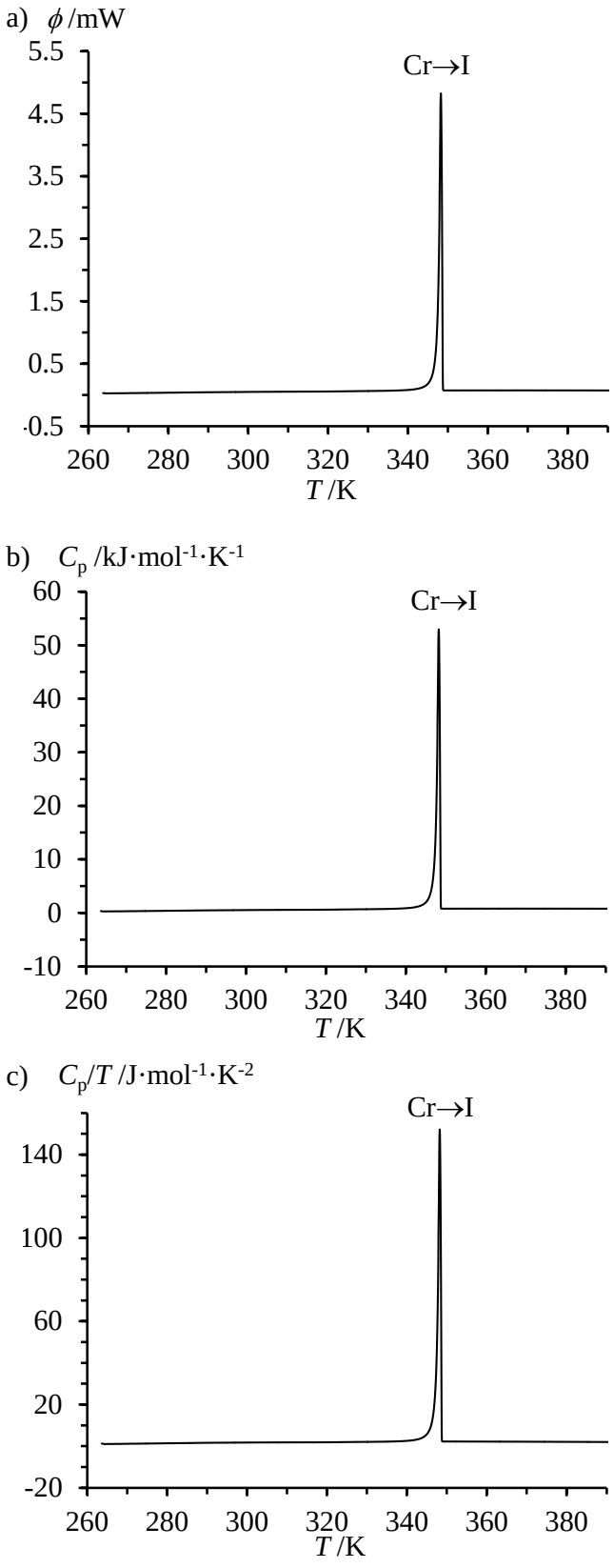

Figure S8 a) DSC trace recorded for the second heating of **C12L**$^{3',2}$ and its transformation into b) molar heat capacity (eqn 8) and c) molar heat capacity per temperature unit.

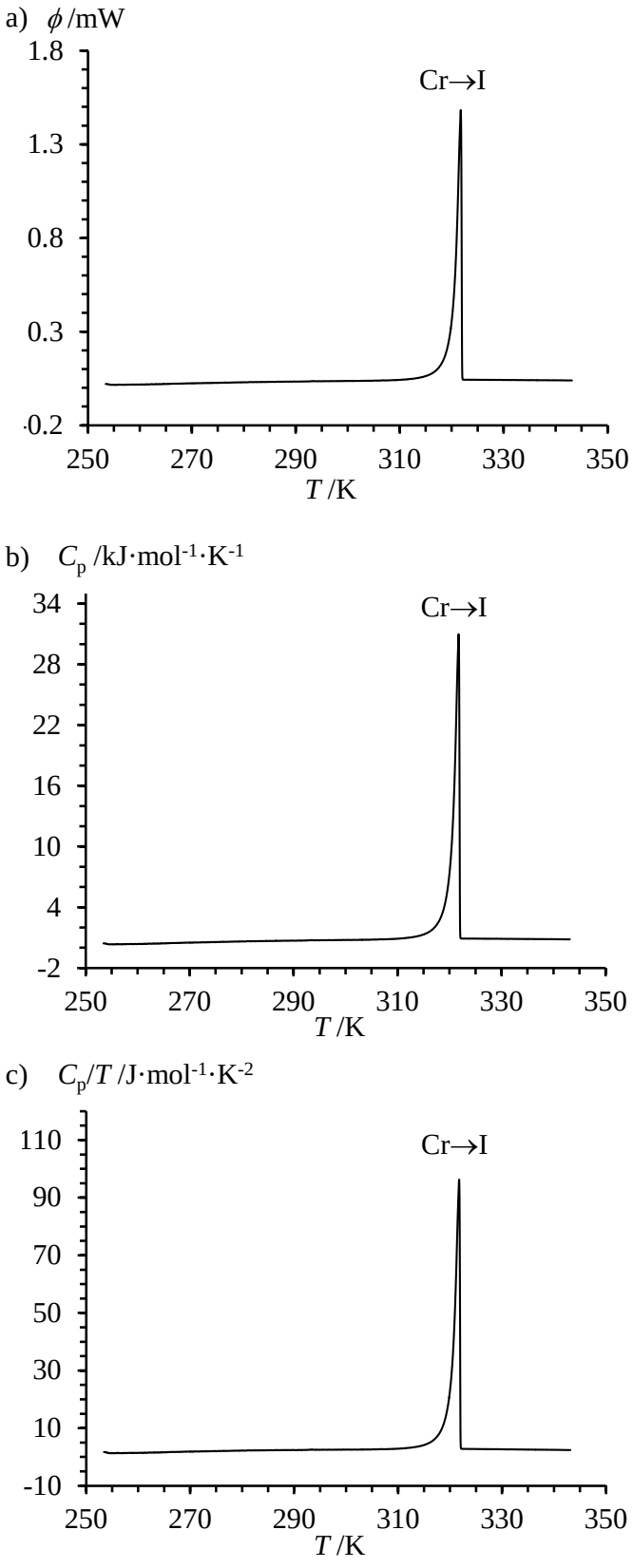

Figure S9 a) DSC trace recorded for the second heating of **C12L**$^{3',3}$ and its transformation into b) molar heat capacity (eqn 8) and c) molar heat capacity per temperature unit.

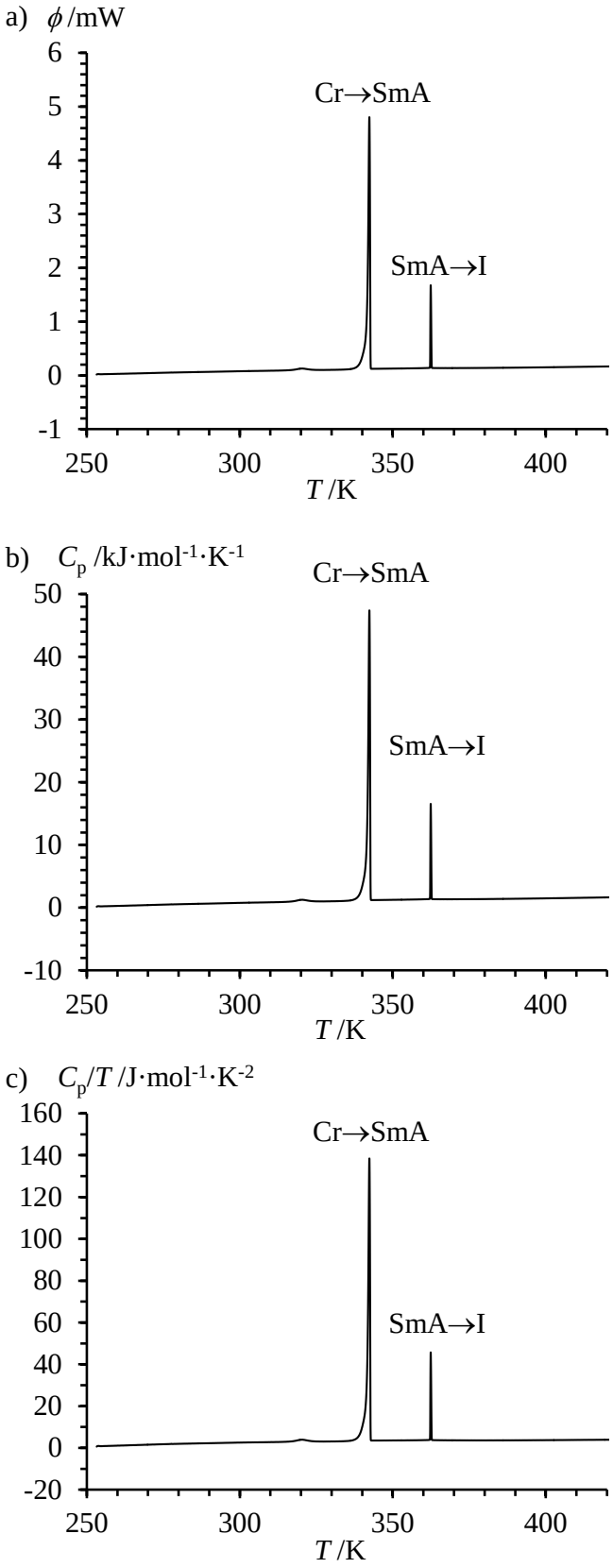

Figure S10 a) DSC trace recorded for **C12L$^{0',0}$** and its transformation into b) molar heat capacity (eqn 10) and c) molar heat capacity per temperature unit.

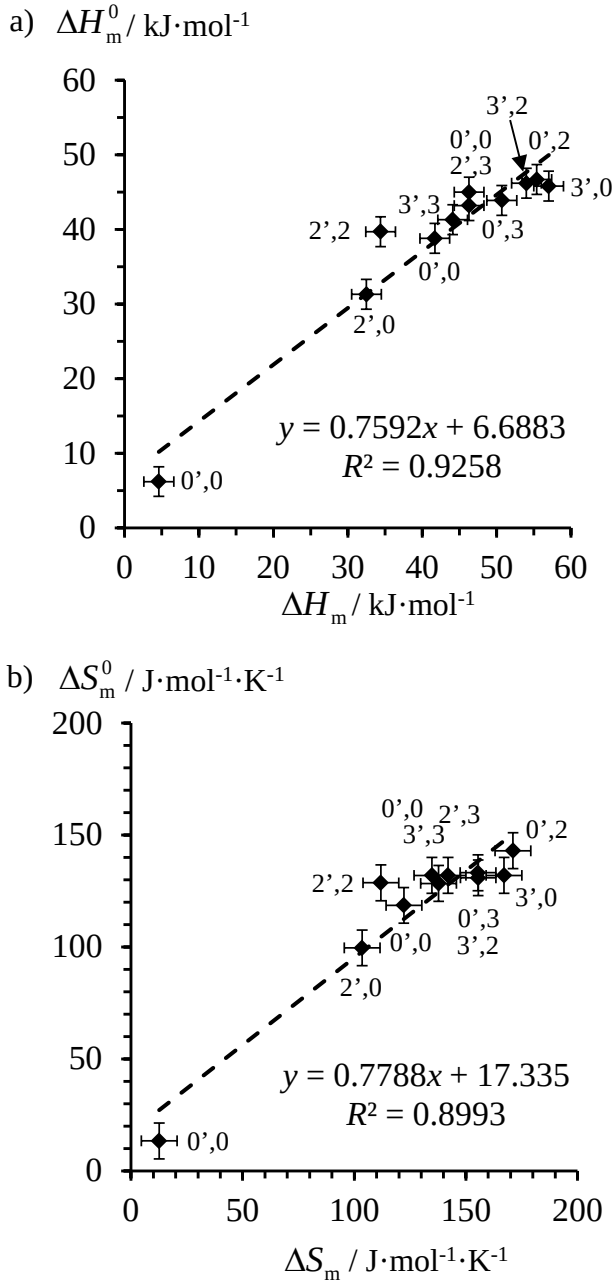

Figure S11 Correlations between a) ΔH^0_m and ΔH_m and b) ΔS^0_m and ΔS_m for the compounds **C12L**$^{i',j}$.

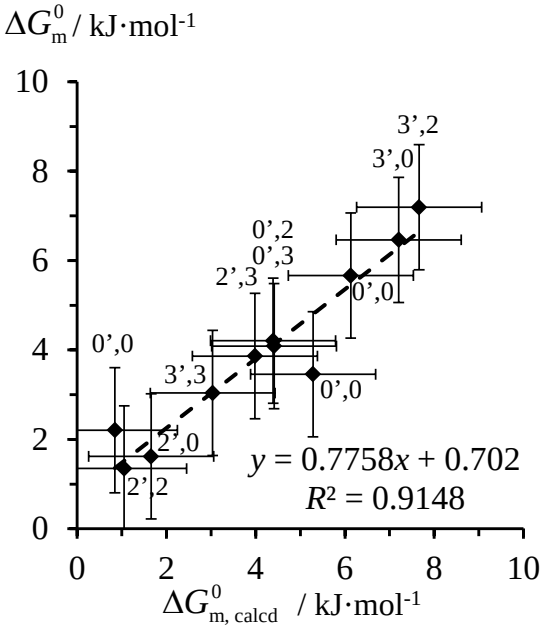

Figure S12 Correlation between $\Delta G^0_m = \Delta H^0_m - T^0 \Delta S^0_m$ and $\Delta G^0_{m,calcd} = \Delta H_m - T^0 \Delta S_m$ for the compounds **C12L**$^{i',j}$.

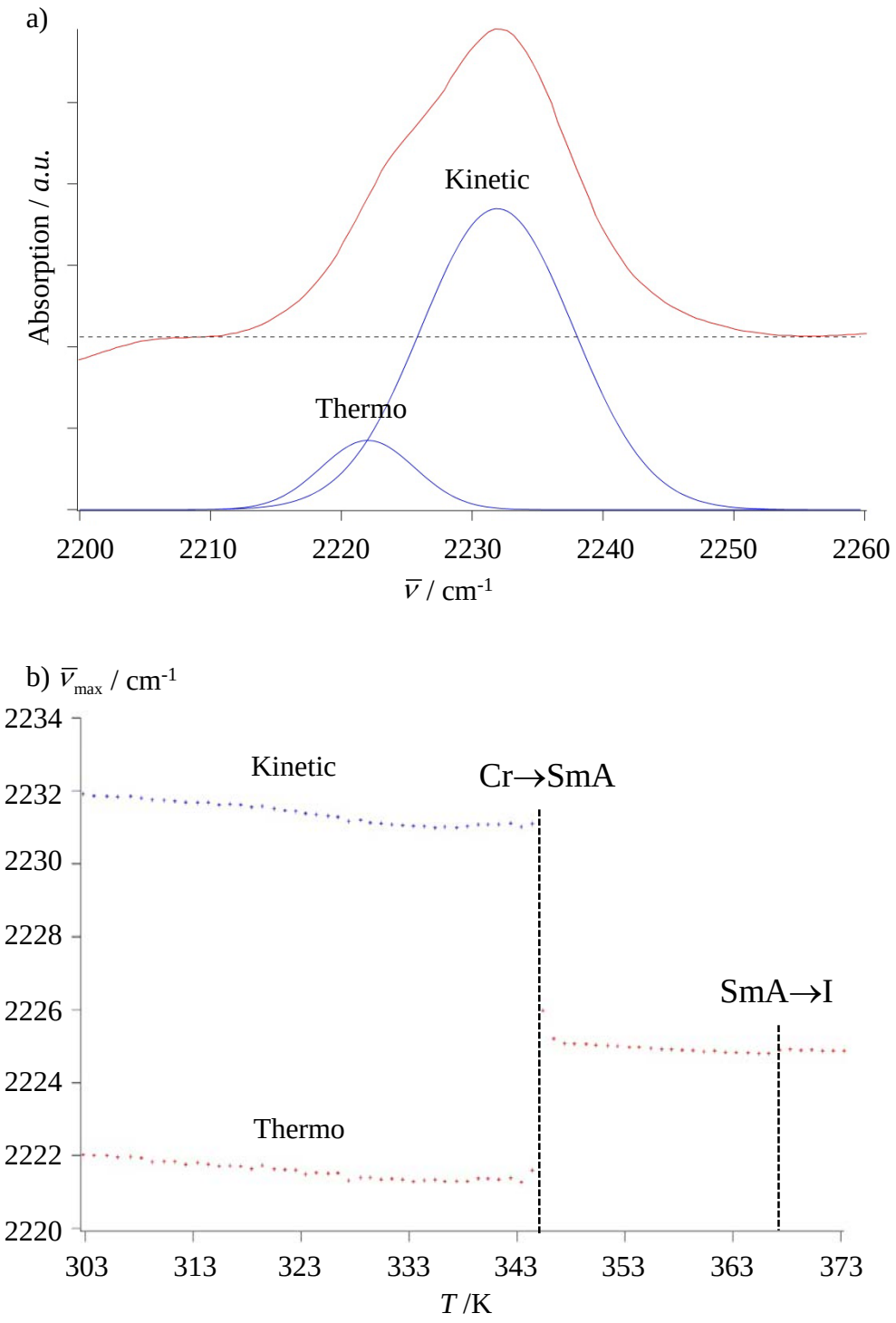

Figure S13 a) Infra-red spectrum of **C12L$^{0',0}$** recorded at 303 K in the 2200-2260 cm^{-1} range (red trace) and its deconvolution into two gaussian absorption bands (blue traces), and b) variable-temperature evolution of the associated maximums of the CN strecthing vibrations.

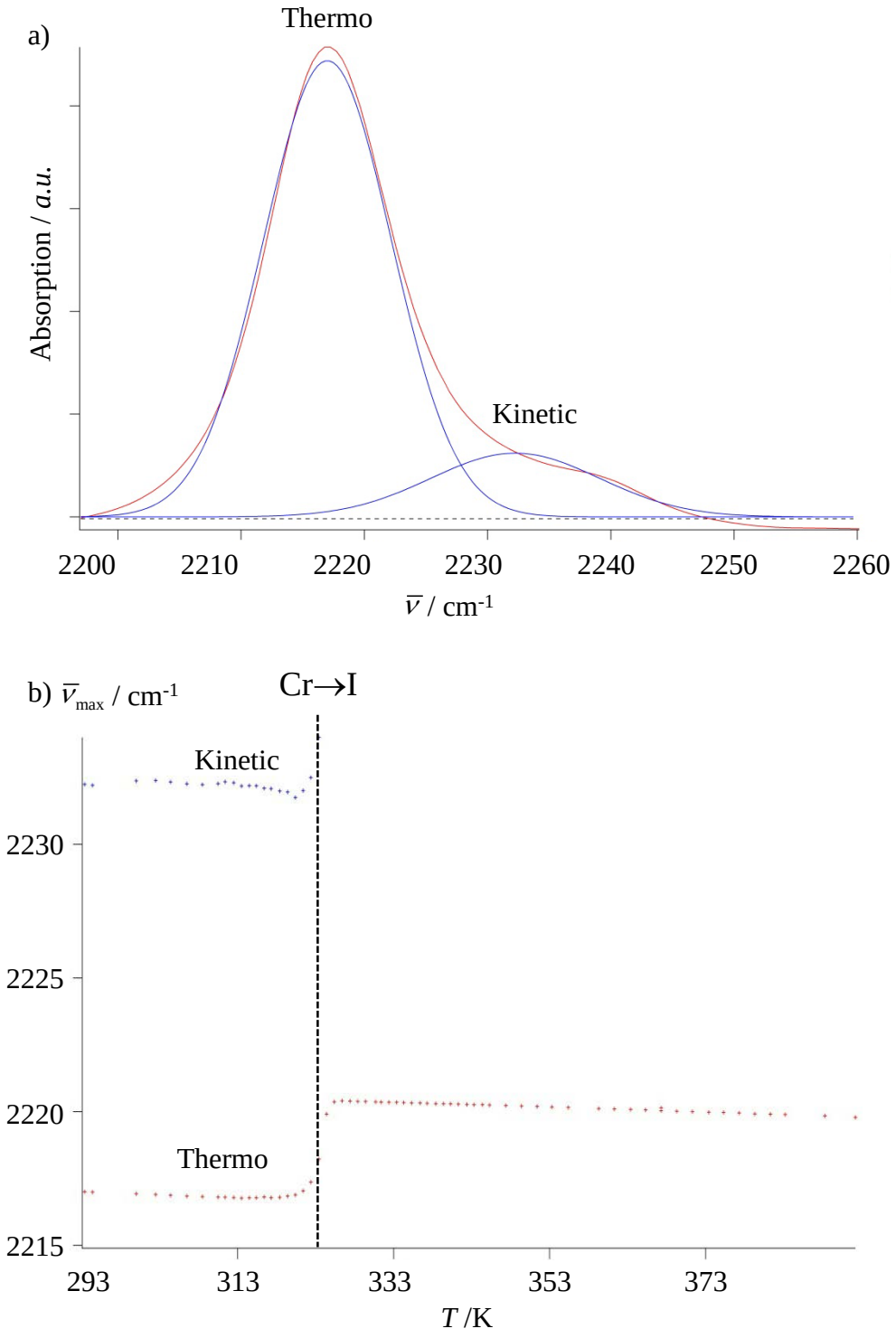

Figure S14 a) Infra-red spectrum of **C12L**$^{3',3}$ recorded at 303 K in the 2200-2260 cm^{-1} range (red trace) and its deconvolution into two gaussian absorption bands (blue traces), and b) variable-temperature evolution of the associated maximums of the CN strecthing vibrations.

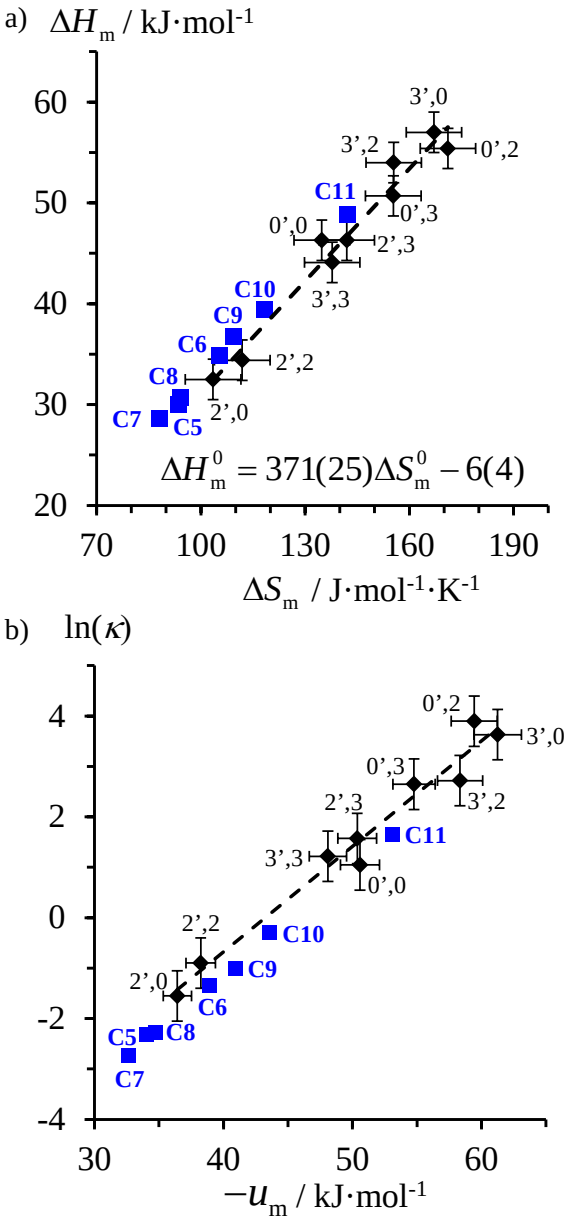

Figure S15 (a) ΔH_m *versus* ΔS_m (eqn 1) and (b) the logarithm of the force constants $\ln(\kappa)$ *versus* the potential well depth u_{min} for the melting of **C*n*L**$^{i',j}$.

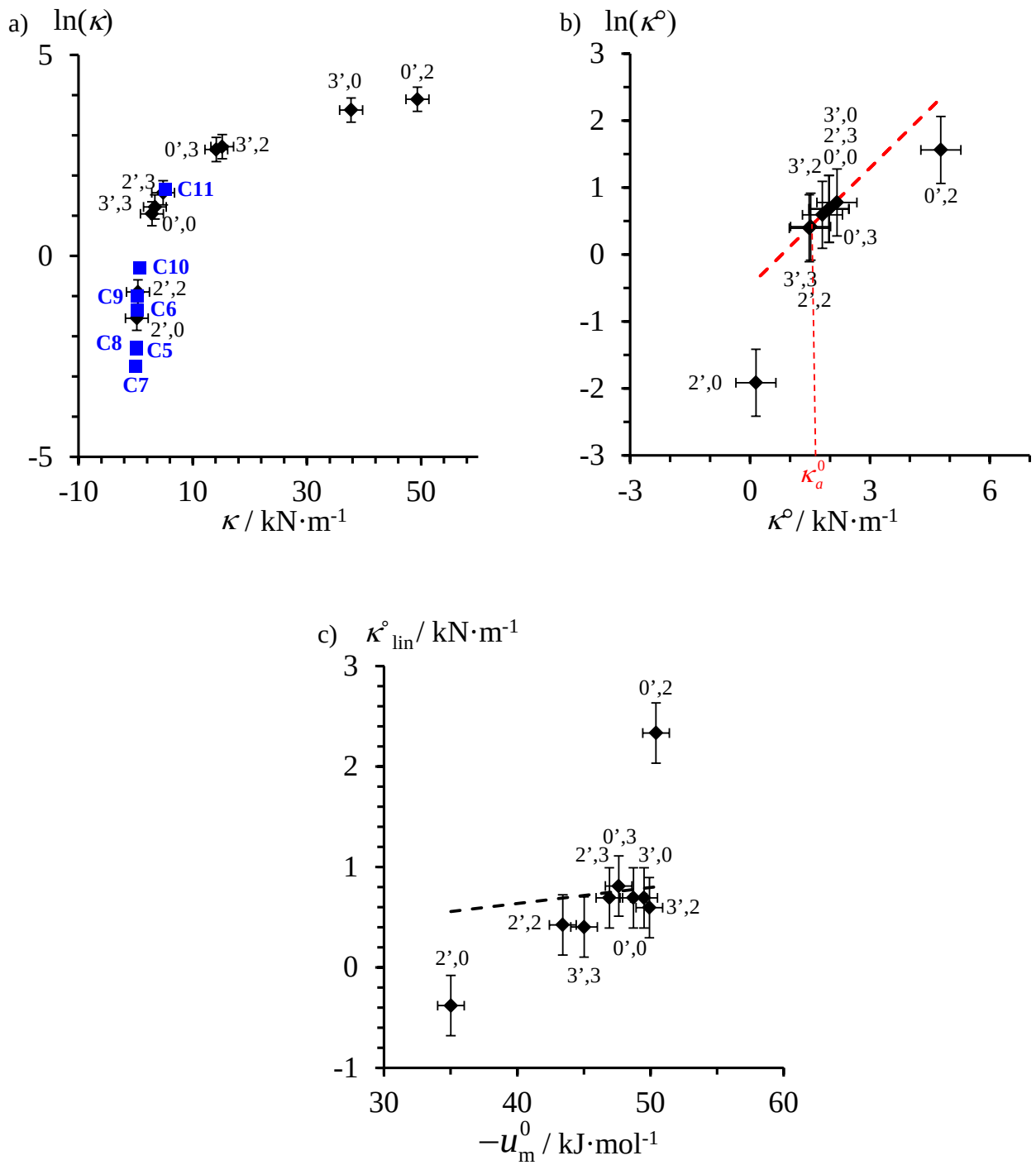

Figure S16 Plots of the logarithm of the force constants $\ln(\kappa)$ *versus* κ for thermodynamic melting parameters of **C*n*L**$^{i',j}$ (a) collected at the different melting temperatures and (b) calculated at the reference temperature. c) Pseudo-linear correlation between the 'linearized' force constants and the potential well depths u_{min} (see text).

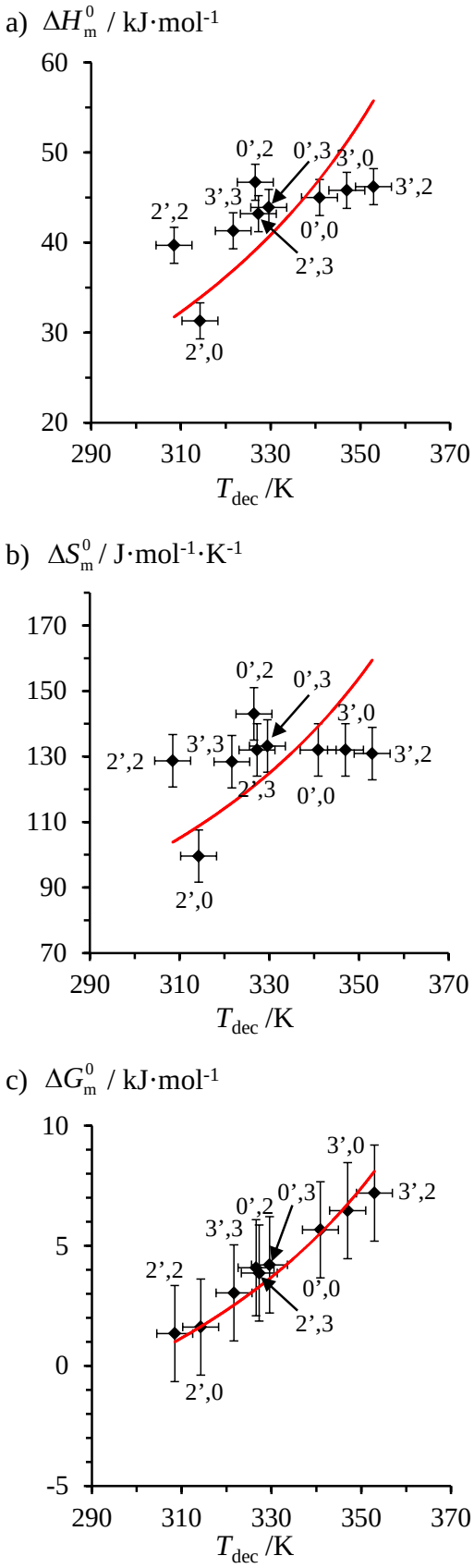

Figure S17 Plots of (a) ΔH^0_m, (b) ΔS^0_m and (c) ΔG^0_m *versus* the decohesion temperature (T_{dec}) for **C12L$^{i',j}$**. The dotted red traces show the theoretical curves computed with eqns (13)-(15).

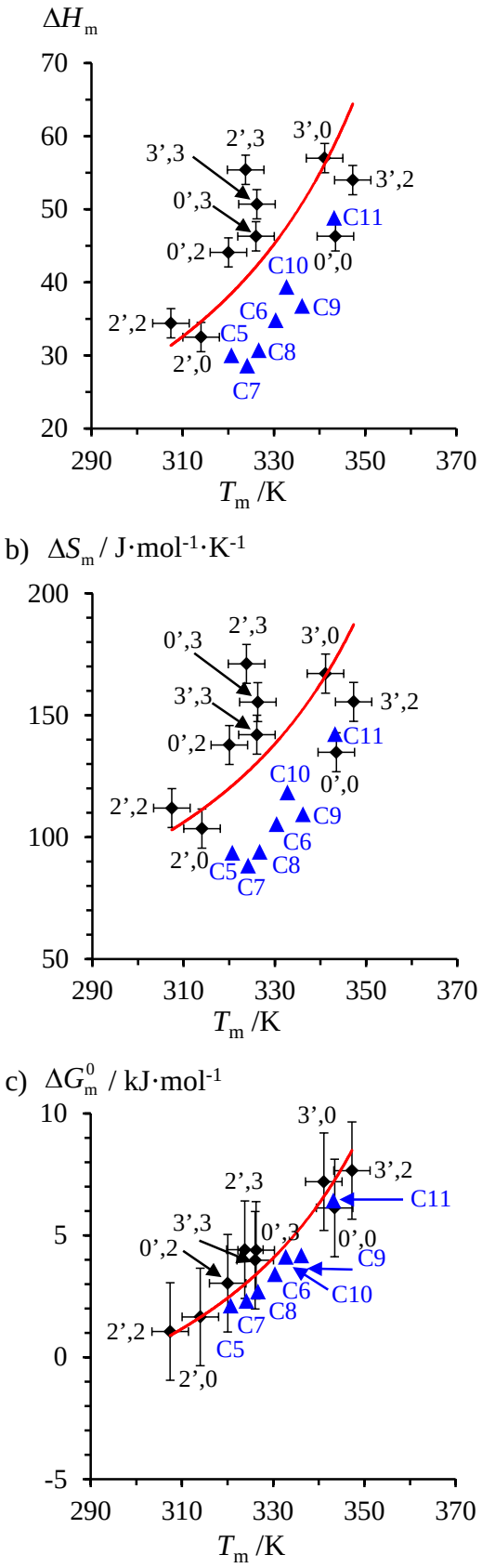

Figure S18 Plots of (a) ΔH_m, (b) ΔS_m and (c) $\Delta G_m^0 = \Delta H_m - T^0 \Delta S_m$ *versus* the melting temperature (T_m) for **C*n*L**$^{i',j}$. The dotted red traces show the theoretical curves computed with eqns (13)-(15)

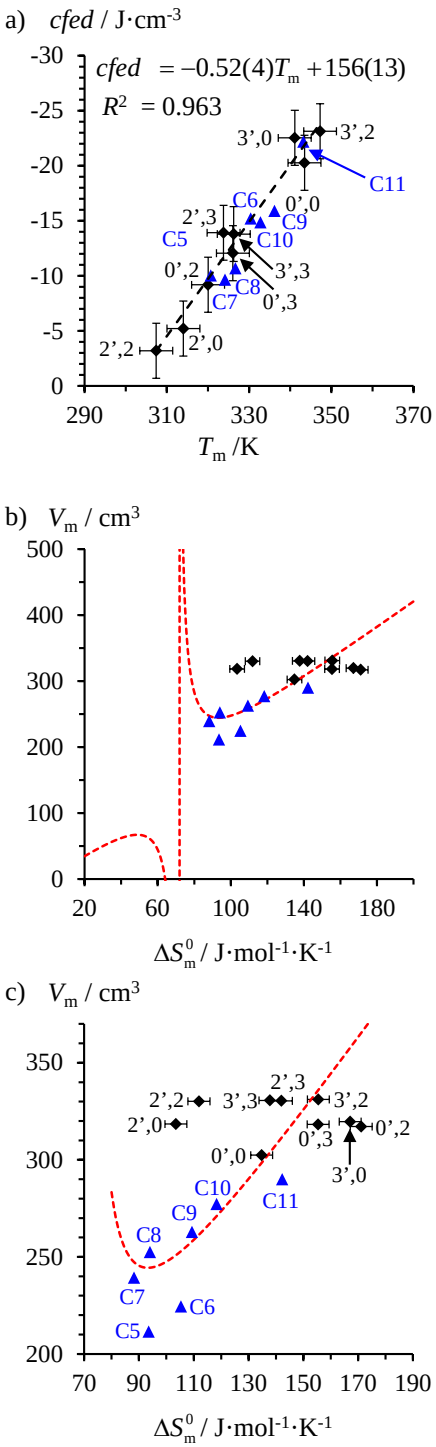

Figure S19 Plots of (a) the cohesion free energy densities (*cfed*) *versus* the melting temperature (T_m) and (b) the molar volumes (V_m) *versus* ΔS_m for **C*n*L**$^{i',j}$. The dotted red trace shows the theoretical curves computed with eqn (17) and (c) shows the assignment of each compound.

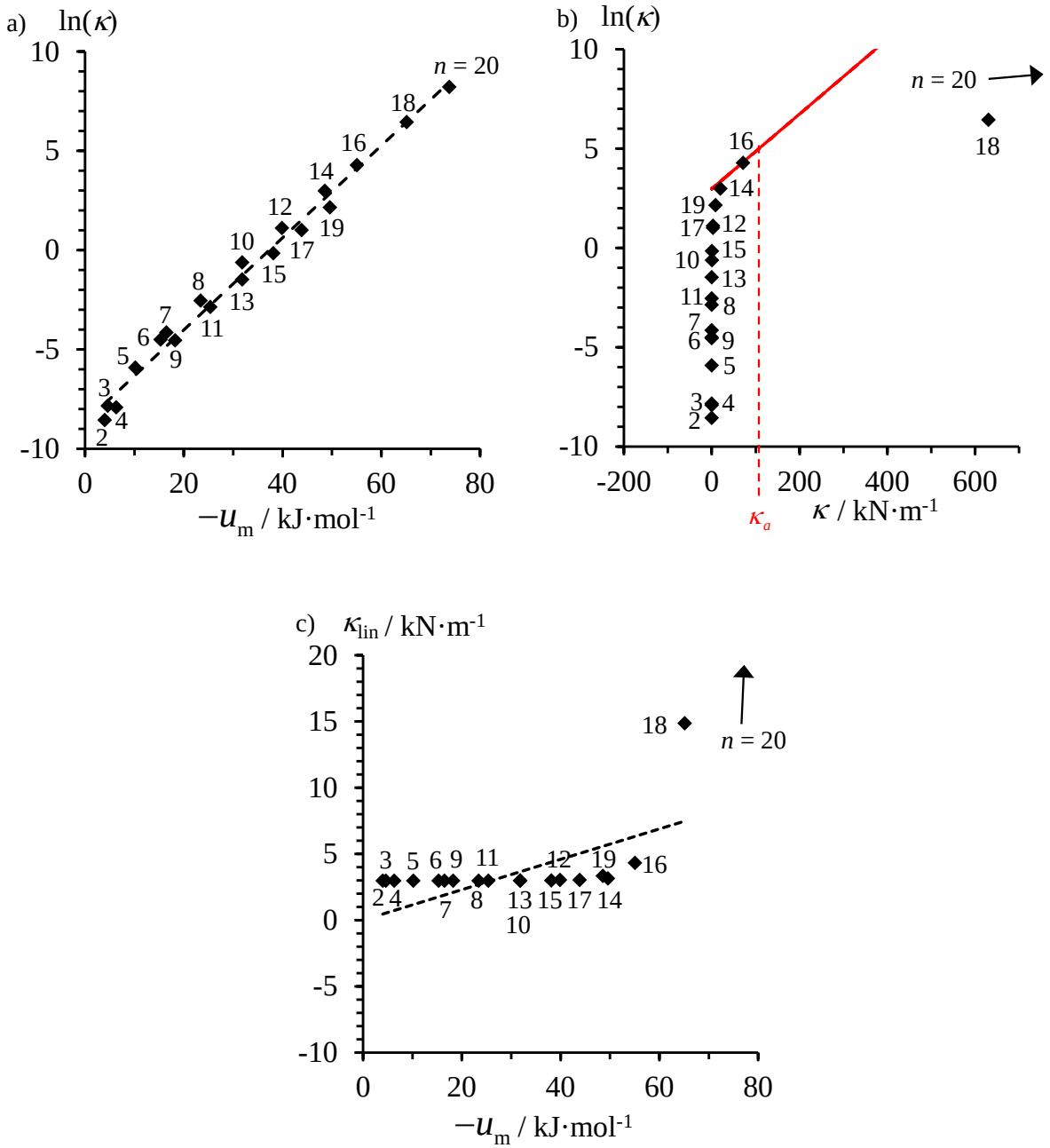

Figure S20 Plots of (a) the logarithm of the force constants $\ln(\kappa)$ *versus* the potential well depth $u_{\min}$, (b) linearization according to a first-order Taylor series $\ln(\kappa^0) \approx \ln(\kappa_a^0) + ((\kappa^0 - \kappa_a^0)/\kappa_a^0)$ about κ_a^0 = 53.1 kN/m^2 and c) pseudo-linear correlation between the 'linearized' force constants and the potential well depths $u_{\min}$ used for estimating $2^{1/6}r_0$ = 0.31(4) Å for the average optimum contact distance between the surface of the alkane entities (eqn 4) for the melting of saturated linear hydrocarbons C_nH_{2n+2}.[19]